



UNIVERSITÀ DEGLI STUDI DI CATANIA

IN CONVENZIONE CON



UNIVERSITÀ DEGLI STUDI DI PALERMO

DOTTORATO DI RICERCA IN

SCIENZA DEI MATERIALI E NANOTECNOLOGIE - XXXI CICLO

VANESSA RITA BERTOLINO

**PREPARATION AND STUDY OF COMPOSITES FILMS
BASED ON BIOPOLYMERS AND NANOFILLERS
CHARGED BY SUBSTANCES WITH SPECIFIC PROPERTIES**

TUTOR: PROF. GIUSEPPE LAZZARA

COORDINATORE: PROF.SSA M. G. GRIMALDI

TESI PER IL CONSEGUIMENTO DEL TITOLO DI DOTTORE DI RICERCA

PREFACE	5
1. GREEN MATERIALS	6
1.1 <i>Introduction</i>	7
1.2 <i>Biopolymers</i>	8
1.3 <i>Chitosan</i>	10
1.4 <i>Alginate</i>	11
1.5 <i>Cellulose</i>	13
1.6 <i>Clays and nanoclays</i>	15
1.7 <i>Halloysite</i>	16
1.8 <i>Kaolinite</i>	18
1.9 <i>Nanotechnology and nanocomposites</i>	19
1.10 <i>Layer-by-layer composites</i>	20
1.11 <i>Layer-by-layer: drug delivery system</i>	21
1.12 <i>Aims and objective of the study</i>	22
2. AQUEOUS BIOPOLYMER/ HNTS MIXTURE	24
2.1 <i>Physico-chemical characterization of halloysite nanotubes (HNTs)-polymer systems in aqueous solution</i>	25
2.1.1 <i>Turbidimetric Measurements</i>	25
2.1.2 <i>Electrostatic interaction</i>	28
2.1.3 <i>Thermodynamic properties by ITC</i>	30
3. NANOCOMPOSITE BASED ON BIOPOLYMER AND HNTS	34
3.1 <i>A chemical-physical characterization of nanocomposites based on biopolymer and HNTs</i>	35
3.1.1 <i>Thermogravimetric results</i>	35
3.1.2 <i>Dynamic-mechanical analysis</i>	38
3.1.3 <i>Wettability and morphology</i>	41
3.1.4 <i>X-ray crystallography</i>	43
4. MULTILAYER NANOCOMPOSITES	45
4.1 <i>Multilayer systems based on HPC/Chit-HNT/HPC</i>	46
4.1.1 <i>Multilayer preparation and structure</i>	46
4.1.2 <i>Thermal behavior under an inert atmosphere</i>	48
4.1.3 <i>Thermal behavior under oxidative atmosphere</i>	50
4.2 <i>Multilayer nanocomposites with halloysite nanotubes between two chitosan layers</i>	51
4.2.1 <i>Preparation of chitosan/ HNTs nanocomposites with three-layered structure</i> ..	52

4.2.2 Morphology investigated using scanning electron microscopy	53
4.2.3 Surface wettability analysis	54
4.2.4 Thermal properties investigated using thermogravimetric analysis and differential scanning calorimetry.....	55
5. LAYER BY LAYER SYSTEMS SUCH AS DRUG DELIVERY	58
5.1 LBL assembly based on electrostatic interactions	59
5.2 Materials properties and LBL systems preparation.....	59
5.3 Size and ζ -potential experiments	60
5.4 Dynamic light scattering investigation.....	61
5.5 CCK-8 assay to investigate the HeLa cell viability	64
5.6 Inhibition of internalization routes	66
5.7 Drug release studies.....	67
6. TEST OF FILMS CYTOTOXICITY ON HELA CELLS	69
6.1 The biocompatibility, the cytotoxicity and the cells proliferation on films surface	70
6.2 Films sterilization	70
6.3 Toxicity studies with CCK-8	70
6.4 Toxicity of DMEM kept in contact with film	71
6.5 Calcein AM/ propidium iodide experiments	71
CONCLUDING REMARKS	74
ACKNOWLEDGMENT	76
REFERENCES.....	78
CURRICULUM VITAE	101
ATTACHED PAPERS	107

Preface

This Ph.D. thesis entitled “Preparation and study of composites films based on biopolymers and nanofillers charged by substances with specific properties” was initiated in November 2015 and finalized in October 2019. The study has almost carried out at the University of Palermo (Physics and Chemistry Department) and some experiments have been done at the Institute of Physics of Santiago De Compostela University during a training of about four months.

The thesis is a contribution to the possibility to replace the traditional plastic materials with bioplastics, composite materials based on environmental friendly resources, such as biopolymers and nanoclays. In detail, the thesis includes six chapters. The first is an introduction to the green materials world, the properties and the current and most important applications of biopolymers, nanoclays and their composites. Chapter 2 reports studies on HNTs stability in aqueous polymer dispersions, considering the structural and the thermodynamic features that influence the interactions between the two components. Chapter 3 is dedicated to the physicochemical characterization of nanocomposite based on biopolymer/ nanofiller, considering the effect of biopolymer charge and the nanoclay morphology on materials obtained. A thermal study on multilayer nanocomposites based on an alternation of layers of hydroxypropyl cellulose and halloysite nanotubes combined to chitosan and the preparation and a thorough physic-chemical investigation on novel biocomposite characterized by halloysite nanotubes sandwiched in two chitosan layers are reported in chapter 4.

The work done during my training at Santiago de Compostela can be divided into two-part. One part focuses on the possibility of designing and characterizing layer-by-layer systems such as drug delivery. Chapter 5 is an in-depth explanation. The second part, that is reported in chapter 6, focuses on the possibility to verify the cytotoxicity of nanocomposites based on chitosan and halloysite nanotubes at different concentrations of components. The possibility of degradation of materials during the first 72 hours in incubation with DMEM is investigated and the possibility of release of toxic substances to cells is verified too.

1. Green Materials

1.1 Introduction

Among the most current problems in environmental degradation are the accumulation of urban wastes and water pollution due to the excessive and irresponsible uses of petrochemical based plastics. The versatility of plastic materials allowed them to be introduced in different fields, resulting in an important improvement in the quality of life but resulting in an increase in ecological problems because of their non-biodegradability.¹ Disposal using incineration of these materials determines an increase in carbon dioxide emission and sometimes, a production of toxic gas, which leads to a contribution to global warming and city pollution. Currently¹, there is a simultaneous and growing interest in developing new materials and innovative process technologies that can reduce the environmental impact on the ecosystems. Specifically, the researchers have focused their attention on renewable and no toxic natural resources. Within this topic, packaging films with either user-friendly or eco-friendly features have become an important object of study. Packaging materials include biobased polymers, bioplastic or biopolymer packaging products made of raw materials originating from agricultural or marine sources.² Various polymers have been used for this purpose, covering a great variety of applications, ranging from containers and packaging materials to substances used in artificial organs and aerospace technology.^{3,4} Some of these biopolymers are used in their pure form, others show better properties as a result of the incorporation of additives.⁵ They generally present poor mechanical properties regarding processability and end-use application, since the fragility and brittleness exhibited during term formation can limit their potential for applications. To overcome this issue, plasticizers are added to provide the necessary workability to biopolymers.⁶ The combination of biopolymeric matrix and additives offer unusual systems of stiffness, strength, and weight that is difficult to attain separately from the individual components. In the last decades, owing to increase in the concept of ecological safety and utilization of renewable materials towards greener society, the use of natural and/or biodegradable plasticizers⁷ with low toxicity and good compatibility with several plastics, resins, rubber and elastomers in substitution of conventional plasticizers, such as phthalates and other synthetic conventional plasticizers attracted the market along with the increasing worldwide trend towards the use of biopolymers.⁸ In this context, the application of natural fibers in the industries as bio-filler/reinforcement materials in composites is considerably improved.⁹ Natural fibers have attracted the interest of

researchers, material scientists, and industries, owing to their specific advantages as compared to conventional or synthetic fibers from the past.¹⁰ Although a total replacement of synthetic plasticizers by natural-based plasticizers is impossible, at least for some specific applications such as a replacement seems obvious and useful.⁸ Finally, to improve the properties of polymers, it is preferable to use a nanofiller, rather than “traditional” fillers of micrometric dimensions. In fact, for any composite, the circumstances for substantial reinforcement and virtuous properties are the homogeneous distribution of the reinforcing component, orientation, good adhesion, and relatively high aspect ratio.¹¹ Nanofillers have a greater surface area and this property lets them usually to provide better performances, e.g. reinforcement, to nanocomposites.¹¹ In such applications, they may confer certain unique attributes and functionalities.¹² Various types of nanoparticles, including nanocarbon, carbon nanotubes, nanoclays, and metal oxides, are currently used to modify the polymer performance.¹³

If nanocomposites indicate a new class of materials with ultrafine phase dimensions, typically of the order of a few nanometers,^{14,15} the combination of biopolymer and nanoclays may generate new sustainable materials, so-called bionanocomposites, with excellent and unique properties.¹⁶ Bionanocomposites have been widely studied and represent a good alternative to the activated carbon in waste-water decontamination. They are good adsorbent materials of toxic substances in the reduction of water pollution¹⁷ and the remediation of organic contamination (better with organo-clays as sorbents).¹⁸ They represent good potential new drug delivery systems.¹⁹ This introduction contains in brief only some of the many characteristics of these “green” materials and the advantages related to their use in many fields, which will be explained in more detail in later chapters.

1.2 Biopolymers

Four are the categories in which it is possible to classify biodegradable polymers based the sources and on the synthesis.²⁰ There are polymers from biomass such as the agropolymers from agro-resources;⁸ polysaccharides, starches (wheat, potatoes, maize),^{21,22} ligno-cellulosic products (wood, straws)²³ and others (pectins, chitosan/chitin, gums)²⁴ protein and lipids, animals (casein, whey, collagen/gelatin),²⁵⁻³¹ and plants (zein, soya and gluten).^{32,33} There are polymers obtained from microbial production,

polyhydroxyalkanoates (PHA) such as poly(hydroxybutyrate) (PHB) and poly(hydroxybutyrate co-hydroxyvalerate (PHBv)). Polymers obtained from chemical synthesis starting monomers of agricultural resources, e.g., poly(lactic acid) (PLA). Polymers such as polycaprolactones (PCL), polyesteramides (PEA), aliphatic co-polyesters (e.g., PBSA) and aromatic co-polyesters (e.g., PBAT), finally, are obtained using chemical synthesis from monomers and polymers of fossil resources.

Because of their naturally occurring structure, biopolymers are fully capable of biodegradation at accelerated rates; the organic components undergo fast degradation induced by a biological system (especially for enzymatic action) determining the release of carbon dioxide, water, minerals and new biomass. Two properties of these materials, biodegradability and renewability, let them be considered excellent alternatives to traditional plastics in many application fields, such as packaging, engineering and textile industry. Another important property of biopolymers is their abundance and consequently their inexpensiveness.¹⁶

Chitosan, alginates, cellulose and their derivatives are some examples of interesting biopolymers. They are polysaccharides and it is interesting to consider the importance of their use in particular in the preparation of nanocomposites due to their specific properties (such as a biological activity). They constitute a large source of materials for applications, especially in the domain of biomaterials for tissue engineering, drug vehicles, controlled release of drugs. Their development has opened a large field of applications.

For all these reasons, the growing interest in polymers such as materials in the last 50 years is very amazing and it is reflected in the increasing number of scientific publications (Fig. 1.2.1 a). There are several fields of application for these materials based on polysaccharides, including material science engineering, biochemistry, agricultural and biological science (Fig. 1.2.1 b,c,d,e,f). In particular the maximum percentage of publications number for polymers such as starch (16%) and pectin (21%) is in agricultural and biological science field (Fig. 1.2.1 b,c), instead the maximum of publications (~20%) for remaining polymers is in materials science (Fig. 1.2.1 d,e,f).

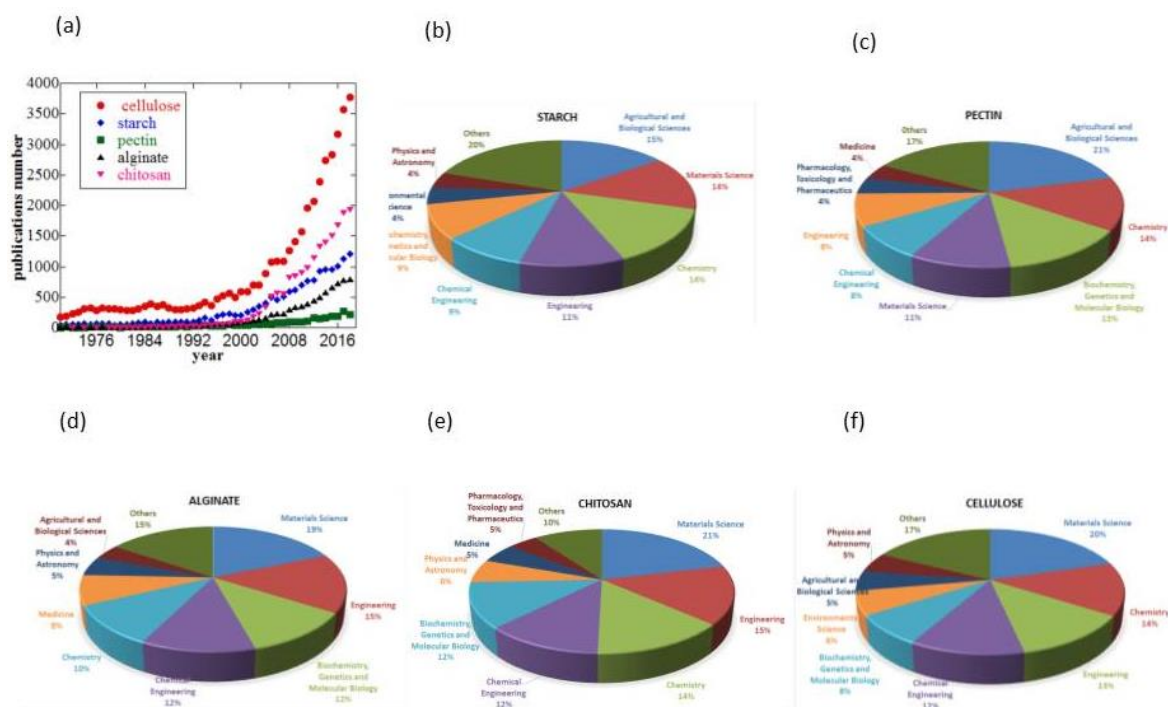


Figure 1.2.1 The number of publications for each year on polysaccharides such as materials (a). The percentage of publications number for studied polymers in different fields (b,c,d,e,f).

1.3 Chitosan

Chitosan is a polysaccharide. It is very similar to cellulose, which consists of β -1,4-linked D-glucosamine with a variable degree of N-acetylation, except that the acetylamino group replaces the hydroxyl group on the C2 position. Thus, chitosan is a copolymer consisting of N-acetyl-2-amino-2-deoxy-D-glucopyranose and 2-amino-2-deoxy-D-glucopyranose, where the two types of repeating units are linked by (1 \rightarrow 4)- β -glycosidic bonds. It is the second abundant natural polymer on earth³⁴ and it is obtained from chitin. The primary source of chitin and chitosan are crustaceans such as crabs, shrimp and lobsters, which are highly abundant biomasses due to the food and beverage and canning industries.³⁵ Chitosan has been widely studied for biosensors, tissue engineering, separation membrane, and water treatment and so on, because of its good biocompatibility, biodegradability, and multiple functional groups.³⁶ In the recent period the researchers have focused their attention on this polymer such as a good candidate to generate biomaterial.³⁷ Chitosan shows non-toxic nature, antimicrobial activity, and good

compatibility with living tissue.^{36,38} Chitosan is readily soluble in dilute acidic solutions below pH 6.0 due to the quaternization of the amine groups that have a pKa value of 6.3 making chitosan a water-soluble cationic polyelectrolyte.³⁹ Furthermore, its polymeric cationic character and its gel and film-forming properties made chitosan extensively examined in the pharmaceutical industry for its potential in the development of drug delivery systems.⁴⁰ Chitin and chitosan can be processed in various forms such as hydrogels,⁴¹ nanofibers,⁴² beads,⁴³ membranes,⁴⁴ scaffolds,⁴⁵ micro/nanoparticles,⁴⁶ tissue engineering,⁴⁷ films,⁴⁸ fibrous mats.⁴⁹ An important application of chitosan membranes was in the biomedical area, in fact, both chitin and chitosan have shown positive effects on wound healing. It was showed they could favor the repair of some tissues and improve the secretion of the inflammatory mediators.⁴⁴ Although the applications of this polymer have been developed in different fields, from molecular separation to food packaging film, from artificial skin to bone substitutes and water treatment, some its properties, such as mechanical strength, thermal stability, scarce water and gas barrier properties resulted not good enough to meet this wide range of applications.^{50,51} The possibility to incorporate inorganic fillers was an effective approach for improving the physico/chemical properties of chitosan and other biopolymers too. Different inorganic fillers have been combined to chitosan for this purpose and in literature, some examples with hydroxyapatite,⁵² clay,⁶ calcium phosphate cements⁵³ are reported.

1.4 Alginate

Others important and abundant naturally derived biopolymers are **alginates**. They are formed by (1-4)-linked b-D-mannuronic acid (M units) and a-L-guluronic acid (G units) monomers linked in a linear manner which vary in amount and sequential distribution along the polymer chain depending on the source of the polymer.⁵⁴ More than 200 different alginates are currently being manufactured.⁵⁵ Different kind of alginates means different physical and mechanical properties; in fact, there is a direct correlation between the polymer properties and its composition (ratio between M and G units) and molecular weight.⁵⁶ Alginate is a naturally occurring anionic polymer typically obtained from brown seaweed (Phaeophyceae), including *Laminaria hyperborea*, *Laminaria digitata*, *Laminaria japonica*, *Ascophyllum nodosum*, and *Macrocystis pyrifera*⁵⁷ by treatment with aqueous alkali solutions, typically with NaOH. Many researchers have extensively investigated on

this polymer due to its biocompatibility, low toxicity, relatively low cost.⁵⁸ Besides it has been used for biomedical applications, because it has several unique properties that have enabled it to be used as a matrix for the entrapment and/ or delivery of a variety of biological agents⁵⁹ and it has been widely used in the food industry as thickeners and emulsifying agents.⁶⁰ The industrial applications of alginates are correlated to their ability to retain water and their gelling. In principle, alginates form gels (or precipitate at low polymer concentrations) in the presence of divalent and trivalent ions such as Ca^{2+} and Al^{3+} .⁶¹ The alginate ability to undergo a sol-gel transition⁶² is correlated to the possibility by two G units of adjacent polymer chains to be cross-linked with multivalent cations (e.g., Ca^{2+} or Ba^{2+}) through interactions with the carboxylic groups in the sugars.⁶³ Gelation was briefly described in the terms of the ‘‘egg box model’’⁶⁴ where multivalent ions, generally calcium ions, are coordinated to guluronate cavities made by paired up of guluronate sequences in the alginate chains.⁶⁵ Alginate gels, in particular hydrogels, found application mainly in the pharmaceutical field. In fact these hydrogels showed an extraordinary resemblance to the natural extracellular matrix⁶⁶ and have been used to provide the structural integrity and bulk for cellular organization and morphogenic guidance, to encapsulate and deliver cells, to act as tissue barriers, to serve as depots for drugs, and to deliver bioactive moieties that encouraged the natural reparative process.⁶⁷

The gelling properties, very important for its use such as immobilization material, are related to the monomeric composition, the sequential arrangements and the lengths of the G-units.⁶⁸ All these reasons have let these alginates hydrogel to have been employed successfully in three-dimensional cell-hydrogel scaffolds for tissue engineering and the encapsulation of transplanted (allogeneic or xenogeneic) cells in alginate hydrogel beads. Natural carbohydrates, such as alginates, possess the supramolecular architecture needed for the preparation of polymeric beads that have been used in biotechnology and also for engineering applications.⁶⁹ Besides, the presence of negative carboxylate functions along polymer chains ensured its high affinity and binding capacity for cations. It could reasonably be utilized as a naturally available low-cost adsorbent for water treatment. In particular, in literature a work has been reported in which the ability of alginate gel beads, specifically Zn^{2+} modified alginate, to adsorb Victoria Blue (VB) dye was higher than other materials.⁷⁰ In another study, it has been demonstrated the efficacy of magnetically separable activated carbon/cobalt ferrite/alginate composite beads as an adsorbent for methylene blue removal from aqueous solution.⁷¹ The capacity of gel beads of alginate filled with halloysite nanotubes to remove crystal violet commonly used as additive for

fertilizers, anti-freezes, detergents, and used also with some medical applications such as antibacterial, antifungal, and anthelmintic has been investigated.⁷² However, alginate hydrogel beads are soft materials because their high water content (ca. 95%). This was also the reason that the beads could undergo to disruption prematurely when compression force occurred during manufacturing or application.⁷³ In some case, they have been subsequently coated with an additional polymer, chitosan, obtaining stronger beads.⁷⁴

Another field in which alginate has been used is the packaging. The growing environmental attention required packaging films with both user-friendly and eco-friendly features.⁶ Alginate is considered a good “green” packaging materials because it has good filming and unique colloidal properties, which include thickening, stabilizing, suspending, film-forming, gel producing, and emulsion stabilizing.⁷⁵ Finally, it was possible to obtain an antibacterial film with this biopolymer.⁷⁶

1.5 Cellulose

Cellulose is the most abundant natural polysaccharide, and due to its biodegradability and renewability, it has been regarded as the greenest available material.⁷⁷ This natural polymer represents about one-third of plant tissues and it can be restocked by photosynthesis.⁷⁸ Wood pulp remains the most important raw material source for the processing of cellulose, most of which is used for the production of paper and cardboard.⁷⁹ Although the use of biopolymers is innovative compared to the use of petroleum-derived polymers, their brittleness and insufficient mechanical and moisture barrier properties at higher humidity conditions restrict their use in a wide range of applications.⁸⁰

There are different studies on cellulosic materials and their mechanical and thermal performances that let us to consider them promising and competitive with conventional plastics. Cotton and other cellulosic fibers, such as kenaf, rami, and flax face competition to synthetic fibers, mostly due to product uniformity, performance, and cost.⁸¹ The all-cellulose composites of ramie fibers embedded in a matrix of regenerated cellulose, which was first introduced by Nishino, Matsuda, and Hirao (2004), had excellent mechanical properties and thermal performance.⁸² Nishino et al.⁸³ investigated the mechanical properties of natural cellulose that shows a high elastic modulus (138 GPa) for the crystalline regions. This result was comparable with the elastic modulus values of high-performance synthetic fibers such as poly(p-phenylene terephthalamide) (156 GPa, Kevlar,

Twaron), Vectran (126 GPa), Technora (88 GPa), and Ekonol (130 GPa).⁸⁴ Also, the maximum macroscopic Young's modulus of natural plant cellulose (up to 128 GPa) was higher than those of aluminum (70 GPa) and glass fibers (76 GPa). Intrinsically, the very high elastic modulus and tensile strength (not specific modulus and specific strength) implied that cellulose possessed the potential to replace glass fiber, and it showed promise as a reinforcement fiber for composites where the density was not a concern.⁸³ Therefore, actual application of cellulose reduces either the consumption of fossil resources or protects the environment. However, the use of cellulose has been limited by the difficulty of its processing and derivatization; this natural polymer is neither meltable nor soluble in conventional solvents due to its hydrogen-bonded and partially crystalline structure.⁸⁵ Chemical modification such as etherification has continued to provide a dominant route towards cellulose utilization in polymer-based materials.⁸⁶ Cellulose derivatives have been applied as components of hydrogel formulations, used as drug-delivery system,⁸⁷ in synthesis of new temperature-responsive hydrogel for functional finishing of cotton knitwear,⁸⁸ in coating formulations to reduce oil uptake in deep-fat frying potato strips and dough discs.⁸⁹ It is important to remember the improvement of micro fibrillated cellulose on tensile properties in composites of phenolic resin.⁹⁰ Hydroxypropyl cellulose (HPC) belongs to the group of cellulose ethers which has been used already for a year by the paper of conservators as glue and sizing material.⁹¹ It is a non-ionic polymer, prepared by reacting alkali cellulose with propylene oxide on anhydrous glucose chain at elevated temperature and pressures.⁹² Carboxymethyl cellulose (CMC) is another example of a polymer obtained by the etherification of cellulose. It has been used in a very wide range of applications, from detergents and soap such as soil-suspending agents to food products such as dietetic food and ice cream, from the textile industry such as coating agents to paper industry for the coating colors.⁹³

It is very important for the results obtained by the combination of fibers from both nonrenewable and renewable resources to produce composite materials that turned competitive with synthetic composites.⁹⁴ Cellulosic fibers represent another class of natural cellulosic biopolymers. Due to their interesting properties, including low cost, biodegradability, recycling, abundance, not abrasiveness, they can be used like biopolymers themselves as well as reinforcing fillers of polymeric matrices.⁹⁵⁻⁹⁷ Studies⁹⁸ have been reported in which it was established that the mixing of fibers with polysaccharides such as thermoplastic starch and its blends or cellulose derivatives, involved a marked improvement in the mechanical properties of biocomposites.⁹⁹ The

nanofibers are composed of extended cellulose chains forming a semi-crystalline structure, so their thermal expansion is as low as that of quartz,⁸³ and their tensile strength was estimated to be about five times that of mild steel, based on the tensile test of kraft pulp single fibers.¹⁰⁰ They have improved mechanical properties of composites based on biopolymers in comparison of pure biopolymers such as polyvinyl alcohol¹⁰¹ or polylactic acid.¹⁰⁰

1.6 Clays and nanoclays

Clays and shales are by far the most abundant types of sedimentary rocks. They represent a typical mineral assemblage in the smallest grain size range. The upper limit of the pelitic size class is a matter of definition. Silt has usually larger grains than 1-10 μ in diameter.¹⁰² For JNCs, joint nomenclature committees, clay is “... a naturally occurring material composed primarily of fine-grained minerals, which is generally plastic at appropriate water contents and will harden with (sic) dried or fired”.¹⁰³ Although plasticity is a part of the JNCs’ definition, but there are clays (e.g., ‘flint clay’) that do not have this property and despite this, they are still regarded as ‘clay’ because of past usage. The JNCs also state that the plastic properties of clay do not need quantification since plasticity is affected by many factors, including chemical composition and particle aggregation.¹⁰⁴ There are different kind of clays. Each one has own mineralogical composition, particle size distribution, organic substances and additives. All these factors can influence their plasticizing property. Clays are abundant, widespread, and inexpensive compared with other raw materials. The great variety of physical, chemical, and thermal treatments that may be used to modify clays and clay minerals provide unlimited scope for future applications, particularly in terms of protecting the environment.¹⁰⁴

The nanoclays are alumino-silicate particles and from the mineralogical view-point, they belong to the family of phyllosilicates composed of two types of structural sheets: octahedral and tetrahedral. The tetrahedral sheet is composed of silicon-oxygen tetrahedra linked to neighboring tetrahedra by sharing three corners, resulting in a hexagonal network.¹³ The remaining fourth corner of each tetrahedron forms a part to the adjacent octahedral sheet. The latter is usually composed of aluminum or magnesium in six-fold coordination with oxygen from the tetrahedral sheet and with hydroxyl groups. The two sheets together form a layer, and several layers may be joined in a clay crystallite by interlayer cations, Vander Waals force, electrostatic force, or by hydrogen bonding.¹³ The

thickness of each layer is ca. 1 nm and the lateral dimensions may change from 300 Å to several microns. These layers organize themselves to form stacks with a regular van der Waals gap called the interlayer or the gallery. It is possible to distinguish clays in three categories, 1:1, 2:1 and 2:1:1 phyllosilicate, according to the different arrangements of the tetrahedral and octahedral sheets. The first one (including phyllosilicates such as kaolinite and halloysite) has one tetrahedral and one octahedral sheet per clay layer. The 2:1 clay minerals, e.g. montmorillonite, laponite and illite, are characterized by one octahedral sheet sandwiched between the two tetrahedral sheets. Finally, the 2:1:1 phyllosilicate, such as cloisite, are composed of an octahedral sheet adjacent to a 2:1 layer. It is possible that an element can replace another element in tetrahedral and octahedral sheets in the mineral crystal without modifying its chemical structure. For example, Al^{3+} can replace Si^{4+} in tetrahedral coordination, and Al^{3+} replaced by Mg^{2+} or by Fe^{2+} and Mg^{2+} replaced by Li^{+} may occur in octahedral coordination. This isomorphous substitutions influence the layered structure of the mineral crystal and determine a charge. The presence of these charges is counterbalanced by ions situated in the interlayer.

The nanoclays properties, such as large surface area, high porosity and tunable surface chemistry make these nanomaterials very versatile and usable in a different fields. They can be used in catalysis,¹⁰⁵⁻¹⁰⁷ in electronic devices,¹⁰⁸ for entrapment of hydrophilic and lipophilic active agents and as a nanofillers for polymers.¹⁰⁹⁻¹¹² Moreover, the nanoclays are largely employed in pharmaceutical applications¹¹³ and in water decontamination¹¹⁴⁻¹¹⁶ because of their sorption ability and biocompatibility. Within this field, halloysite is a new emerging clay with unique properties and appealing perspectives.

1.7 Halloysite

Halloysite belongs to the family of layered aluminosilicate (1:1) clay mineral (chemical formula of $\text{Al}_2\text{Si}_2\text{O}_5(\text{OH})_4 \cdot 2\text{H}_2\text{O}$) and it occurs widely in both weathered rocks and soils. The largest deposits of halloysite are found in Northland (New Zealand) and Dragon Mine (Utah – USA).

The structure and chemical composition of halloysite is similar to that of kaolinite, dickite or nacrite but the unit layers in halloysite are separated by a monolayer of water molecules,^{117,118} that determines an increase of the spacing in the multilayer walls from 7 Å to 10 Å; the interlayer water is weakly held, halloysite-(10 Å) can readily and irreversibly dehydrate to give the corresponding halloysite- (7 Å) form.¹¹⁸

Halloysite has a different morphology but the most common is elongated tubule,¹¹⁹ due to the discrepancy in the two-layered alignment of the tetrahedral sheet of silica bonded to the octahedral sheet of alumina, which causes the wall to curve into a cylindrical shape.¹²⁰ The HNT nanotubes (HNTs) are characterized by a certain polydispersity in size: their length is between 0.2 and 1 μm , the inner diameter can be from 10 to 70 nm, while the outer diameter is ca. 20-200 nm.¹²¹

The different chemical nature of the outer and inner surface of the nanotubes, the first characterized by the presence of Si–O–Si groups, the second characterized by the chemistry of Al–OH groups determines a different charge between the two surfaces. At pH between 2 and 8, the outer and inner surfaces have a negative and a positive charge respectively^{122,123} and the surface ζ -potential of the HNTs falls between that of silica and alumina. The specific surface area of halloysite is 65 m^2/g , pore volume is 1.3 mL/g , the refractive index is 1.54, and specific gravity is 2.53 g/cm^3 .¹²² The lumen, modified or not, of nanotubes can be loaded with drug or molecules with antioxidant and antimicrobial capacity.¹²⁴ Different studies confirm that HNTs represent an ideal substrate for the controlled or sustained release of drugs or bioactive molecules.¹²² Another important application of HNTs is related to their ability to give to systems based on biopolymers better chemical-physical properties, in this case, the nanoclays act as reinforcing agent.¹²⁵ Sometimes it could be useful to functionalize the halloysite nanotubes to improve the interaction or the compatibility to biopolymers. There are different studies in which it was demonstrated the possibility to improve the HNTs biocompatibility with non-covalent functionalization too. Chang et al. prepared and conducted studies on a supramolecular complex based on amylose and HNTs, kept together using mechanical forces. The components were mixed by ball mill and in this way, the mechanical force wrapped helical amylose around the walls of HNTs.¹²⁶ The biocompatibility of nanotubes made these systems potentially adequate as biosorbents for heavy metal ions¹²⁷ and dyes,¹¹⁵ biomedical applications,¹²⁸ biological nanoreactors¹⁰⁶ and nano-fillers in biopolymer matrix.¹²⁹ Furthermore halloysite nanotubes are biocompatible materials that have properties comparable to carbon nanotubes for some applications. They have also been found to be suitable for the encapsulation of biologically active molecules, such as Tetracycline, Khellin, and Nicotinamide Adenine Dinucleotide.¹³⁰ Summing up, the most important characteristics of HNTs and other clays for the wide use in different applications are particle size, surface chemistry, particle shape, surface area, and other physical and

chemical properties such as viscosity, color, plasticity, green, dry and fired strength; absorption and adsorption; abrasion; and others.¹³¹

1.8 Kaolinite

Kaolinite (Kao) is the major mineral component of kaolin. The kaolinite ($\text{Al}_2\text{Si}_2\text{O}_5(\text{OH})_4$), the anhydrous form of halloysite, is produced by a slow and complex hydrothermal alteration (“kaolinization”) of feldspars, feldspathoids and other aluminiferous silicates present as essential components in numerous rocks, mainly of the type granitic and gneissic. These minerals, in an acid environment, in the presence of water and CO_2 and under conditions of low temperature and pressure, release alkaline and alkaline-earth ions in solution and are transformed into aluminum hydrated silicates among which kaolinite prevails.⁶ The latter is a phyllosilicate (1: 1) consisting of a tetrahedral silica layer and an alumina octahedral layer. The thickness of an octahedral or tetrahedral sheet is about 2.4 Å, and this also results in the thickness of an interlayer space. It follows that the basal reticular distance is about 7.2 Å.¹³² This structure contains limited substitutions of other elements, such as some Fe can substitute Al and some Al can substitute Si. Because of the limited substitutions, the charge on the kaolinite layer is minimal so that there is a very little charge on the layer.¹³³ The morphology of kaolinite is different from that of the halloysite. Kao is characterized by a sheet-like geometry. To understand better it is possible to say “in the earliest stage of weathering, spheroidal aggregates consisting of microcrystalline halloysite are formed on the plagioclase surface. With progressive weathering, spheroidal halloysite converts to tubular halloysite. As weathering advances, tubular halloysite converts to platy halloysite, which in turn converts to kaolinite...”¹³⁴ Halloysite is attributable to the structure of kaolinite in which two water molecules per stoichiometric unit are interposed between the layers. The presence of these water molecules is probably the reason for the roll-up in nanotubes for the first one.^{122,135}

The major uses of kaolins are in the paper, ceramic, paint, plastic, rubber, and cracking catalyst industries because of some of their characteristics, e.g. the non-reactivity at pH between 4-9, the color (white), the ability to cover or hide if used as pigments, the softness and not abrasiveness, the low heat and electricity conductivity, the hydrophilic nature and so the high solubility in water. Besides these clays are not expensive.¹³³

1.9 Nanotechnology and nanocomposites

Nanotechnology is the ability to assemble and manipulate complex structures, with dimensions of the order of nanometers, and constitutes a new scientific and technological approach aimed at controlling the fundamental behavior of matter at the atomic and molecular level. In this context, in the last ten years, nanomaterials have aroused enormous interest with the belief that they can provoke a real technological revolution comparable to that generated by electronics and information technology. Their design and synthesis require the interaction between different scientific disciplines and interdisciplinary approaches. The nanocomposite technology is of great interest both in science and in industry. There has been an interest in combining polymeric materials and inorganic and organic structures to obtain the so-called ceramics with properties typical of ceramics (resistance to high temperature, stiffness, etc.) and of polymers (plasticity, low density, ease of transformation, etc.). Moreover, the catalytic, mechanical, electrical, thermal, optical, electrochemical properties of nanocomposites are different from those of the constituents.¹³⁶⁻¹³⁸ The nanocomposites are materials characterized by a dispersion of the ultrafine phases typically of the order of a few nanometers in polymeric matrices. The extent of the interactions is strongly linked to the nature of the dispersed phase; it is maximized by passing from isodimensional particles to nanotubes.^{6,139} Compared to conventional composite materials, nanocomposites have particular mechanical characteristics linked to the high surface/ volume ratio of the reinforcement phase; in general, the interfacial area between the matrix and the reinforcing phase (or phases) is typically an order of magnitude higher than that of conventional composite materials. Already low contents of nanofillers (less than 5-6% by weight) cause a notable increase of some chemical, physical and mechanical properties^{140,141} (gas permeability, solvent resistance, maximum temperature of use, thermal and dimensional stability, heat and flame resistance and mechanical stiffness¹⁴²⁻¹⁴⁴) minimizing the undesired effects resulting from the addition of traditional inorganic additives (increase density, reduction of processability, alteration of fracture toughness, opacity, etc.).¹³⁸

The first nanocomposite was prepared in 1961 when Blumstein demonstrated the polymerization of a vinyl monomer intercalated in the structure of montmorillonite,¹⁴⁵; however, only in 1988 the first industrial application has been carried out by Okada et al.¹⁴⁶ at the Toyota Central Research laboratories in Japan. They created a nanocomposite

system with a nylon 6 matrix loaded with montmorillonite and they found an extraordinary improvement of all the properties: increase of the tensile modulus, increase of tensile strength, reduction of thermal expansion coefficient, reduction of permeability, increase of resistance to impact.¹⁴⁷ This material (marketed by UBE Industries) is currently used for the manufacture of the belt in the engines of Toyota cars and for the production of films for packaging.¹³⁸ In recent years the scientific attention has been directed to a peculiar category of nanomaterials, the bio-nanocomposites that are called "eco-sustainable" due to the presence of a biopolymer matrix. The advantage of developing and disposing of these materials is important for the industrial world. Thanks to the availability of biopolymers, in the last decades studies have been carried out to improve the performances to extend them to the application sectors, especially electronics, the transport industry and packaging.

In the field of transport, the use of nanocomposites translates into an increase in production speed, an increase in thermal stability and mechanical properties, promotion of recycling and weight reduction. In the field of packaging, the use of nanocomposites has translated into the possibility of using thin layers of materials, guaranteeing a sufficient barrier level and the possibility of exploring new bio-packaging materials as biodegradable films from renewable sources.¹⁶ Unfortunately, the use of biodegradable films for food packaging has been strongly limited by the poor barrier properties and weak mechanical properties shown by natural polymers. It is for this reason that polymers are often mixed with other polymers or, less frequently, chemically modified to extend their applications to different circumstances.¹³⁶

1.10 Layer-by-layer composites

The layer-by-layer (LBL) method represents an easy and successful strategy for the manufacture of thin films with a multilayer structure. It is easier than the traditional method based on Langmuir-Blodgett (LB) technique, whose use is limited for amphiphilic molecules.¹⁴⁸ Langmuir Blodgett films are in fact monolayers or multilayers of a particular material which are usually obtained as monolayers by deposition at a liquid-gas interface (usually water-air) and as multilayers by building up monolayers on a chosen substrate.¹⁴⁹ The main difficulty of the Langmuir method is to prevent leakage of amphipathic material from the monolayer-covered region to the pure water surface. The multilayers can be built on substrate one layer at a time up to either an even or odd number of layers.¹⁴⁹ Additionally, LB method requires special instrumentation¹⁵⁰ and presents

several limitations on the shape/ size of the substrates as well as on the stability and quality of films.¹⁵¹

The LBL method is based on the electrostatic attractions between oppositely charged molecules¹⁵² and the hydrophobic interactions.¹⁵³ It is possible to obtain a layer-by-layer film through charge-transfer interactions.¹⁵⁴ Besides there are different methods to deposit the layers: spin-coating, spray-coating and solvent casting.¹⁵⁵ Antifogging and antireflective coatings were fabricated using a Spin-LbL assembly process, and this process is driven by electrostatic interactions between the positively charged ZrO₂ NPs and negatively charged SiO₂ NPs.¹⁵⁶ In literature different are the study of the preparation of multilayer assemblies using LBL spray-coating. It is reported of nanomaterials-based superhydrophobic (super water-repellent) coatings on Portland cement concrete (PCC) surfaces. These coatings are synthesized with nanomaterials such as polytetrafluoroethylene (PTFE), polyether ether ketone (PEEK) and silanized diatomaceous earth (DE). The study reveals that the spray duration and coating type are significant variables.¹⁵⁷

The benefits to adding an inorganic nanofiller to a biopolymer to obtain alternative plastics for several purposes within the packaging,¹⁵⁸ biotechnology,¹⁵⁹ and engineering¹⁶⁰ applications have already been extensively discussed. In this contest, the hybrid materials with a multilayer morphology exhibit different specific characteristics and functionalities. An intermediate clay layer between the polymer causes a flame retardant action on nanocomposites.¹⁶¹ Alginate/ montmorillonite nanocomposites with a multilayer structure show excellent flame and fire shielding property.¹⁶² LBL of polyacrylamide and graphene oxide let to fabricate fire retardant coatings for cotton fabric.¹⁶³ The success of this layer-by-layer assembly of polyelectrolyte multilayer thin films is based upon the fact that the adsorption of the polyelectrolyte chains leads to charge overcompensation on the film surface.¹⁶⁴

Finally, the resulting ease of preparation and versatility of multilayer assemblies has led to their use in such varied applications as contact lens coatings and antifouling covers.¹⁶⁵ Besides, recent studies have shown that there are many other promising applications for multilayered materials in such areas as drug delivery, sensors, wound healing, and membrane filtration.¹⁶⁶

1.11 Layer-by-layer: drug delivery system

In recent decades research has focused its attention on multicomposites because these systems make it possible to combine more properties (reinforced plastics).¹⁶⁷ Sometimes it is possible to improve stability for highly labile biomolecules or biomolecular assemblies; other times it is important to control molecular orientation or develop methods for the controlled assembly of multicomponent nanostructures.¹⁶⁸ In the biological world there are many examples of multicomponent nanostructures and the research tries to imitate it. In particular, it is possible to deposit or create molecular layers onto a planar solid supports¹⁶⁸ or such as a work in which Layer-by-Layer electrostatic self-assembly of polyelectrolyte nanoshells is created on individual carbon or halloysite nanotube used as templates.^{169,170} Based on this idea and the awareness that the fabrication of micro- and nano-sized capsules (or shells) which enable the encapsulation of various materials are of both scientific and technological interest.¹⁷¹ These capsules have been usually studied such as carriage-system for controlled release and targeting of drugs.¹⁷² It is known in literature a work in which these kinds of nanotubes, whose outer surface was modified by polymer chains of chitosan, are used as "carrier" systems for doxo with a resulting good control on delivery-release and antitumoral efficacy on MCF-7 cells.¹⁷³ Lee et al. have studied the cytotoxicity of HNTs functionalized by DNA to improve their solubility in water and the loading and following the release of doxo on A549 cells.¹⁷⁴ In this study halloysite nanotube is used to create around its outer surface with specific charge some layer in which a drug is kept using electrostatic interaction to obtain a system for a controlled and specific drug release. In fact, layer by layer system is realized exploiting the different surface charges of the polymer and of the drug itself and strong electrostatic interactions between the different layers to incorporate the drug, doxorubicin hydrochloride (doxo) and to improve the release in some specific conditions.

1.12 Aims and objective of the study

The research aim is to design, prepare and characterize composite films of polymers with nanofillers loaded with substances having specific properties. An extensive chemical-physical investigation was carried out based on the determination of properties (thermal stability, wettability, mechanical resistance), that provided useful information for the evaluation of technological applications. Furthermore, their combination with the

investigations on the structure of such materials (electron microscopy, dielectric spectroscopy, X-ray diffraction) provided the tools to correlate the mesoscopic structure with the properties of these nanocomposites. Both the polymers and the nanofillers will be chosen among the materials defined as "green"¹⁷⁵ and readily available. In this way, the aim is to reduce the environmental impact caused by the accumulation of non-totally biodegradable waste and to contain the cost of producing plastics that can be applied from the packaging field to tissue engineering, from the pharmaceutical industry to possible treatments in the field of conservation and restoration of Cultural Heritage. Biopolymers, that have been used, are chitosan, alginate, cellulose derivatives. They were chosen because of their biodegradability and low cost being readily available (they come from renewable resources). Their mixtures have also been used. As nanofillers we used nano-clay, and in particular halloysite nanotubes (HNTs). They have already been used in the preparation of polymeric nanocomposites as drugs transport¹⁷⁶/ release vehicles and in the treatment of wastewater,¹⁷⁷ or as reinforcing agents¹⁷⁸ (improve the mechanical properties) of the composites, if mixed in certain quantities. Furthermore, nano-clays are among the materials considered "green"¹⁷⁹ and can undergo various functionalizations¹⁸⁰ that can selectively improve their use.

In particular, the research project is schematized in three parts. The first part focused on the polymer- nanofiller interactions in aqueous solution. Additional detailed information is reported in the attached paper I.

The second part focused on the study of bionanocomposites. The solvent casting method was used to obtain the films, which were characterized both thermally and mechanically. The different interaction between polymer and nanofiller was evaluated, based on both the polymer charge and the morphology of the nanofiller. The possibility to obtain bionanocomposites with a multilayers structure was evaluated (additional information in attached papers II, III, IV).

Finally, the third part is focused on the research conducted during my training at Santiago de Compostela. In particular, layer-by-layer systems based on biopolymers and halloysite nanotubes and the study of cytotoxicity of bionanocomposites were considered (two manuscripts are in preparation).

2. Aqueous biopolymer/ HNTs mixture

2.1 Physico-chemical characterization of halloysite nanotubes (HNTs)-polymer systems in aqueous solution

Studies on the adsorption of biopolymers onto halloysite nanotubes (HNTs) in water were conducted. Three systems, HNTs-chitosan, HNTs-pectin, HNTs-hydroxypropyl cellulose (HPC), are characterized by turbidimetric technique to evaluate the stability of functionalized nanotubes in water. The choice of these three polymers is not accidental. It was intended to compare the different behavior of nanotubes in water in the presence of polymers with a different charge. In particular, we have used chitosan, a cationic polysaccharide, because of the presence of protonable amino groups; pectin from citrus, an anionic polysaccharide; and finally hydroxypropyl cellulose, a neutral polymer. ζ -Potential measurements are conducted to determine the surface charge properties. Polymer adsorption onto HNT surface is investigated by isothermal titration calorimetry (ITC). The standard variations in free energy, enthalpy, and entropy of the process were obtained and discussed. This study focuses on designing nano-objects, using the adsorption of polymers on the nanotubes surface, which can conveniently tune nanotubes charge and hydrophilicity for different applications.

In the following details on the above-mentioned properties and the insights provided are briefly discussed.

2.1.1 Turbidimetric Measurements

Figure 2.1 shows the optical density (OD) values as a function of time for each dispersion. The colloidal stability of the HNT dispersion in water can be investigated using the time dependence of the optical density.¹⁸¹ This parameter is related to the concentration of nanoparticles in suspension.

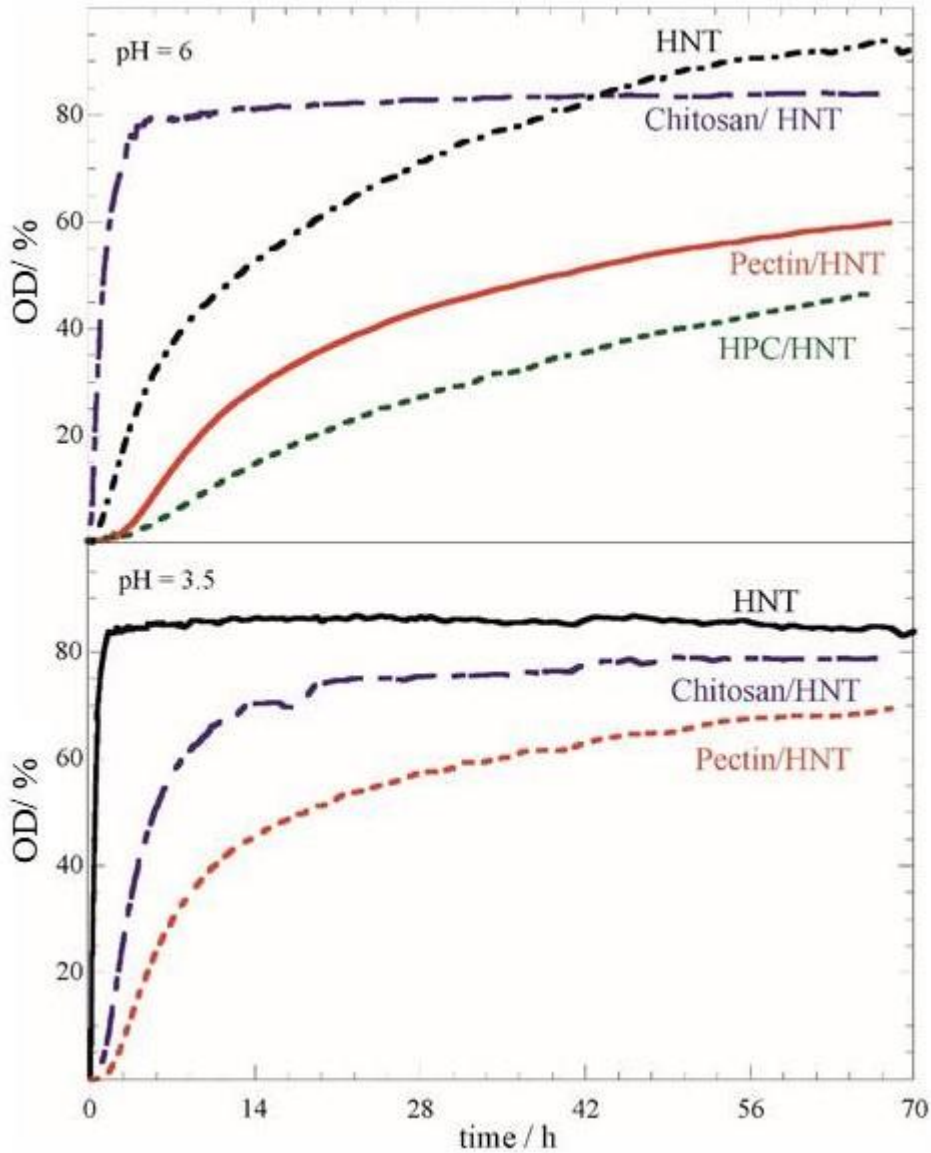


Figure 2.1. Optical density (OD) measured at $\lambda = 800$ nm as a function of time for HNT and polymer/HNT aqueous dispersion at different pH values. (Adapted with the permission from ref.182)

The optical density (OD) versus time curves can be fitted to the empirical exponential expression, that is adequate for sedimentation processes in colloidal systems:¹⁸³

$$OD = OD_{inf} [1 - \exp(-t/t_0)] \quad (\text{eq.2.1})$$

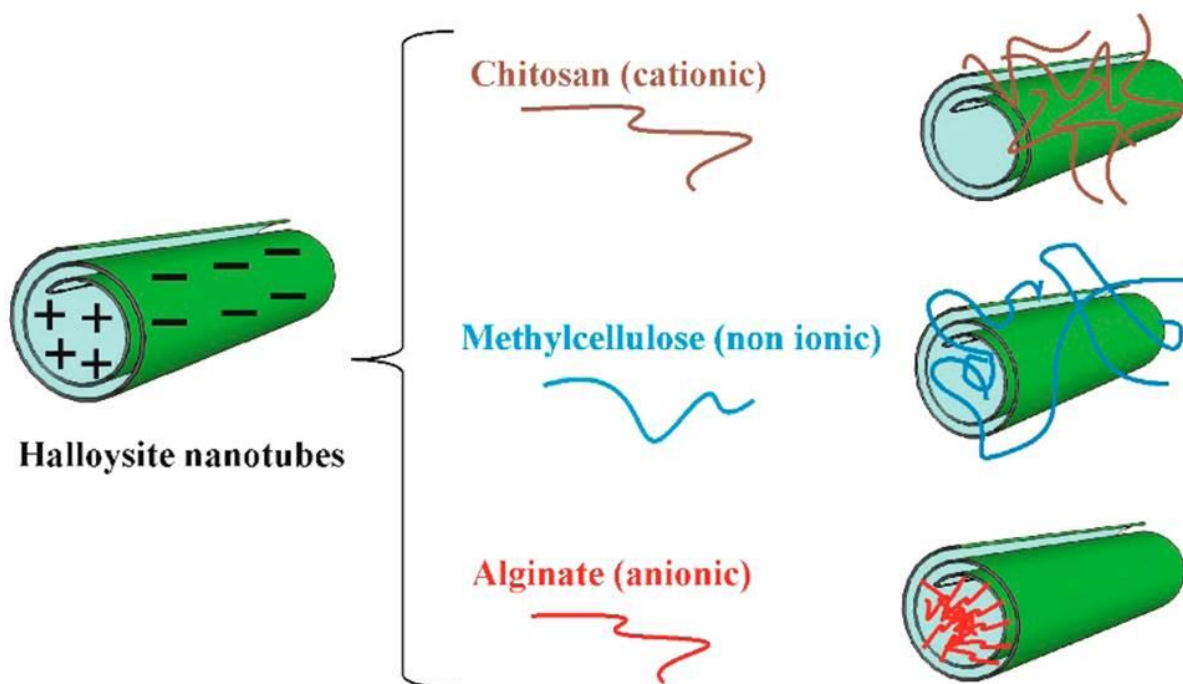
where OD_{inf} is the level-off value of the optical density, t is the time, and t_0 is the characteristic time for the sedimentation process. Table 1 shows parameters (OD_{inf} , t_0), calculated by the best fit based on eq.2.1 for each system.

Table 2.1 Fit Parameters for HNT Sedimentation Kinetics and Viscosity Values for the Aqueous Polymer Solutions^a

	pH	OD _{inf} / %	t ₀ / 10 ³ s	η _r
HNT	3.5	85.3 ± 0.1	1.57 ± 0.02	
HNT	7	90.3 ± 0.7	57.0 ± 1.2	
HPC/HNT	7	72.4 ± 1.9	224 ± 9	1.078
Pectin/HNT	3.5	66.9 ± 0.5	45.7 ± 0.9	1.445
Pectin/HNT	7	64.0 ± 0.6	91.0 ± 1.9	1.044
Chitosan/HNT	3.5	77.7 ± 0.4	21.1 ± 0.4	2.850
Chitosan/HNT	7	82.0 ± 0.2	5.4 ± 0.1	1.108

The kinetic and thermodynamic stability of the systems considered is influenced by the particle size, their charge, the viscosity of the medium (η_r) and the interactions of the components.

It is possible to hypothesize an interaction mechanism based on electrostatic interactions (Scheme 2.1). Chitosan, with its positive charges, could prefer to interact with negative external nanotube surface; pectin, instead, could interact with the inner nanotube surface. Both polymers, however, stabilize HNT particles in water according to the electrostatic mechanism.



Scheme 2.1 Mechanisms of polymers/ HNT interaction based on electrostatic interaction. (Adapted with permission from ref. 182).

2.1.2 Electrostatic interaction

The ζ -potential trends for chitosan- and pectin-based mixtures show that an electrostatic mechanism of nanotube stabilization exists.

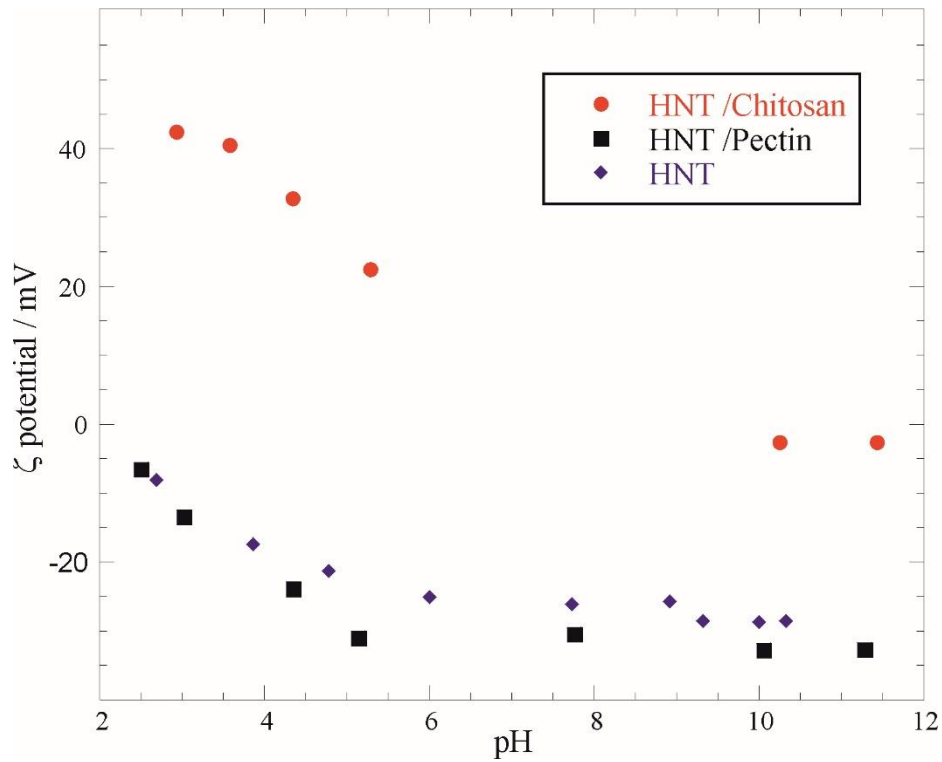


Figure 2.2. ζ -Potential values as a function of pH for HNT/chitosan and HNT/pectin citrus dispersions. Both systems had an HNT/polymer ratio of 10:1. (Adapted with permission from ref.182).

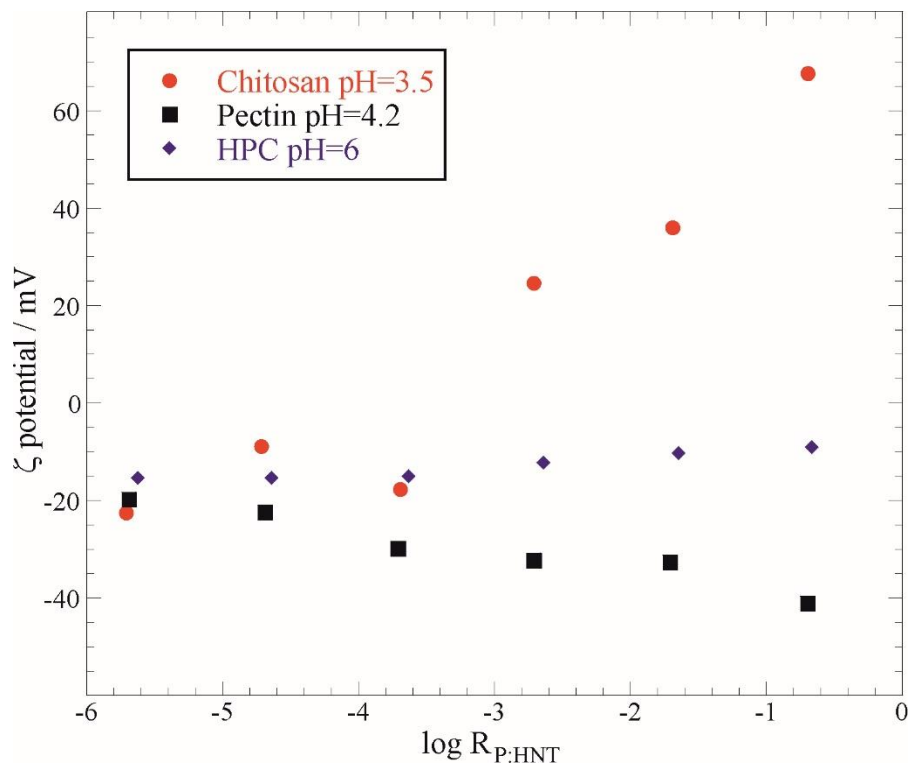


Figure 2.3 ζ -Potential values as a function of RP:HNT for HNT/polymer dispersions. (Adapted with permission from ref.182).

ζ -potential values are influenced both by the pH of dispersions (Fig. 2.2) and by components concentration (Fig. 2.3). The pH of dispersions influences the protonation equilibria of polymers and consequently determines changes in ζ -potential trends. Chitosan stabilizes HNTs in water under acidic pH, exactly the opposite for pectin. In particular the first should adsorb on the HNTs outer surface, resulting in a more positive overall charge. Pectin, instead, should adsorb within the HNT lumen, that is positively charged, resulting in a more negative overall nanotubes charges. ζ -potential is constant for the non-ionic HPC, but this is the biopolymer that better stabilizes HNTs in water such as evidenced by turbidimetric studies.

2.1.3 Thermodynamic properties by ITC

Isothermal titration calorimetry is the technique used to investigate the trend of the heats of titration ΔH_i as a function of polymer/ HNT mass ratio ($R_{P:HNT}$). The sigmoidal profile obtained for each system (Fig. 2.4) is analyzed based on a simple Langmuir-type adsorption model (see scheme 2.2).

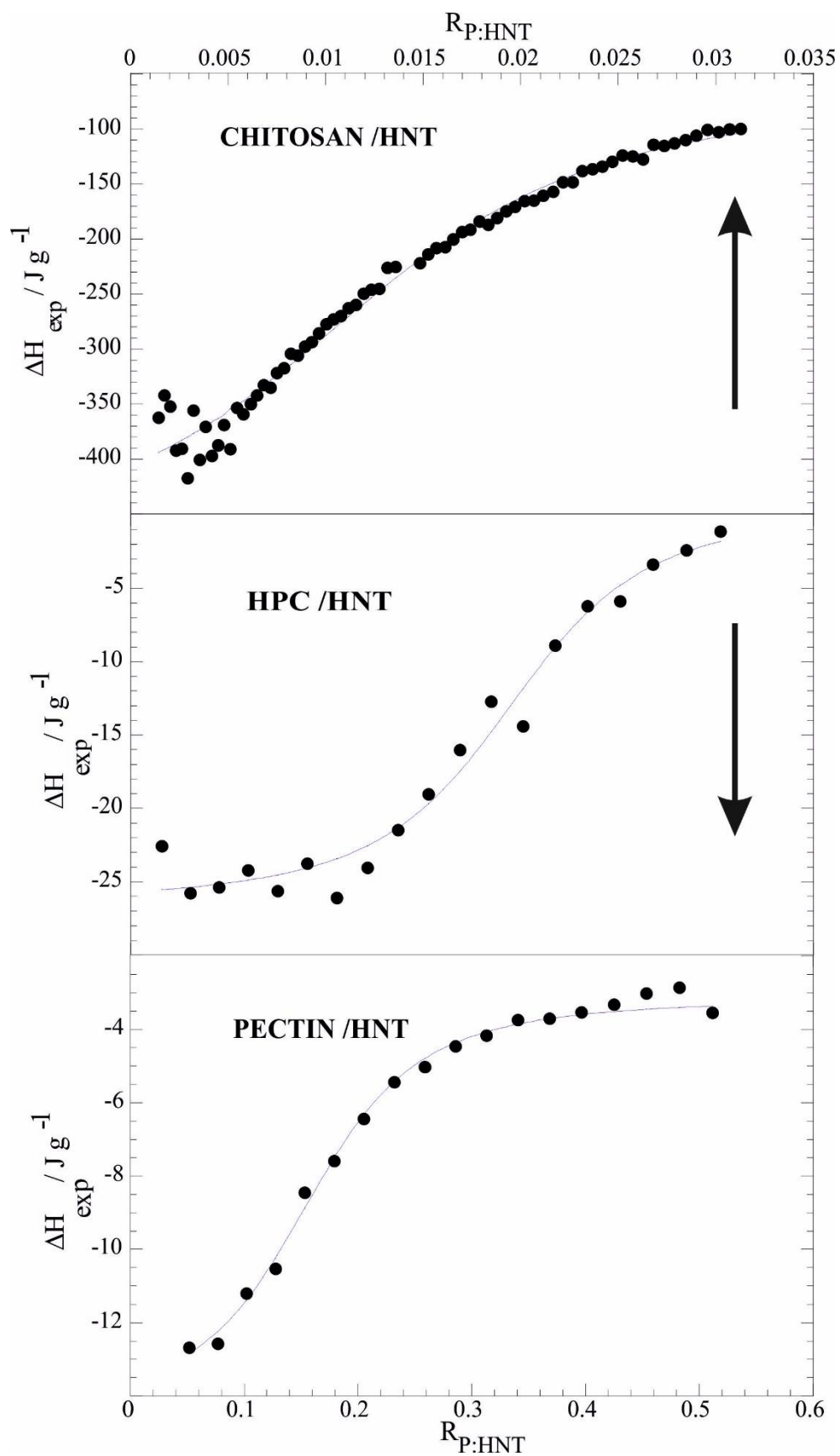
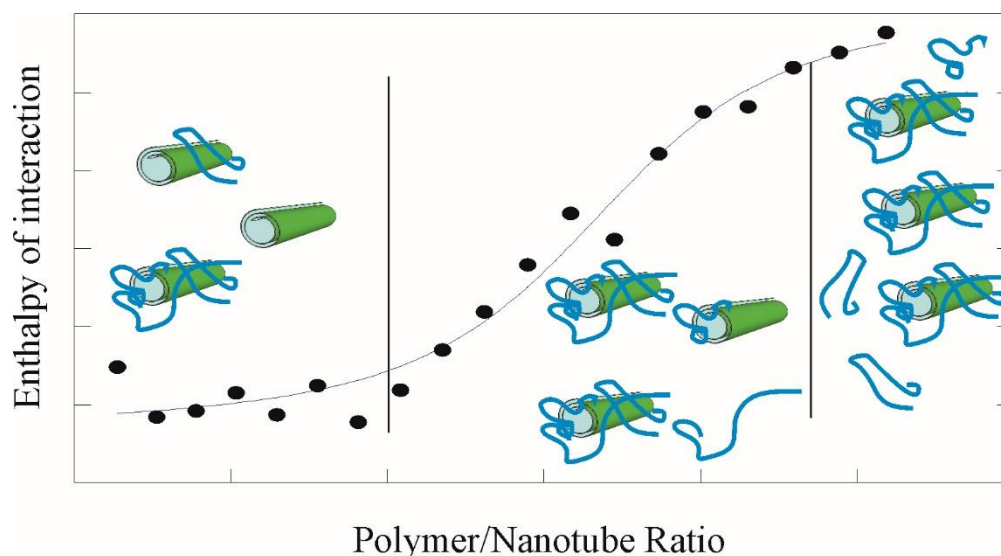


Figure 2.4. ITC data for HNT titration with chitosan, pectin and HPC. (Adapted with permission from ref.182).



Scheme 2.2. Schematic representation of interactions between the components based on a model of adsorption of the polymer on the nanoparticle. (Adapted with permission from ref. 182).

The fitting of the experimental data provides the equilibrium constant (K_{ads}), the maximum weight (in grams) of polymer adsorbed per surface unit of nanoparticle (Z) and the enthalpy of adsorption per mole of polymer ($\Delta H^{\circ}_{\text{ads}}$). Details on the model and fitting procedure are reported in ref ¹⁸². Thereby, standard free energy ($\Delta G^{\circ}_{\text{ads}}$) and entropy ($\Delta S^{\circ}_{\text{ads}}$) for the adsorption process are calculated as

$$\Delta G^{\circ}_{\text{ads}} = -RT \ln K_{\text{ads}} \qquad T\Delta S^{\circ}_{\text{ads}} = \Delta H^{\circ}_{\text{ads}} - \Delta G^{\circ}_{\text{ads}} \qquad (\text{eq.2.2})$$

The obtained parameters are reported in table 2.2.

Table 2.2. Adsorption Parameters from ITC Measurements for Polymer-HNT Dispersions

	$K_{\text{ads}} / \text{dm}^3 \text{g}^{-1}$	$Z / \text{g m}^{-2}$	$\Delta H^{\circ}_{\text{ads}} / 10^3 \text{kJ mol}^{-1}$	$\Delta G^{\circ}_{\text{ads}} / \text{kJ mol}^{-1}$	$\Delta S^{\circ}_{\text{ads}} / \text{kJ mol}^{-1} \text{K}^{-1}$
Chitosan	10.2±1.5	2.6×10 ⁻⁴	-47.0±1.6	-19.8±0.4	-157.8±0.1
Pectin	12±2	2.5×10 ⁻⁴	-0.73±0.03	-20.2±0.4	-2.40±0.02
HPC	393±92	5.15×10 ⁻³	-2.17±0.07	-28.9±0.6	-7.17±0.03

For all cases the $\Delta H^{\circ}_{\text{ads}}$ are negative and it means that the interactions between the components are favored and represent the driving forces for the adsorption process. $\Delta S^{\circ}_{\text{ads}}$

values are negative too for all systems. Despite the loss of counterions and hydration water from polymer and/or nanoparticle surface, the entropic contribution results in negative because of a reduction of configuration freedom of the polymer adsorbed to the nanotubes. It is possible to assert that the stability of dispersions is controlled by the interactions (electrostatic and steric) between the dispersed particles. In the case of HPC/ HNTs system, the better stabilization of nanotubes could be attributed to a steric rather than electrostatic stabilization; the repulsion is the dominant factor and the system remains stable.

3. Nanocomposite based on biopolymer and HNTs

3.1 A chemical-physical characterization of nanocomposites based on biopolymer and HNTs

Nanocomposites based on biocompatible components are prepared and characterized (attached article). The systems properties are highlighted to factors such as composition, filler geometry and polymer charge. Three polymers with different charges (alginate, methylcellulose, chitosan) are chosen and they are combined to two nanoclays with similar chemical composition but different morphology (kaolinite sheets and halloysite nanotubes). In this way, it is possible to evaluate the effect of biopolymer charge and the nanoclay morphology on materials. A chemical-physical investigation (contact angle measurements, dynamic mechanical analysis, thermogravimetry) is conducted. Studies on the activation energy of the polymer degradation process are also conducted. Friedman's method is used to calculate E_a without making any assumption on the reaction mechanism.¹⁸⁴ All polymers used are non-toxic, biocompatible and biodegradable and HNTs are widely used for the development of systems for the release of drugs, tissue engineering, decontamination and food additives.¹⁸²

Some details on the experimental result and discussion are reported below.

3.1.1 Thermogravimetric results

For each systems, it is determined the water content loss at 120 °C (MD_{120}) and the polymer degradation temperature (T_d). Table 3.1 shows the values.

Table 3.1. Degradation temperature and water content for biopolymers.^a

POLYMERS	$T_d / ^\circ\text{C}$	$MD_{120} / \text{wt}\%$
Alginate	251.1	15.3
Chitosan	304.6	11.2
Methylcellulose	360.2	3.5

^aThe error estimated by at least three independent measurements is ± 0.5 °C for T_d and ± 0.1 wt% for MD_{120} .

Interesting is the figure A that shows the degradation temperature as a function of the concentration of nanofiller, that is halloysite nanotubes or its anhydrous form, kaolinite.

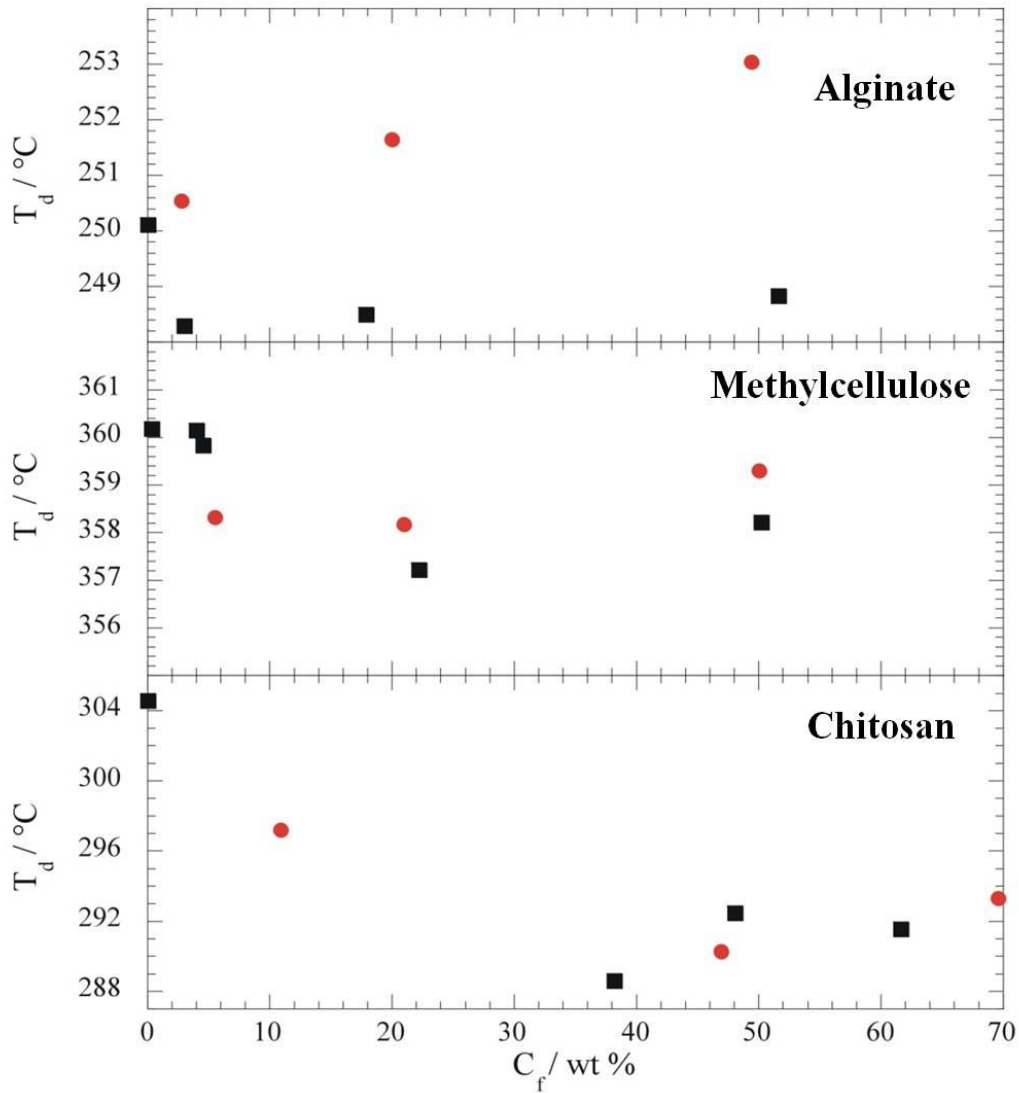
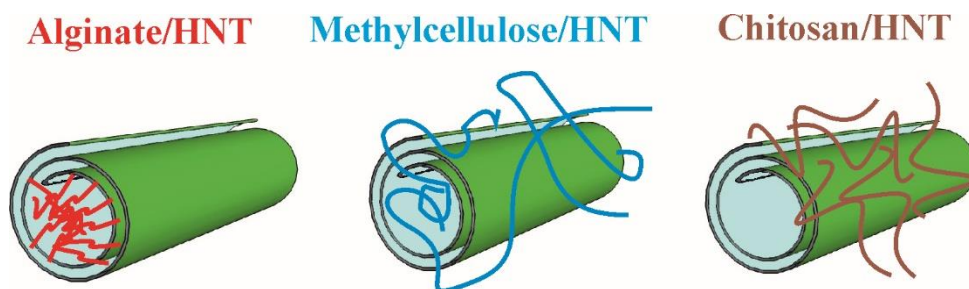


Figure 3.1. Degradation temperatures as functions of concentration of nanofiller (●, HNT; ■, kaolinite). The error estimated by standard deviation on at least three independent measurements is ± 0.5 °C for T_d . (Adapted with permission from ref.6).

T_d values show that the filler morphology affected the polymers' degradation. In fact for the alginate, it is possible to obtain a polymer stabilization with the addition of HNTs. This result is not obtained with kaolinite. For methylcellulose and chitosan, a slight destabilization is achieved with both nanofillers. This behavior is related to the interactions between the components such as shown in the previous chapter. Just to remember (scheme 3.1):

Scheme 3.1. Mechanism of polymer/ HNT interaction based on electrostatic forces. (Adapted with permission from ref. 6).



The different charge between the inner and the outer surface of nanotubes, positive and negative respectively determines that the alginate, anionic polymer, prefers to fit in the tubular cavity and consequently is thermally stabilized. The first-order derivative functions of the mass loss percentage (DTG curves) confirm this entrapment of alginate in nanotubes. In figure 3.2 DTG curves for nanocomposites based on polymer and HNTs at $C_f = 50$ wt % are shown.

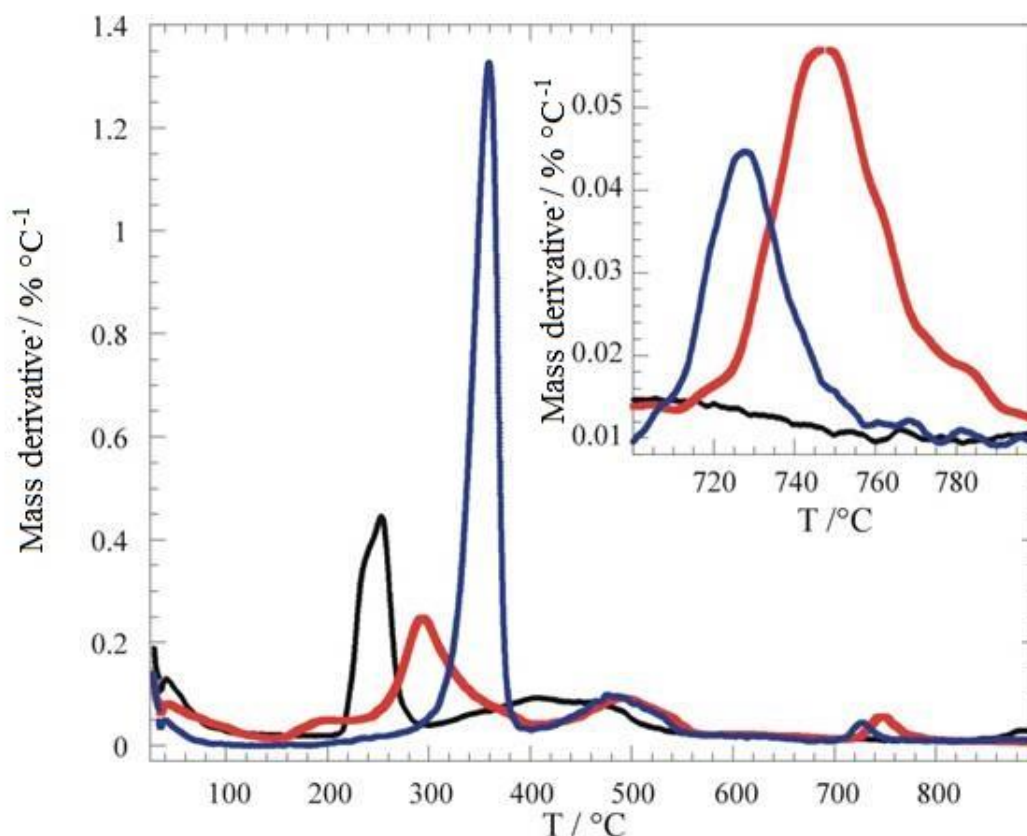


Figure 3.2. DTG curves of the polymers (— for methylcellulose, — for alginate, — for chitosan) containing 50 wt% of HNT. (Adapted with permission from ref.6).

For chitosan and methylcellulose nanocomposites it is possible to observe the typical peak of the dehydroxylation of alumina groups of the HNT lumen at a temperature between 700-800 °C. The nanocomposite based on alginate does not show this peak and this fact seems to confirm an entrapment of polymer in nanotubes with an ionic exchange involving alginate COO⁻ groups and Al-OH groups.

Another important value that adds information on the effect of filler and its morphology on polymer thermal stability is the activation energy of polymer degradation. Friedman's method is used to calculate E_a without making any assumption on the reaction mechanism.

The following equation (eq.3.1) is used:

$$\ln\left(\frac{\beta d\alpha}{dt}\right) = \ln[Af(\alpha)] - E_a/RT \quad (\text{eq.3.1})$$

where β is the heating ramp, da/dT is the first derivative of α to temperature and $f(\alpha)$ is a function of the extent of conversion (α) that depends on the degradation mechanism. In this case, the E_a values, at each α value, are obtained from the slopes of the $\ln(\beta da/dT)$ versus $1/T$ plot. Table 3.2 contains activation energy values for each system studied.

Table 3.2. Activation energy values for pristine biopolymers and nanocomposites.

Material	$E_a / \text{kJ mol}^{-1}$
Alginate	236 ± 12
alginate/ HNT	400 ± 30
alginate/ Kao	250 ± 20
Methylcellulose	191 ± 8
methylcellulose/ HNT	209 ± 3
methylcellulose/ Kao	193 ± 3
Chitosan	197 ± 25
chitosan/ HNT	212 ± 24
chitosan/ Kao	266 ± 20

The results confirm an increase of the energetic barrier to the degradation process for alginate with HNT but not with Kao. For other polymers, there is not a strong enhancement, but there is no effect with nanofiller morphology.

3.1.2 Dynamic-mechanical analysis

Elastic modulus (E) and breaking stress (σ_r) are two important parameters that characterize the mechanical properties of material. Both parameters can be determined by means of a typical stress-strain curve (Fig. 3.3).

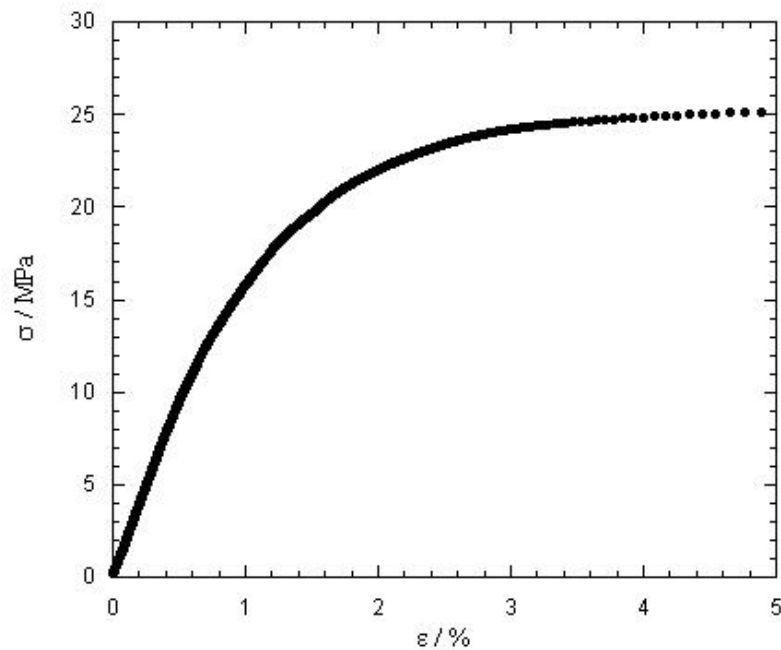


Figure 3.3. Stress as function of strain obtained under static regime for nanocomposite based on methylcellulose with 13 wt % of HNT. (Adapted with permission from ref.6).

The biopolymers show mechanical properties comparable to those of traditional plastics^{185,186} and other biopolymer^{187,188} but it is more interesting to see the effect on these parameters after the combination to HNT and Kao. Figure 3.4 shows E and σ_r values for the film of pristine biopolymer and their nanocomposites.

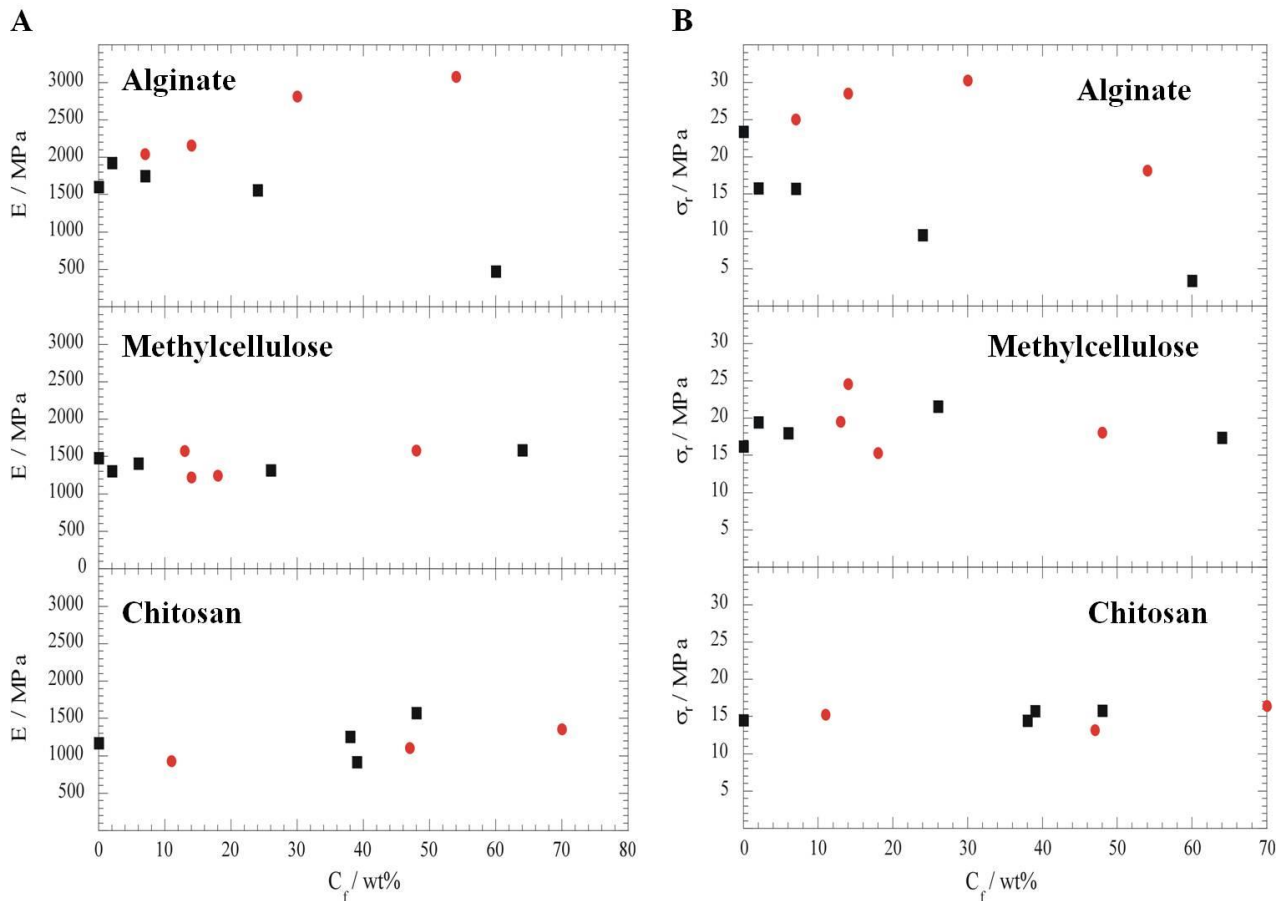


Figure 3.4. (A) Young's modulus of the polymer films as a function of the nanofiller amount (●, HNT; ■, kaolinite). (B) Tensile strength of the polymer films as a function of the nanofiller amount (●, HNT; ■, kaolinite). (Adapted with permission from ref.6).

Methylcellulose and chitosan do not show an important change in mechanical properties after the addition of nanofiller. Different is the result of alginate. The presence of HNT into alginate film causes an increase in elastic modulus even at high concentration and in tensile strength for $C_f < 30$ wt %. The presence of kaolinite has an opposite effect; it determines a decrease of tensile strength. This result confirms that the electrostatic interactions and morphology influence the mechanical properties of nanocomposites too.

Dynamic mechanical analysis is conducted in the oscillatory regime as a function of temperature. In this way, it is possible to determine the glass transition temperature of polymers or some structural change and to observe the variation of curves due to the addition of nanofiller. Figure 3.5 shows the curves of $\tan \phi$ recorded for each system analyzed.

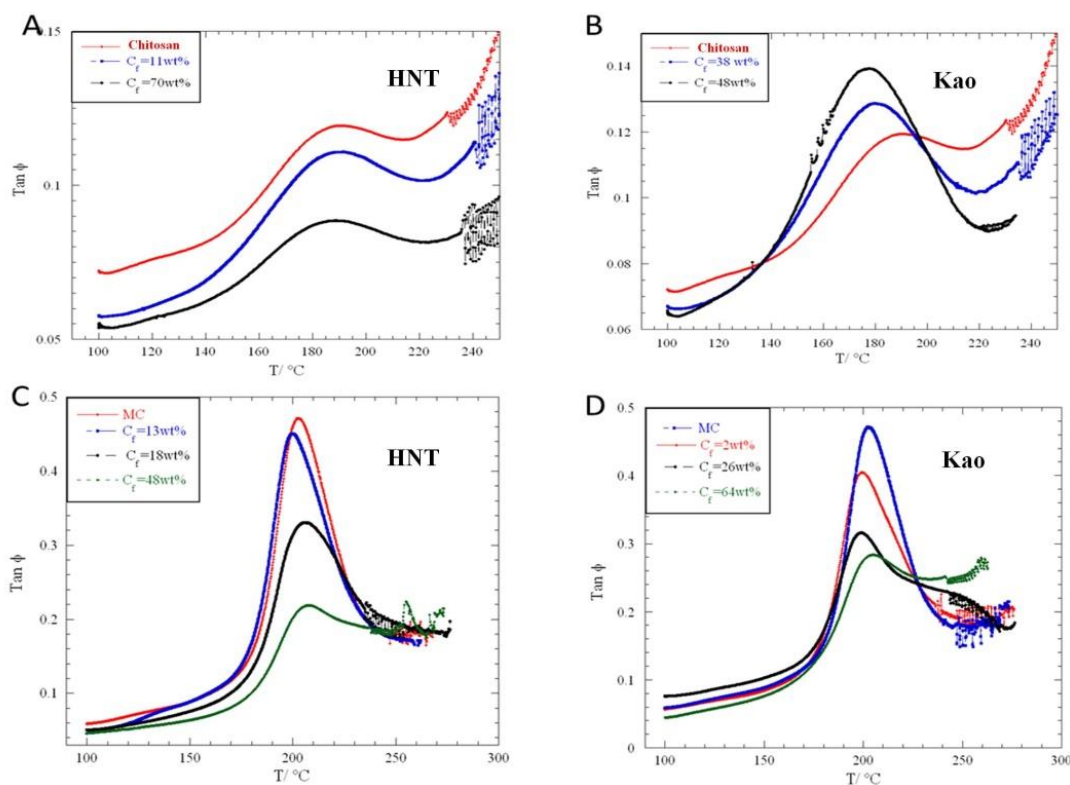


Figure 3.5. Tan ϕ as a function of temperature for chitosan and methylcellulose and respectively their nanocomposites. (Adapted with permission from ref.6).

There are not the curves of alginate and their nanocomposites because alginate does not show structural changes and phase transitions up to the degradation of the polymer matrix. For nanocomposite based on chitosan, the addition of HNT determines a weak decrease in T_g value but an evident reduction of peak intensity due to a higher capacity of the pure polymer to dissipate energy as the viscous response at elevated temperature.¹⁸⁹ The addition of kaolinite involves a decrease in T_g but an increase in the peak intensity; this fact seems to confirm a different interaction of chitosan with the two nanofiller related to its surface charge and its preference to interact to the external surface of nanotubes. For nanocomposite based on methylcellulose, the addition of HNTs and kaolinite does not influence the T_g value, but there is in both cases a reduction in peak intensity, confirming a nonspecific interaction between the neutral polymer and the surfaces of the nanotube.

3.1.3 Wettability and morphology

Table 3.3 shows the contact angle (Θ_i) at deposition ($\tau = 0$) for pristine biopolymer and bionanocomposites.

Table 3.3. Contact angle values at water drop deposition on films of pristine polymer and their nanocomposites.

C_f / wt%	Filler	θ_i / °
Alginate		
0	-	67
54	HNT	61
60	Kao	61
Methylcellulose		
0	-	54
48	HNT	61
64	Kao	66
Chitosan		
0	-	90
47	HNT	65
39	Kao	74

^aThe estimated error of at least three independent measurements is $\pm 1^\circ$.

The values are extrapolated by fitting on kinetic data (eq.3.2):

$$\theta = \theta_i \exp(k_\theta \tau^n) \quad (\text{eq.3.2})$$

where θ_i is the zero-time contact angle (τ), k_θ represents the constant for the decay speed of the exponential function that appears in the equation while n can take values between 0 and 1, that represents pure adsorption and pure spreading, respectively.

Chitosan shows the highest value of hydrophobia, but the presence of nanofiller, in particular HNTs, determines an important decrease in θ_i . A slight decrease is obtained for nanocomposite based on alginate compared to the value of pure polymer. Methylcellulose shows an opposite behavior, the addition of nanofiller implies an increase in hydrophobia.

The morphology studies clarify the change on the wettability of the nanocomposite surface. In fact, scanning electronic microscopy (SEM) micrographs (Fig. 3.6) show a uniform distribution of HNTs on alginate and chitosan surface. Considering that HNTs have a strong hydrophilic character, the presence of nanotubes on surface justifies the greater wettability of nanocomposites. For methylcellulose/ HNTs nanocomposites it is possible to see an increment of surface toughness and consequently an increase of hydrophobic character of their surface.

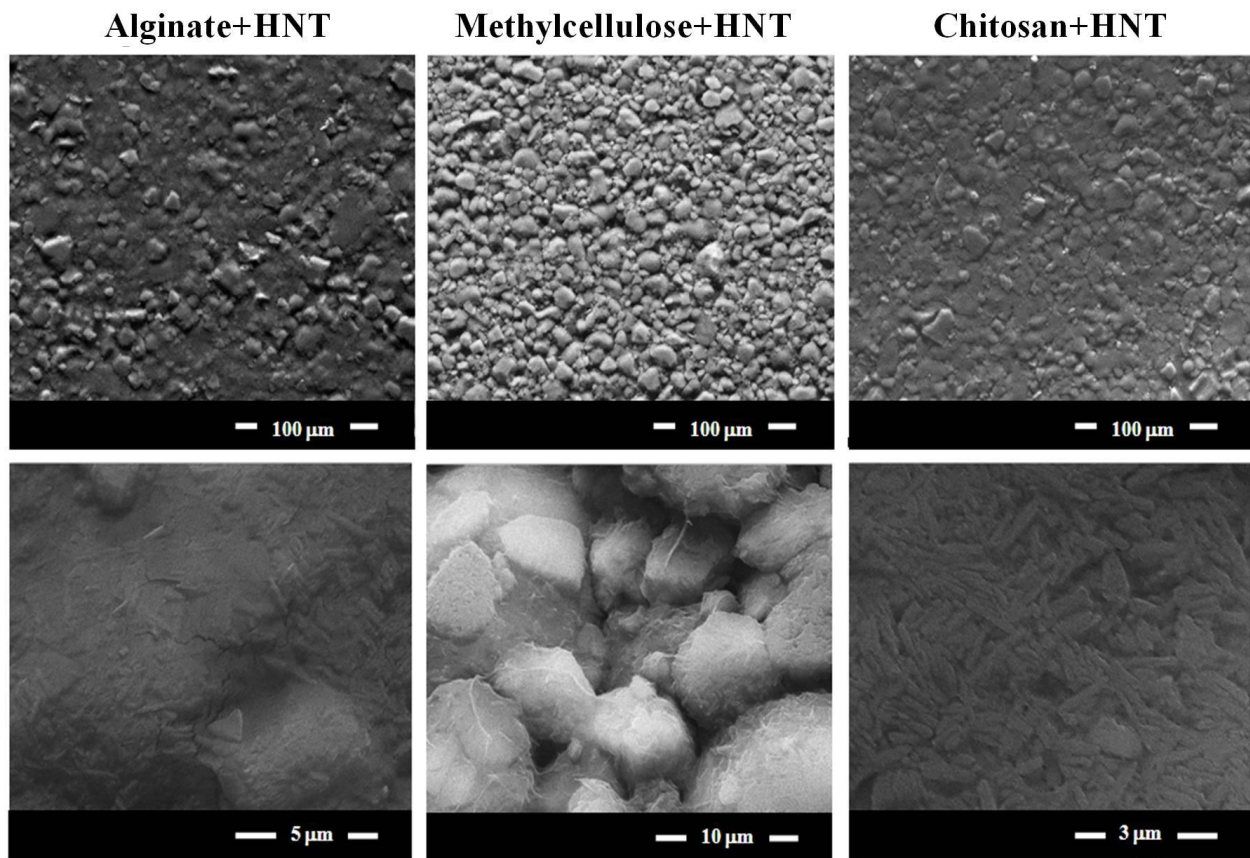


Figure 3.6. SEM images obtained on nanocomposites with 50 wt % of HNTs. (Adapted with permission from ref.6).

3.1.4 X-ray crystallography

X-ray diffraction pattern is registered for HNT and their nanocomposite based on alginate and methylcellulose (Fig.3.7). It is not measured the pattern for the chitosan/ HNT system because it is known in the literature.

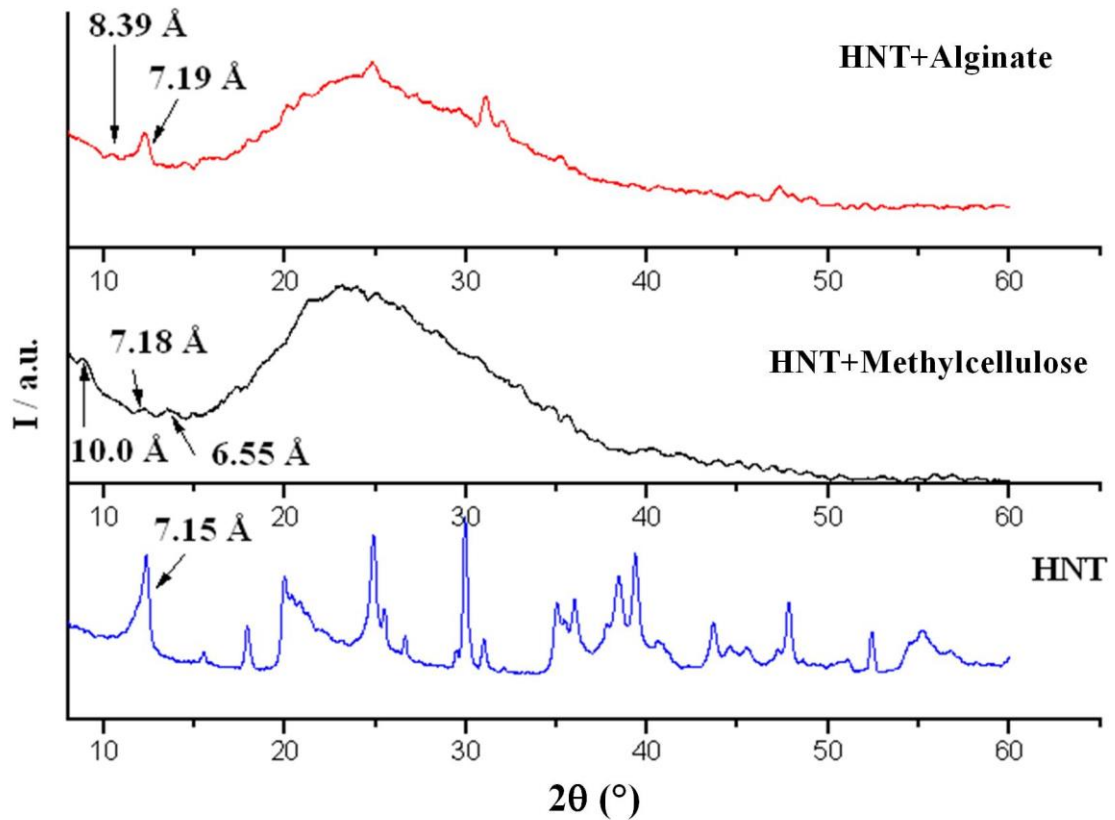


Figure 3.7. Diffractograms respectively for HNT/ alginate with $C_f = 30$ wt %, HNT/ methylcellulose with $C_f = 18$ wt %, HNT. (Adapted with permission from ref.6).

The results confirm the coexistence of two phases: HNT with intercalated polymer and HNT without polymer; the first phase is revealed by the presence of peaks at 8.39 Å and 10.0 Å for composites based on alginate and methylcellulose respectively and the second is characterized by the presence of peak at ca.7 Å, that coincides with interlayer space of nanotubes.

4. Multilayer Nanocomposites

4.1 Multilayer systems based on HPC/Chit-HNT/HPC

Multilayer composite biofilms are prepared and thermally characterized. The systems are prepared through a sequential casting method, with the alternation of hydroxypropyl cellulose (HPC) in ethanol and an aqueous chitosan/ HNT dispersion respectively. It is valued the influence of HPC/ HNTs ratio on the thermal properties of films using differential scanning calorimetry (DSC) and thermogravimetry (TG). It is interesting the comparison between the two techniques data because TG measures are conducted under inert atmosphere (N₂ flow), while DSC measures are conducted in an oxidative atmosphere (air). In this way DSC lets us know the enthalpy and the temperature for the oxidative degradation of composites, while TG lets us evaluate the effect of HNTs using kinetic studies on the pyrolytic process.

4.1.1 *Multilayer preparation and structure*

Table 4.1 shows the composition of the nanocomposites.

Table 4.1. A description of nanocomposites composition and the corresponding amounts of HPC solutions and chitosan/ HNTs dispersions used in sequential casting.

$R_{(C+H)/HPC}$	Amount of HPC solution (First layer) / g	Amount of chitosan/HNTs dispersion (Second layer) / g	Amount of HPC solution (Third layer) / g
0.92	8.18	4.96	8.02
1.89	8.15	10.24	8.07
2.81	8.05	15.03	8.00

Different composition of systems is expressed in terms of different ratio ($R_{(C+H)/HPC}$) between the weight of the middle layer (chitosan + HNTs) and the external layers (HPC). Each layer is obtained using the solvent casting method. The use of different solvent and the low solubility of chitosan in ethanol ensure the multilayer morphology of nanocomposites studied. This is confirmed by the scanning electron microscope (SEM) images (Fig. 4.1 b).

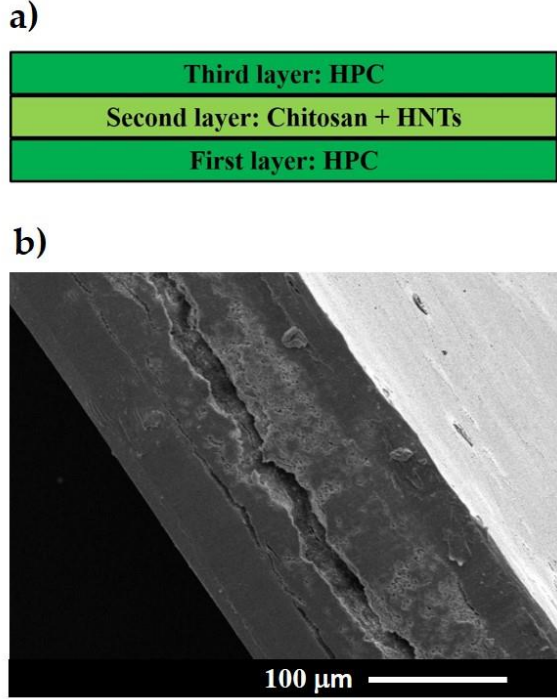


Figure 4.1. Preparation scheme of multilayer nanocomposite (a). SEM image for nanocomposite with $R_{(C+H)/HPC} = 2.81$ (b). (Adapted with permission from ref.190).

The thickness of the intermediate layer is changed while that of the outer layers is kept constant. The thickness of the HPC (outer layer) is calculated by the eq. 4.1

$$h_{(HPC)} = m_{HPC}/\delta_{HPC} \cdot \pi \cdot r^2 \quad (\text{eq. 4.1})$$

where m_{HPC} and δ_{HPC} are the mass and density of HPC, respectively; r is the radius of the Petri dish used to obtain the system. The thickness of chitosan and HNTs is calculated by the eq.4.2

$$h_{(C+H)}^* = h_{(C)} + h_{(H)} \quad (\text{eq. 4.2})$$

Considering the thickness of chitosan (h_C) and the thickness of HNTs (h_H) using eq. 4.1 and the densities of two components neglecting the reciprocal interactions, it is possible to calculate the values that are collected in table 4.2.

Table 4.2. Thicknesses of films, the outer HPC layers and intermediate chitosan/HNT layer for the prepared nanocomposites.

$R_{(C+H)/HPC}$	$h_{(HPC)}$ (First layer) / μm	$h_{(HPC)}$ (Third layer) / μm	h_{C+H} (middle layer) / μm	Nanocomposite thickness / μm
0.92	71.2	69.8	2.67	144
1.89	70.9	70.3	5.52	147
2.81	70.1	69.7	8.11	149

4.1.2 Thermal behavior under an inert atmosphere

Thermogravimetric curves for three nanocomposites are compared (Fig. 4.2).

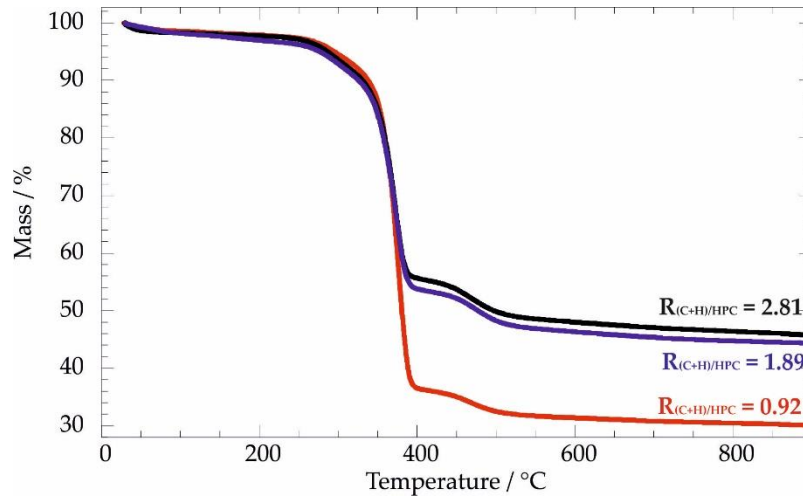


Figure 4.2. Thermograms of multilayer systems with different interlayer thickness. (Adapted with permission from ref.190).

The typical trend obtained with TGA has three characteristic loss. The first one is in the interval of 25-150 °C and indicates the humidity of composite; the second one is between 200-400 °C and is due to organic losses; the last one, in the range of 420-550 °C, is attributable to the two water molecules present in the nanotubes of interlayer. ⁶ It is interesting a comparison on thermal results obtained in the same condition (heating rate = 10 °C · min⁻¹) between nanocomposites (table 4.3).

Table 4.3. Mass losses and residual masses at 900 °C for pure HPC and nanocomposites determined by TG measurements at $\beta = 10 \text{ °C min}^{-1}$.

R(C+H)/HPC	ML ₁₅₀ / %	ML ₄₀₀ / %	ML ₆₀₀ / %	MR ₉₀₀ / %	T _{CHIT} / °C	T _{HPC} / °C
0	0.65	92.4	//	4.07	289.2	369.7
0.92	1.74	61.3	4.28	30.1	290.2	376.4
1.89	1.83	43.2	6.33	44.8	291.6	373.4
2.81	2.31	42.1	6.49	45.8	286.5	374.5

The analysis of differential thermogravimetric curves (DTG) lets us identify the steps of sample degradation.

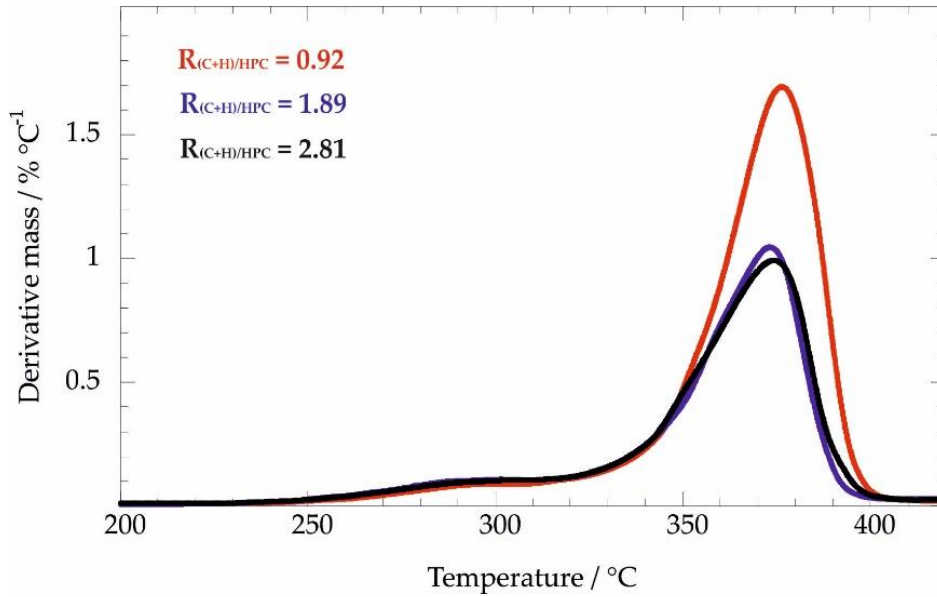


Figure 4.3. DTG of nanocomposites at different compositions. (Adapted with permission from ref.190).

In Fig. 4.3 it is possible to observe a shoulder for each system at 290 °C attributable to degradation of chitosan and a peak at 370 °C due to HPC degradation.

The presence of a multilayer structure and the combination with the chitosan/nanotubes layer cause a slight stabilization of HPC. For a deeper understanding, the kinetic process of polymer degradation is studied. Thermograms are registered at different heating rates and analyzing the data between 200-400 °C using Friedman method (eq. 4.3), it is possible to determine the activation energy (E_a) values for all nanocomposites.

$$\ln\left(\frac{\beta d\alpha}{dT}\right) = \ln[Af(\alpha)] - \frac{E_a}{RT} \quad (\text{eq. 4.3})$$

where α is the conversion degree, A is a pre-exponential factor and R is a gas constant.

Fig. 4.4 shows the E_a for each multilayer.

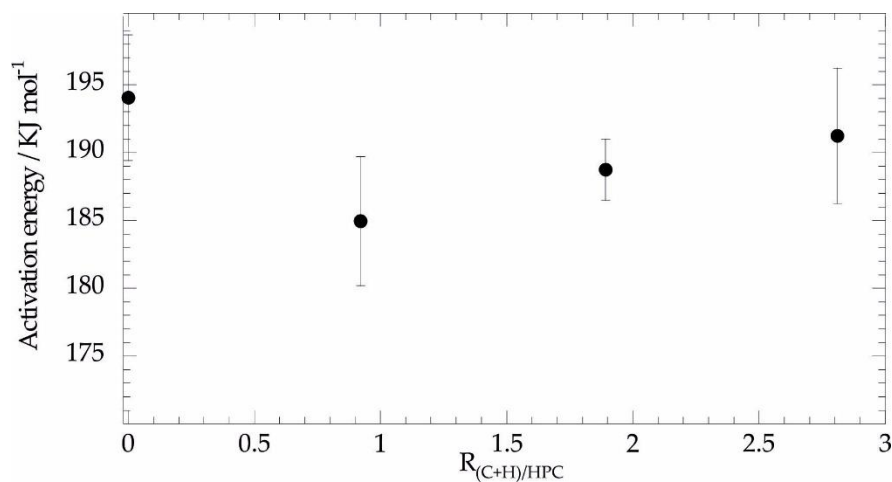


Figure 4.4. The average activation energy for the HPC degradation process as a function of the multilayer composition. (Adapted with permission from ref.190).

The results obtained clarify that the presence of chitosan/ HNT interlayer and the same multilayer structure does not affect the kinetic of the HPC degradation process.

4.1.3 Thermal behavior under oxidative atmosphere

Differential scanning calorimetry measurements are conducted on all nanocomposites. Unlike the thermogravimetric measurements carried out in a nitrogen current, here the measurements are conducted in air, therefore in oxidative conditions. Fig. 4.5 the trend of heat flow as a function of temperature for three nanocomposites with different $R_{(C+H)/HPC}$.

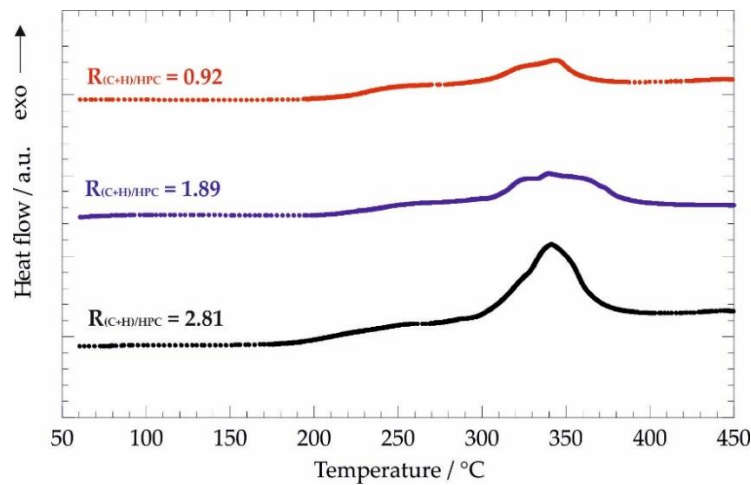


Figure 4.5. Differential scanning calorimetry curves for nanocomposites with different weight ratios between the inner and outer layers. (Adapted with permission from ref.190).

All three nanocomposites undergo an exothermic process. The analysis of recorded results lets us determine the temperature (T_{ox}) and the enthalpy variation (ΔH_{ox}), which are the maximum and the peak integration respectively. Fig. 4.6 shows the different values of T_{ox} and ΔH_{ox} obtained for systems in comparison to pure polymer too.

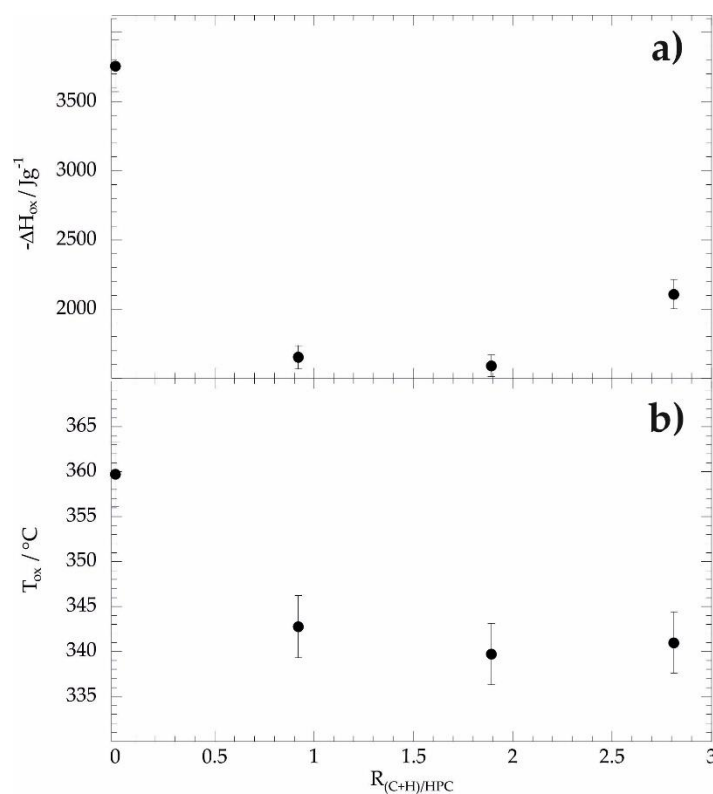


Figure 4.6. The enthalpy variation (a) and temperature (b) of the oxidative process as functions of different composition of nanocomposites. (Adapted with permission from ref.190).

As expected the presence of interlayer determines a fire retardant action on multilayer systems.

4.2 Multilayer nanocomposites with halloysite nanotubes between two chitosan layers

A sequential casting of chitosan and halloysite nanotubes is conducted to have a stratification of HNTs between two layers of chitosan. Multilayer composite biofilms are obtained such as confirmed by water contact angle measures, in fact despite the hydrophilic character of nanotubes, the surface of composites has a strong hydrophobic character. Thermal properties are analyzed under inert and oxidative atmospheres and the results are correlated to the sandwich-like morphology of hybrid materials. The kinetic of chitosan degradation is investigated using Friedman's method, which is a non-isothermal thermogravimetric approach. Also, in this case, the formation of a well-compacted middle layer of HNTs affects the activation energy value of polymer degradation. Finally,

differential scanning calorimetry shows the effect on the ignition temperature of chitosan by the presence of HNTs.

4.2.1 Preparation of chitosan/ HNTs nanocomposites with three-layered structure

Different methods can be conducted to prepare multilayer assemblies through several deposition procedures that include spin-coating, co-extrusion, spray-coating and solvent-casting.¹⁹¹ In this study chitosan/ HNTs composite are prepared by using a novel method that consists of a water casting procedure, in which the sequential deposition is controlled by the pH conditions.

In the specific, an aqueous chitosan solution is prepared. The pH is fixed at 3.5 by adding dropwise of glacial acetic acid. The solvent casting method let us obtain a chitosan film dried when its weight is constant over time. A second dispersion composed by halloysite nanotubes in water is deposited and after the evaporation of solvent, it is possible to see a well compacted HNTs layer. The strength for the success of the stratification is the poor solubility of chitosan in a low acidic solution such as that of halloysite nanotubes in water (pH = 6). Finally the deposition of the third layer, aqueous chitosan solution at pH = 3.5. Fig. 4.7 gives a schematic illustration of the preparation performed.

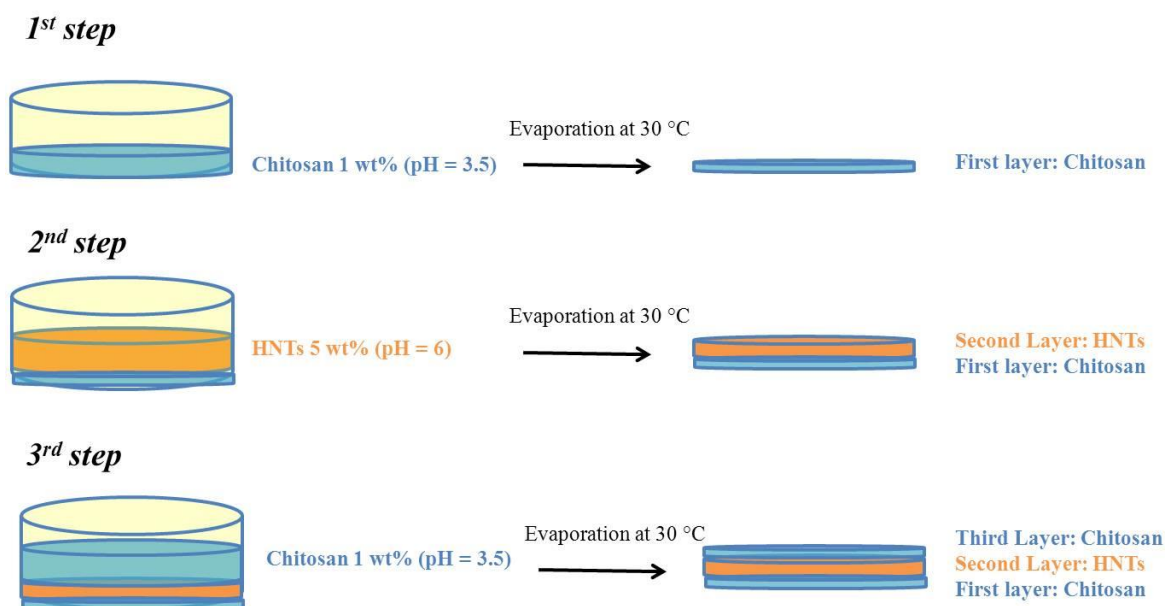


Figure 4.7 Schematic representation of the sequential deposition to obtain the assemblies of three layers. (Adapted with permission from ref.192).

4.2.2 Morphology investigated using scanning electron microscopy

Nanocomposites with different composition are prepared, in particular, it is specified the ratio ($R_{\text{HNTs:CHIT}}$) between HNTs and the total amount of chitosan (outer and inner layers). Both scanning electron microscopy (SEM) images (Fig. 4.8) and the surface wettability study confirm the presence of the HNTs layer only in the middle layer.

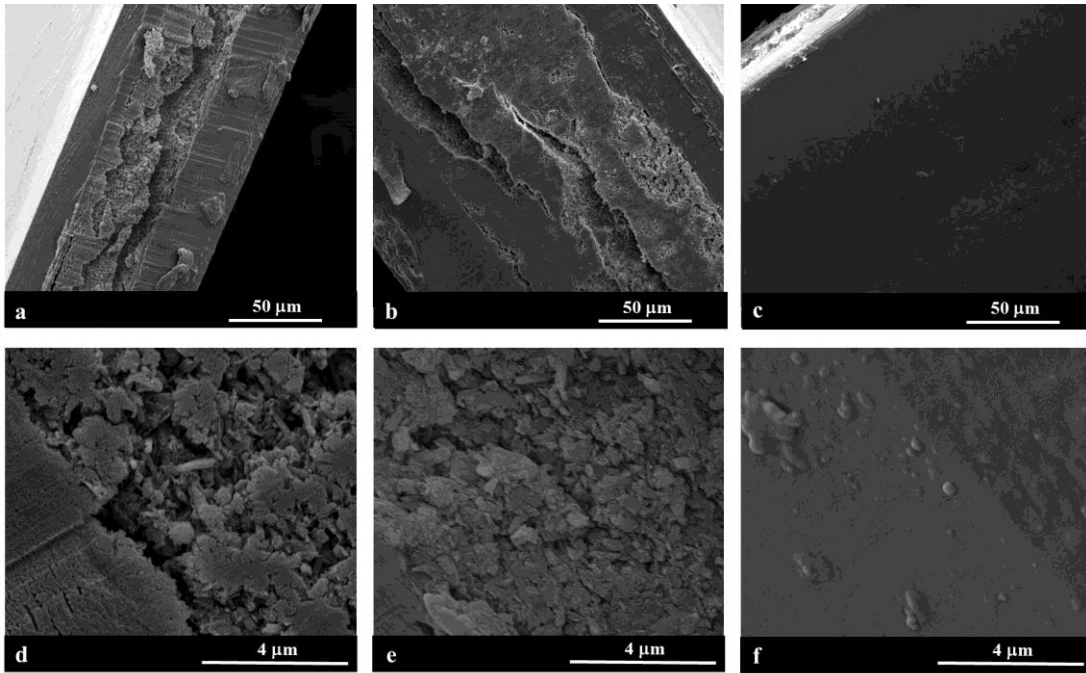


Figure 4.8. SEM images of cross-section for multilayer composite with $R_{\text{HNTs:CHIT}} = 0.62$ (a, d) and $R_{\text{HNTs:CHIT}} = 1.27$ (b, e). SEM images of surface for multilayer composite with $R_{\text{HNTs:CHIT}} = 1.27$ (c, f). (Adapted with permission from ref.192).

The images in Fig. 4.8 provided the thickness of the intermediate layer. In Fig. 4.9 it is reported a schematic representation of the structures with calculated thicknesses, in which it is shown that the volume fraction of the middle layer and the overall thickness depend on $R_{\text{HNTs:CHIT}}$.

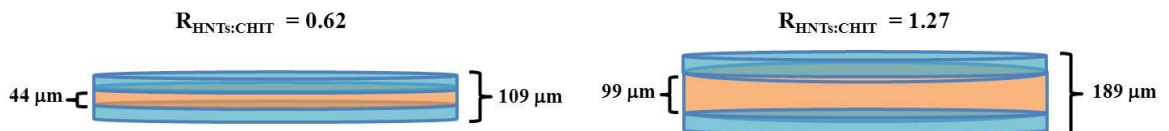


Figure 4.9 SEM images let us calculate the thickness of multilayer assemblies obtained using sequential solvent casting method. (Adapted with permission from ref.192).

4.2.3 Surface wettability analysis

Contact angle measurements are conducted. A water drop is deposited on the film surface and its behavior is monitored as a function of time. As a general result, the drop on surface forms a contact angle that is intended to decrease due to two processes: adsorption and spreading. The data fitting is done using equation 4.4:¹⁹³

$$\theta = \theta_i \exp(k_\theta \tau^n) \quad (\text{eq.4.4})$$

where θ_i is the zero-time contact angle (τ), k_θ represents the constant for the decay speed of the exponential function that appears in the equation while n can take values between 0 and 1, that represents pure adsorption and pure spreading, respectively.

The parameters are shown in table 4.4.

Table 4.4. Fitting parameters data of kinetic deposition of a water drop on the film surface. Initial contact angle (Θ_i), exponential parameter correlated to adsorption and spreading processes (n) and kinetic constant (k).

$R_{\text{HNTs:CHIT}}$	$\theta_i / ^\circ$	N	k / s^{-1}
0	86 ± 3	0.641 ± 0.004	0.0078 ± 0.0001
0.33	79 ± 3	0.63 ± 0.01	0.0046 ± 0.0001
0.48	74 ± 4	0.78 ± 0.01	0.0085 ± 0.0001
0.62	84 ± 4	0.62 ± 0.01	0.0038 ± 0.0001
0.94	78 ± 5	0.78 ± 0.01	0.0013 ± 0.0003
1.27	75 ± 4	0.80 ± 0.01	0.0032 ± 0.0001

All nanocomposites undergo both processes in fact n values are between 0 and 1, more precisely n varies from 0.64 (n value for pristine chitosan) to 0.80 (n value for composite with $R_{\text{HNTs:CHIT}}$ highest of all). k values do not have a trend correlated to the presence of HNTs layer, so it is possible to deduce that HNTs do not affect the kinetic of two processes. The most interesting result is on Θ values. All films show the strong hydrophobic character typical of the chitosan layer, so this fact confirms the good retention of nanotubes in the center of the systems and it is in agreement with morphology study using SEM images.

4.2.4 Thermal properties investigated using thermogravimetric analysis and differential scanning calorimetry

The literature reports that the mesoscopic structure of nanocomposites influences their thermal properties. A homogenous dispersion of nanofiller into polymer matrix usually determines a good thermal stabilization. There are different examples for good dispersed HNTs in polymers with an increase in degradation temperature due to a barrier effect and entrapment process towards the volatile products.^{194–196} The HNTs confined in a layer in the middle of a multilayer composite do not influence the thermal properties of nanocomposites.¹¹⁰

The activation energy (E_a) of chitosan degradation is calculated for all nanocomposites through Friedman's method, which is the same method used to analyze the kinetic data discussed in 3 and 4 chapters and that is used in different kinetic studies reported in the literature.¹⁸⁴ Fig. 4.10 collects all activation energy values calculated for the investigated systems.

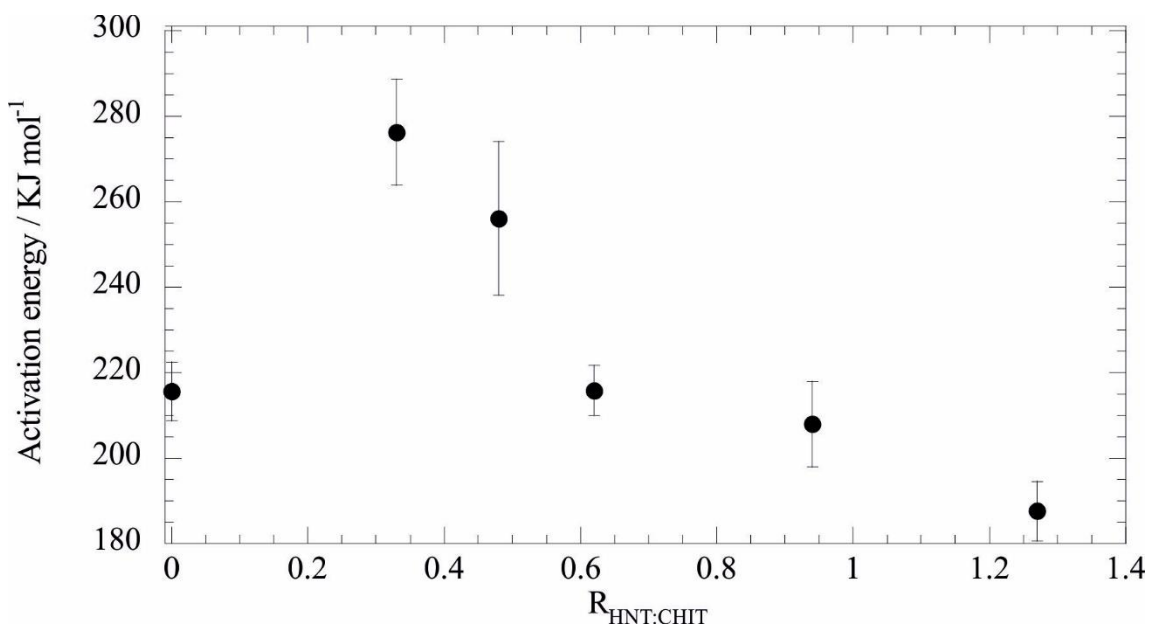


Figure 4.10. The average activation energy of chitosan degradation for nanocomposites with different compositions. (Adapted with permission from ref.192).

The filler concentration influences the kinetic of chitosan degradation in multilayer assemblies. In particular, the chitosan degradation is accelerated by a large amount of HNTs (E_a of multilayers $<$ E_a of pure chitosan). In agreement with the one mentioned above only the designed multilayer morphology could influence the kinetic of process. A

thermal destabilization for composite with the highest $R_{\text{HNT:CHIT}}$ value is consistent with the formation of a well compacted intermediate layer of HNTs between the outer layers.

The other two important parameters that characterize thermally the films are determined using differential calorimetry (DSC) and they are the enthalpy (ΔH_{ox}) and degradation temperature (T_{ox}) under oxidative atmosphere (a different condition from that of TGA). Fig. 4.11 shows ΔH_{ox} and T_{ox} for multilayer with different composition.

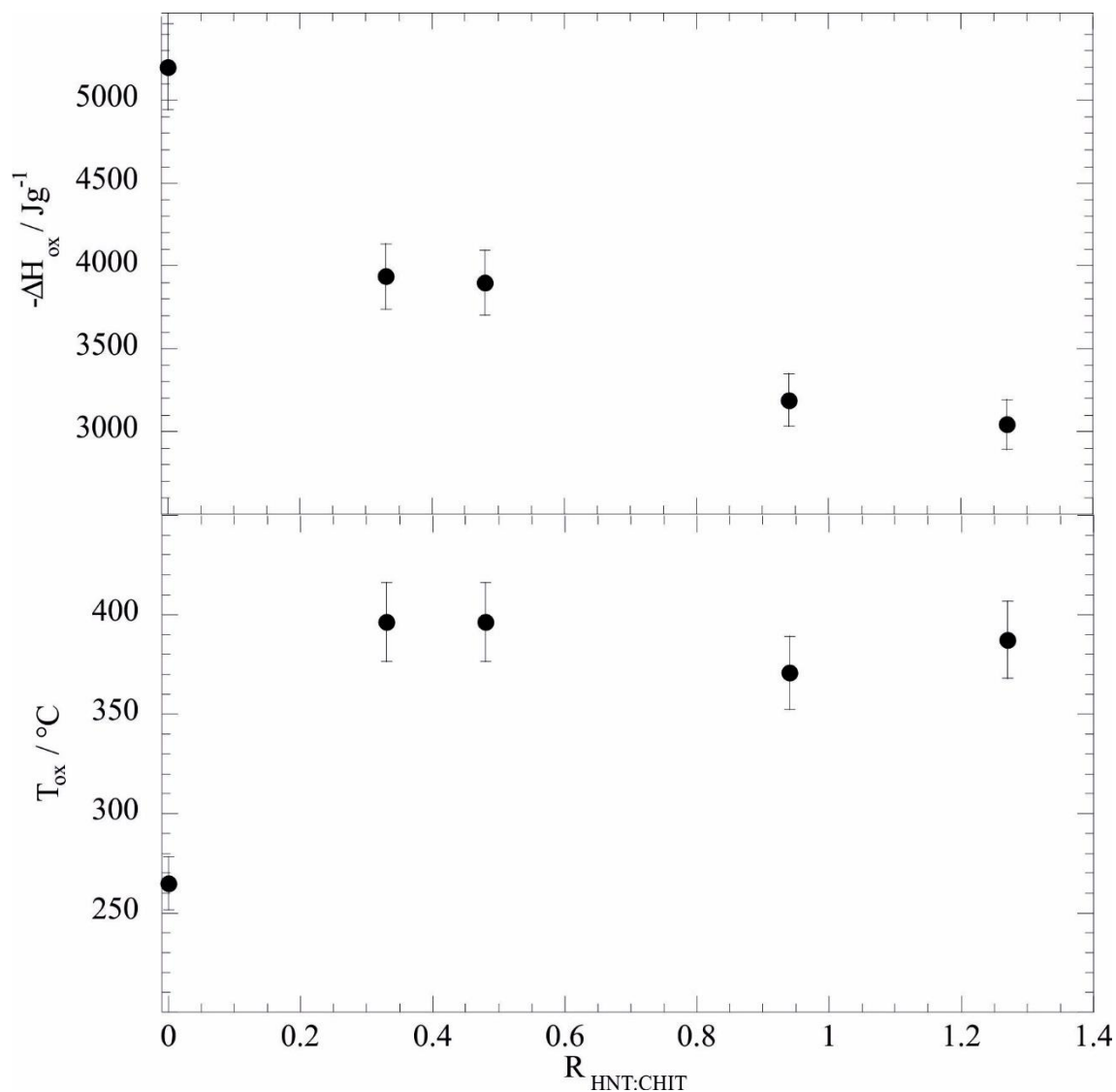


Figure 4.11. Enthalpy (up) and oxidative degradation temperature (down) as functions of the composition of the nanocomposites. (Adapted with permission from ref.192).

The degradation temperature is affected by the presence of nanotubes, showing greater resistance to the ignition process of materials than pure chitosan. Nanocomposites based on chitosan and sepiolite gave similar results.¹⁹⁷ The enthalpy values of oxidative degradation are lower for nanocomposites than pure chitosan. This is in agreement with the degradation

temperature results: HNTs induce a fire retardant action on nanocomposite especially for nanocomposites with more nanotubes.

5. Layer by layer systems such as drug delivery

5.1 LBL assembly based on electrostatic interactions

The sequential adsorption of oppositely charged polyelectrolytes onto a charged surface from dilute aqueous solutions has become a very attractive means of preparing versatile polymer films and coatings.^{198,199}

Two different layer-by-layer systems, based on adsorption biopolymers onto halloysite nanotubes (HNTs) in water using electrostatic interactions are prepared. ζ -Potential confirmed different surface charge of functionalized nanotubes upon polymer and drug adsorption step by step. Dynamic light scattering was used to evaluate the stability of functionalized nanoparticles in time. Cytotoxicity studies, confocal studies (nanotubes internalization) and inhibition of internalization routes are conducted on HeLa cells. Spectrophotometric measurements confirm a slow and controlled release of drugs by systems at two different pH, 5.5 and 7.4. Modified nanotubes by interactions with polymers lead to the formation of layer-by-layer systems with tunable stability, surface properties and the ability to incorporate drugs to be released in response to external stimuli.

5.2 Materials properties and LBL systems preparation

Cationic polymers, chitosan (CHIT) and poly (allylamine hydrochloride) (PAH) for the first layer around nanotubes, and anionic polymers, hyaluronic acid (HA) and poly(sodium 4-styrene sulfonate) sodium salt (PSS) are chosen respectively as the second layer. The same drug, doxorubicin hydrochloride (DOXO), is the third layer for each system. Finally, the second polymer of each system is used to close the layer-by-layer assembly.

Poly allylamine is a functional polymer with primary amino groups. It forms hydrogen bonds and has good solubility in water because of the amino group, but it is almost insoluble in benzene, ether, ester, acetone and other common organic solvents.²⁰⁰ There is a lot of work in literature in which this polymer is used to create LBL systems.^{201,202} It is sometimes used²⁰³ and in this work too in combination with poly(sodium 4-styrene sulfonate) sodium salt.

Hyaluronic acid (HA) is a linear polysaccharide that consists of alternating units of a repeating disaccharide, β -1,4- D -glucuronic acid- β -1,3- N -acetyl- D -glucosamine.²⁰⁴ HA is an essential component of the extracellular matrix in which its structural and biological properties mediate its activity in cellular signaling, wound repair,

morphogenesis, and matrix organization.²⁰⁵ It has been largely studied as medical materials.²⁰⁶ It is easily modified to alter the properties of materials (hydrophobicity and biological activity), which takes place.²⁰⁷ Its chemical modifications are extensively reviewed.²⁰⁸ It is known that this polymer is widely used in anticancer drug delivery since it is biocompatible, biodegradable, non-toxic, and non-immunogenic; moreover, HA receptors are overexpressed on many tumor cells.²⁰⁹

After the preparation of aqueous dispersion of halloysite nanotubes (HNTs) and aqueous dispersion of polymers, layer by layer systems are prepared following this protocol: an amount of HNTs aqueous dispersion is added to the same amount of cationic polymer dispersion; obtained dispersion is kept 2 min in sonication and then 20 min on shaker. After that, the pellet is obtained using centrifugation (6 min at 6000 rpm) and washings for 2 times with MilliQ. The second layer is created adding a share of anionic polymer dispersion on pellet and the process from sonication to centrifugation is repeated with the only difference about shaker time; in fact, with second layer, drug (third layer) and last layer the time in which the dispersion is kept on shaker is 24 h.

5.3 Size and ζ -potential experiments

These techniques are used to investigate the surface charge of systems at each addition and to clarify the presence of a new layer step by step. Another indication from these experiments is on the best preparation conditions: the measurements are conducted modifying one variable at a time between the polymer concentrations (first/ second layers) and the ionic strength of dispersion.

In tables 5.1 and 5.2, the values of peak size, parameter related to the nanoparticles' dimensions and ζ -potential values are reported for the system chosen to investigate the drug delivery on HeLa cells.

Table 5.1. Results obtained by size and ζ potential measurements.

<i>Systems</i>	<i>peak size diameter (nm)</i>	<i>ζ-potential (mV)</i>
HNTs	470.5	-12.4
HNTs-CHIT	897.8	45.3
HNTs-CHIT-HA	173.7	-38.4
HNTs-CHIT-HA-DOXO	790	-2.95
HNTs-CHIT-HA-DOXO-HA	-	-30.5

Table 5.2. Results obtained by size and ζ potential measurements.

<i>Systems</i>	<i>peak size diameter (nm)</i>	<i>ζ-potential (mV)</i>
HNTs	1371	-16.1
HNTs-PAH	611.5	43.7
HNTs-PAH-PSS	1555	-34.8
HNTs-PAH-PSS-DOXO	448.4	28.3
HNTs-PAH-PSS-DOXO-PSS	2195	-40.5

The most meaningful datum of the two tables is the ζ -potential values because the parameters about dimensions are related to a lot of conditions. It is interesting to observe that both systems show a good alternation of the sign of the surface charge for each layer so this evidence is in agreement with the presence of sufficient electrostatic interactions for the success of layer by layer systems.

5.4 Dynamic light scattering investigation

Dynamic light scattering (DLS), the measurement of scattering due to light-particle interaction as a function of time, let us detect the size of particles and its trend over time. This technique could give information on the stability of the system. The measurements are conducted for all analyzed systems in two different solvents: saline phosphate buffer (PBS) and Dulbecco's Modified Eagle Medium (DMEM). PBS is a buffer

solution commonly used in biological research. It is a water-based salt solution containing disodium hydrogen phosphate, sodium chloride and, in some formulations, potassium chloride and potassium dihydrogen phosphate. The buffer helps to maintain a constant pH. The osmolarity and ion concentrations of the solutions match those of the human body (isotonic).²¹⁰ DMEM is a widely used basal medium for supporting the growth of many different mammalian cells. Cells successfully cultured in DMEM include primary fibroblasts, neurons, glial cells, HUVECs, and smooth muscle cells, as well as cell lines such as HeLa, 293, Cos-7, and PC-12.²¹¹ Figure 5.1 shows the diameter of particles for each step in the layer by layer system preparation.

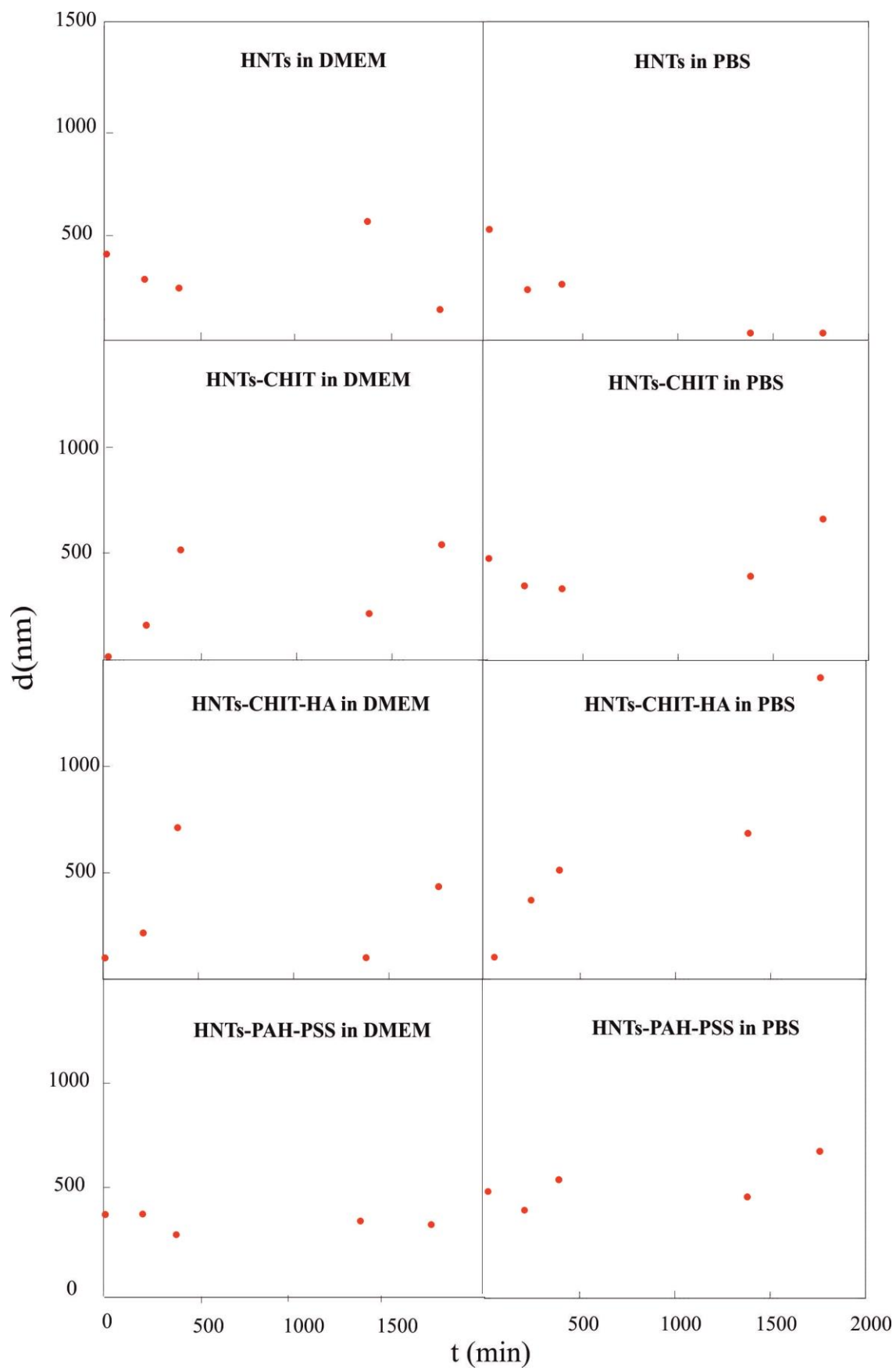


Figure 5.1. Diameter particles as a function of time determined using DLS measurements. (Adapted with permission from ref. 212 in preparation).

After 23h and 46 hours, all systems in DMEM have visible aggregates. After 3 days the systems HNTs-CHI-HA and HNTs-PAH-PSS have determined a color change of DMEM (from pink to orange). After 23h and 46 hours, all systems in PBS have visible aggregates.

5.5 CCK-8 assay to investigate the HeLa cell viability

CCK-8 is the acronym of CELL COUNTING KIT- 8 and is the most common assay in vitro nanotoxicity assessment.²¹³ This study is performed in a 96-well plate. A solution of 50000 “Hela” cells/ ml in DMEM is used. 100 µl (5000 cells) are put in each well and kept in incubation for 24 h. The medium is changed (cleaned) and 100 µl of a nanoparticles (NP) solution in DMEM with the desired concentration of NPs. The measurements are conducted in triplicate for each concentration. The reference cells (blank sample) have to be incubated without NPs but with the same conditions of the experiment cells. Cells with NP systems are kept in incubation for different time (24 h, 48 h, 72 h). After the incubation, 10 µl of CCK8 are added in each well, in blank too. The plate is put in incubation for 1.30h (incubation time depending on the kind of cells used). Absorbance measurements are directly conducted on the plate.

The measurements are conducted on systems with five different concentrations of drug and consequently of halloysite nanotubes concentrations. The studied systems are indicated with an acronym (NP1, NP2, etc.), as detailed below:

NP1: HNTs in DMEM (HNTs concentrations: 0.4mg/ml, 0.2mg/ml, 0.1mg/ml, 0.05mg/ml, 0.025mg/ml);

NP2: HNTs+ CHIT;

NP3: HNTs+ CHIT+ HA;

NP4: HNTs + PAH;

NP5: HNTs + PAH+ PSS;

NP6: HNTS + CHIT+ HA + DOXO + HA (Doxo concentrations: 19microM, 9.5microM, 4.75microM, 2.375microM, 1.187microM);

NP7: HNTs+PAH+PSS+DOXO+PSS (Doxo concentrations: 19microM, 9.5microM, 4.75 microM, 2.375microM, 1.187 microM).

Figure B shows the survival rates as a function of HNTs concentration (systems without drug) and the survival rates as a function of doxo concentration (system with drug) at a different time from the system administration. It is very interesting to observe the

different survival rates for the systems with and without the drug. The systems of HNTs and that of layer by layer on HNTs (without doxo) show a considerable number of live cells even after 72 h at the largest concentrations. The presence of drug reverses situation with a lot of cells died after the first hours.

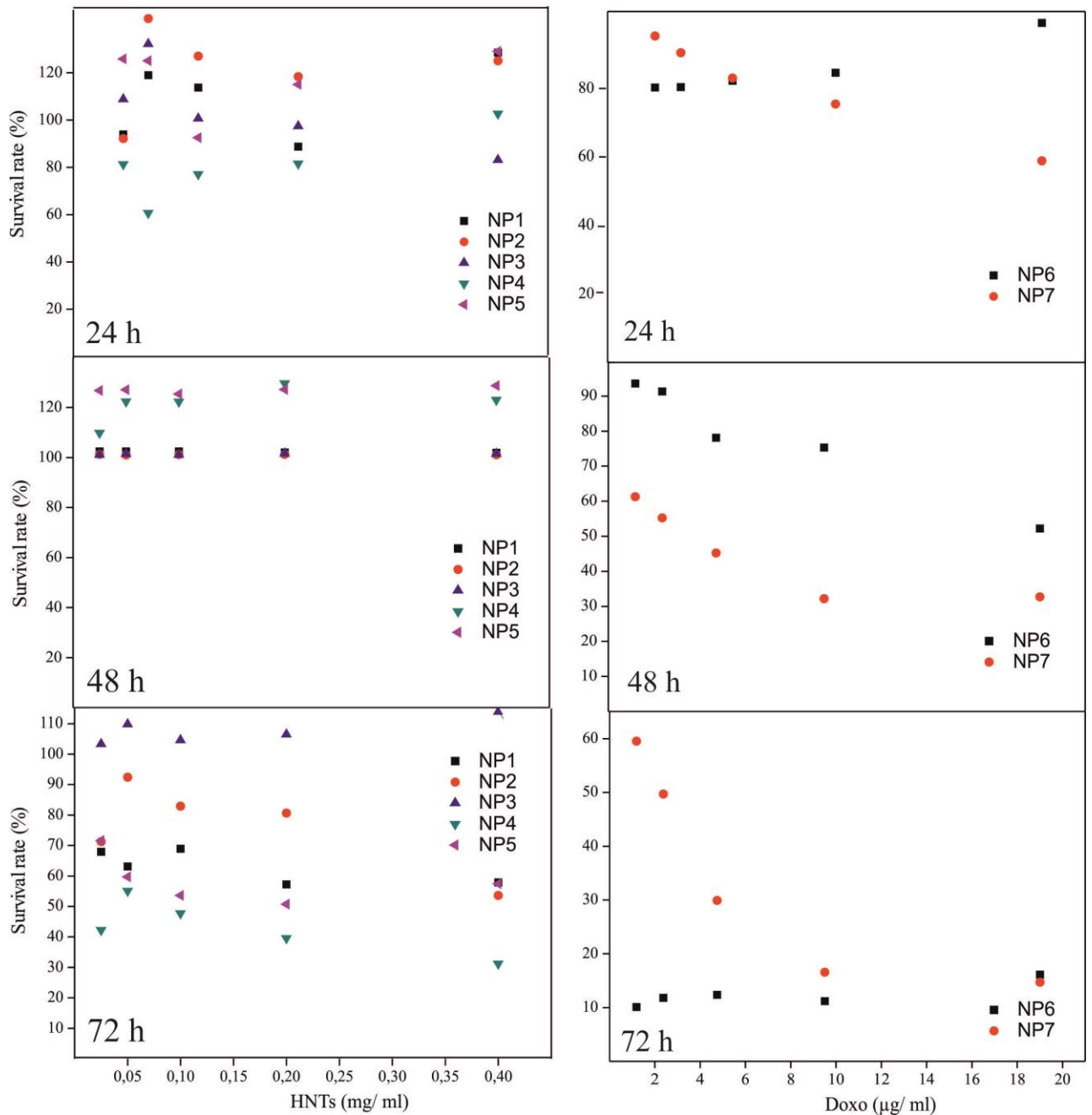


Figure 5.2. Survival rates of HeLa cells after a different contact time of analyzed systems. NP1, NP2, NP3, NP4, NP5 are systems without the drug. NP6 and NP7 are systems with doxorubicin hydrochloride. (Adapted with permission from ref. 212 in preparation).

5.6 Inhibition of internalization routes

After CCK-8 assay to investigate the HeLa cell viability, it is interesting to understand the mechanism of interaction between the drug and the cell using internalization routes. Three inhibitors solutions in DMEM are prepared: sucrose 0.4 M, chlorpromazin 30 μ M, Nystatin 80% 30 μ M. As the fourth inhibitor is used the refrigerator at 4 °C. It is prepared a DMEM solution of 50000 cells/ml (Hela). An aliquot (100 μ l corresponding to 5000 cells) is put in each well. Cells are incubated for 24 h. The medium is changed, 100 μ l of an inhibitor solution is added and it is necessary a contact time of 1 h at 37 °C. The same conditions (incubation time and temperature) are necessary for blank samples (cells with inhibitors but without NPs). After this incubation time, it is necessary to clean DMEM with inhibitors and in each well it is added a DMEM solution with NPs and inhibitor at the desired concentration of NP. Other 3 hours of incubation this time and then the medium is aspirated and cleaned with PBS. Finally, it is added new medium and the systems are incubated for 48 h. After this time, 10 μ l of CCK8 are put in each well (blank too), incubated for 1.30 h and absorbance measurements are conducted.

The experiments of internalization routes are conducted only on the systems with the drug: NP6 and NP7 at doxo concentration of 9.5 microM (C2) after 48h.

Table 5.3 shows the absorbance (Abs) values and the survival rate percentage calculated comparing the absorbance values measured for the systems and their respective references (blank). The inhibitors used are indicated such as R1, R2, R3 and R5, which indicate respectively sucrose, chlorpromazina, nystatin and nevera.

Table 5.3. The survival rate percentage calculated using the absorbance measured after the interaction of NPs system with inhibitors.

Inhibitors- inhibitors routes	Abs value	% survival rate
R1-NP7	0.705	78
R2, NP7	0.203	103
R3, NP7	0.970	86
R1, NP6	0.202	22
R2, NP6	0.198	100
R3, NP6	0.241	21
R5, NP6	0.412	44
R5, NP7	0.995	105
R1, blank	0.903	
R2, blank	0.198	
R3, blank	1.123	
R5, blank	0.943	

5.7 Drug release studies

Interesting is to follow the kinetics of drug delivery over time.

The complete layer-by-layer systems are investigated in solution at two different pH using a spectrophotometer that allow us to record the absorption spectrum from 200 to 800 nm.

Doxo has a characteristic absorption peak at 480 nm,²¹⁴ so it is possible to investigate the release over time.

Fig. 5.3 shows the absorbance values as a function of time for the system HNTs-CHI-HA-DOXO-HA and the system HNTs-PAH-PSS-DOXO-PSS at pH 5.5 and pH 7.4.

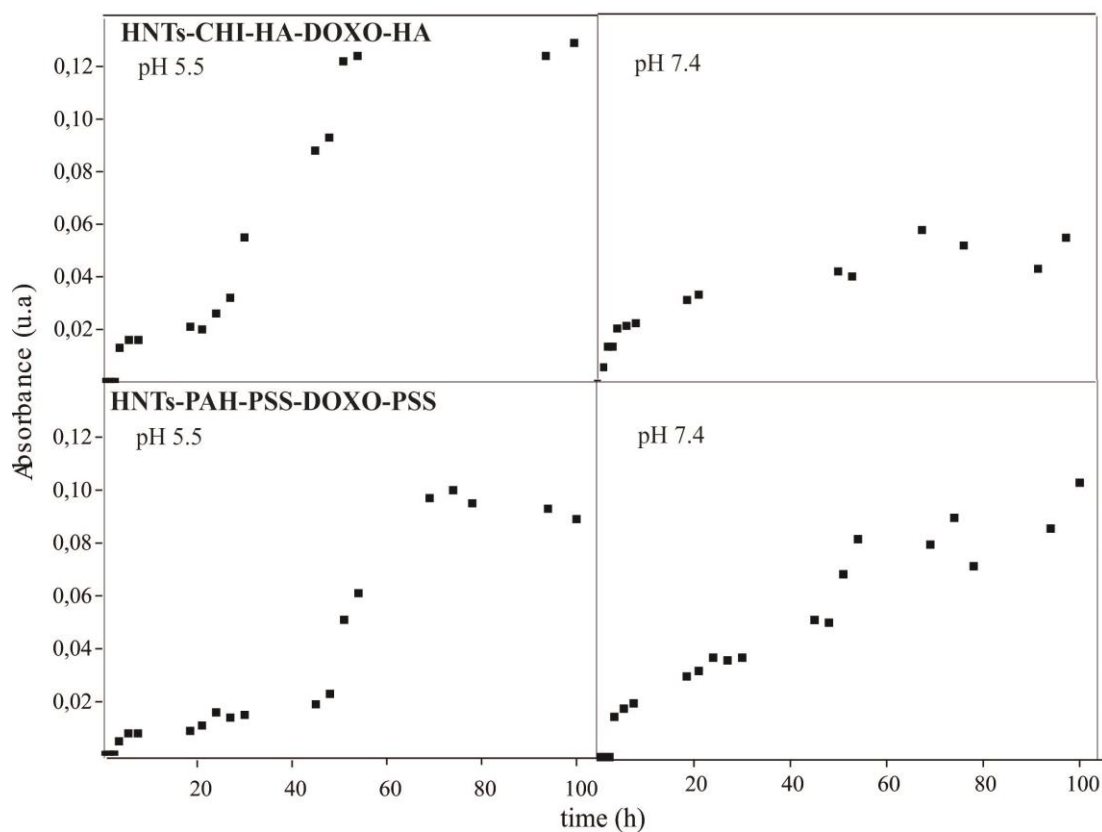


Figure 5.3. Absorbance values of doxo released by the two systems LBL with the drug. The release is monitored for 100 h and at two pH, 5.5 and 7.4. (Adapted with permission from ref. 212 in preparation).

The release is slow and lasting up to 60-100 h. The different systems have similar release curves at the same pH, in particular at pH 5.5 it is possible to note two steps of release for both systems.

Results confirm experimental evidence obtained using tests on cells.

6. Test of films cytotoxicity on HeLa cells

6.1 The biocompatibility, the cytotoxicity and the cells proliferation on films surface

Nanotechnology has promised invaluable progress in science and technology, the onus rests on the scientific community to predict the unknown outcome on the biological system for its safe proliferation. In this context the main objective of this research is focused on the real applicability of these systems as drug carriers with specific functions, avoiding that they may be themselves toxic to cells. Films cytotoxicity study with CCK-8 are conducted: films based on pristine chitosan and based on polymer combined to HNTs are compared. Surfaces are investigated using calcein AM/ propidium iodide experiments to clarify the cell proliferation on films. Finally, the nanocomposites are analyzed to clarify if toxic substances for cells are obtained from possible degradation of films in the culture medium.

6.2 Films sterilization

This sterilization is important and it is necessary at the beginning of each experiment with cells (the toxicity studies, toxicity of medium kept in contact with films, proliferation studies). Piece of films is hydrated with DMEM and is fixed to the bottom of the well. 1 ml of ethanol (70%) is placed on film pieces for 5 min. After this time, ethanol is aspirated. The same procedure, with water and not ethanol, is repeated another time. 1 ml of PBS is put and the plate is incubated for 15 min and then aspirated. The plate is put under UV light for 5 min. Finally, 1 ml of DMEM is put in each well and incubated for 30 min. After this time, it is necessary to remove DMEM.

6.3 Toxicity studies with CCK-8

The toxicity experiments are conducted on films based on chitosan and HNTs with different concentrations of filler (C_f) in different time intervals: 24, 48 and 72 hours. This study is performed in a 96-well plate. Pieces of sterilized films have been fixed to the bottom of the well at the end of the sterilization (previous step). A solution of 50000 cells/ml (Hela cells) is prepared and 100 μ l (5000 cells) are put in each well in a very fast way. The plate is incubated for 24 h and after this time, 10 μ l of CCK-8 are added in each well, in those containing blank cells too. The plate is incubated again for 1.30 h for Hela cells.

Finally DMEM of each well is moved to another empty well to do absorbance measurements and in this way it is possible to avoid the interference of the films.

It is interesting to see the different behavior after 48 and 72 hours. It could be strange to observe a survival rate percentage higher after 72 hours of incubation than after 48 hours, but it is reasonable with a cell proliferation following a minimum re-adaptation time in which some cells die.

6.4 Toxicity of DMEM kept in contact with film

The films are covered with DMEM and left in incubation for 72h. DMEM is recovered and used as a culture medium for cells. After 24h the absorbance measurement is conducted. The survival rate ranged between 60 to 75% evaluated up to 50 % of HNTs content.

This experiment is important to understand if a film degradation process is taking place and if this can release some toxic substances for the cells in solution, but if this were the case, the cell survival values would be much lower.

6.5 Calcein AM/ propidium iodide experiments

This experiment is used to test the behavior of cells after a certain time interval of incubation with the various nanocomposites. The experiment consists to prepare a solution of 50000 cells/ml (Hela cells) in DMEM. 700 μ l are put in each well immediately after the sterilization. This quantity of cells corresponds to a density of $5 \cdot 10^4$ cells/cm². The plate is incubated for 24 h. DMEM is aspirated and well are washed with 1 ml of PBS to remove each possible traces of DMEM. For confocal visualization by microscopy, it is necessary to prepare a solution of 5 ml of PBS with 10 μ l of solution A (transparent) and 15 μ l of solution B (red). It is added 1 ml of the previous solution to each well and the plate is incubated for 10 min. After that, a drop of PBS is put on the microscope “porta”. A piece of film with the cells is carefully moved over the drop. Samples are ready to be measured in a fluorescent microscope in a very fast way. Figure 6.1 shows images obtained by confocal microscopy after treatment on films with calcein AM / propidium iodide. In this way, it is possible to see in red dead cells and in green alive cells.

F1, F2, F3 and F4 indicate chitosan film with a C_f of 10% wt, 20 wt%, 40 wt% and 50 wt % respectively.

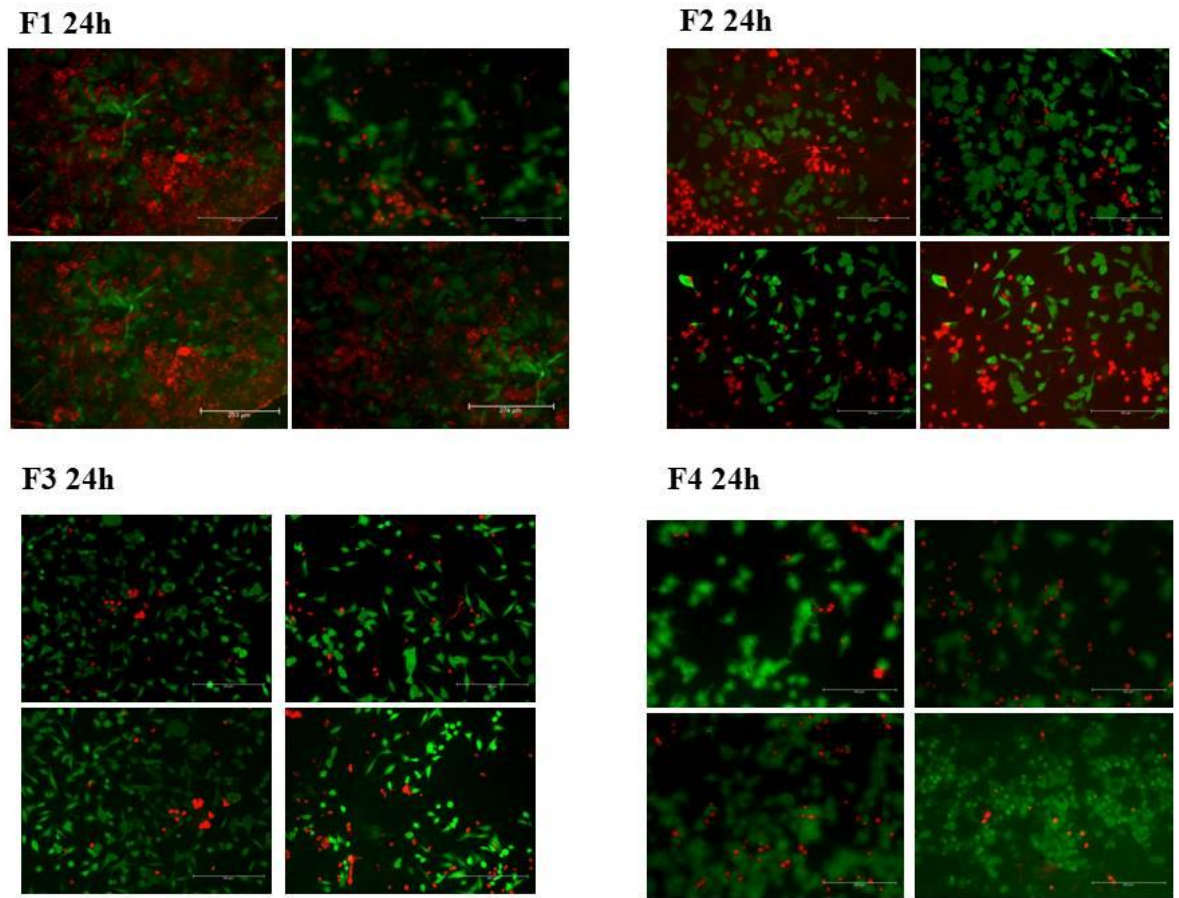


Figure 6.1. Four different images taken at different points on the same piece of nanocomposites for each sample. (Adapted with permission from ref. 215 in preparation).

After 24 h, F1 film shows a lot of dead cells, F2 shows a heterogeneous survival rate, F3 and F4 have a prominent cells proliferation.

The measurements are repeated for each sample after 48 and 72 hours. Figure 6.2 shows the results obtained.

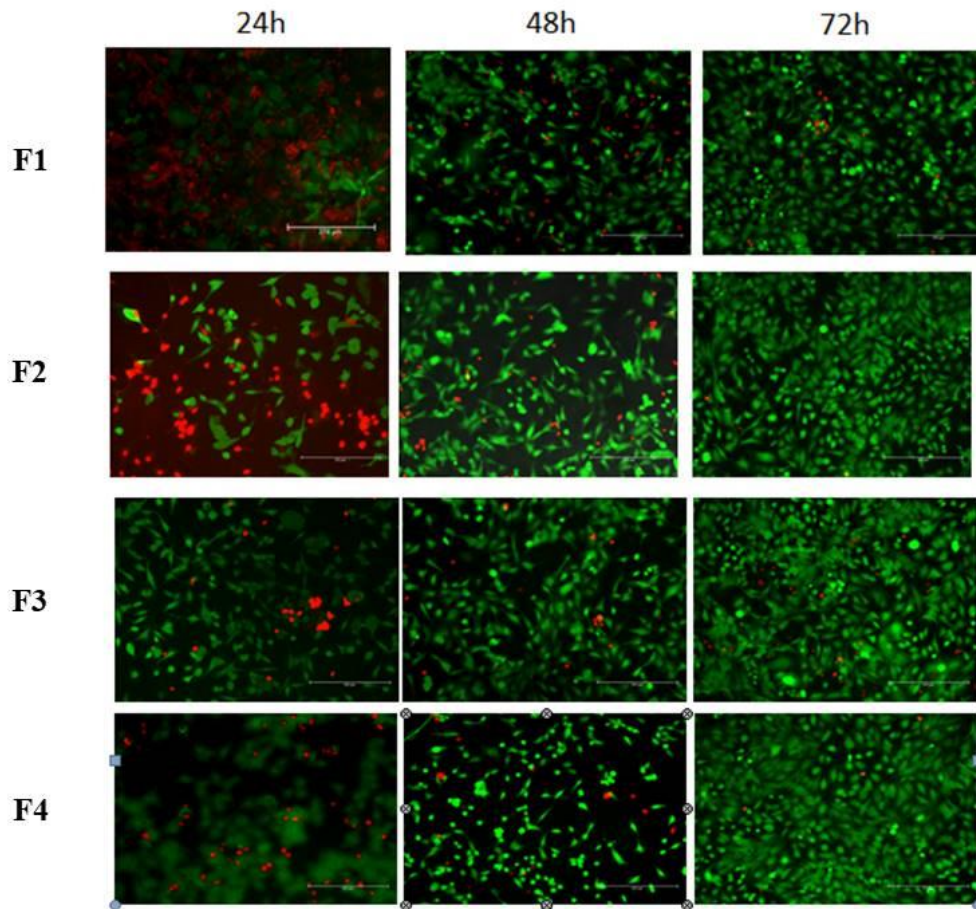


Figure 6.2. The life cells control on nanocomposites in time. (Adapted with permission from ref. 215 in preparation).

For each nanocomposite it is possible to observe a cells proliferation after 72 hours. It is possible to hyphotheseize that after an initial period of cell death due to the “new” presence of film, the cells in direct contact with the films recognize the material as good and send the growth signal to the companions, causing a consistent proliferation.

Concluding remarks

Halloysite/biopolymer systems were investigated in aqueous media and solid films. Biopolymers with different charges-anionic (pectin), neutral (hydroxypropyl cellulose) and cationic (chitosan) were considered. Studies on the adsorption onto halloysite nanotubes in aqueous media were conducted by direct thermodynamic methods. It was demonstrated that the stability of dispersed particles in solution was not correlated to a change in the water/polymer solution viscosity, but it is controlled by dispersed particle interactions (electrostatic and steric). In particular, when repulsion is the dominant factor as in the case of the HNT/ HPC system, the system remains stable and in a dispersed state. The better stability of this system could be attributed to a steric rather than electrostatic stabilization.

Biopolymer/nanoclay composite films were successfully prepared by the casting method from water and characterized. The nature of the matrix and the shape of the filler exercise a key role in the morphological and macroscopic properties of the materials. The concentration of nanoclay was systematically varied for each nanocomposite, and a compact film was always obtained. These materials resulted in competitive with many traditional plastics from the mechanical and thermal viewpoint and, therefore, they are promising for packaging applications. The obtained results confirmed a different interaction between the components based on the morphology of the nanoclay and the biopolymer charge. The polymer encapsulation into the nanotubes cavity improved tensile and thermal properties of the nanocomposites.

Multilayer composite biofilm based on halloysite nanotubes and sustainable polymers were prepared by a sequential casting method, which turned out to be an easy strategy to prepare multilayer with promising surface and thermal properties. A chemical-physical investigation (contact angle measurements, differential scanning calorimetry, thermogravimetry) was conducted to characterize the composites. Calorimetric measurements have shown that layered composites have potential flame retarding capacity compared to pure polymers. The attained knowledge represents a fundamental point to fabricate composite with a sandwich-like structure that can perspective for several technological purposes.

Modified nanotubes by interactions with polymers lead to the formation of layer-by-layer systems with tunable stability, surface properties and the ability to incorporate drugs to be released in response to external stimuli. In this context, two different layer-by-

layer systems such as drug delivery, based on adsorption biopolymers onto halloysite nanotubes (HNTs) in water using electrostatic interactions, were proposed and characterized. Cytotoxicity studies, confocal studies (nanotubes internalization) and inhibition of internalization routes were conducted on Hela cells and demonstrated the release of drugs with a high cell mortality rate already after one hour of incubation.

Finally, it was considered necessary to evaluate the cytotoxicity of the Halloysite nanocomposite films with different compositions. Typically, the nanocomposite showed cell proliferation after 72 hours. In particular, after an initial period of cell death, the cells in direct contact with the films show a consistent proliferation.

Acknowledgment

I would like to thank all the people who assisted me during the PhD period. I was lucky enough to do another "research" activity during my PhD. God has given me a beautiful child and not always a woman is very much understood in her role as mother. I do not think I have sacrificed my path to this. It was only a year longer, but richer. The serenity was given to me by the support received from all my colleagues: Lorenzo (my adventure partner and roommate), Filippo and Giuseppe (my guardian angels) but in particular to my great Prof. Giuseppe Lazzara, a person of big know-how but of great humility who knows how to make you feel like a person before a doctoral student. He sustained me and supervised my research at the University of Palermo. A special thanks go to all of them.

I thank Prof. Stefana Milioto who allowed me to work in her laboratories. I am grateful to Prof. Pablo Taboada who supervised me at the University of Santiago de Compostela and for stimulating discussions on the perspective of halloysite such as drug carriers.

I thank my colleagues for the XXXI cycle. They completed the path started together in the first part of this year. I was very excited about them. I shared with them many aspects of this journey: entrance exam, anxieties, lessons, laughter and evenings. I am grateful to them for every moment.

I thank my colleagues and friends Francesco e Lorena. They were a reference for me during my stay in Palermo.

I thank my parents. They have always believed in me, although they have not yet understood what a research doctorate is.

I thank my husband. He allowed me to continue this course of study helping me with our daughter. He supported me as never before. He indulged me in all my needs. He is my pillar.

I thank my best friends Dorotea, Giovanna e Chiara. They have always supported me not only in my research path but in every aspect of my life.

Finally, but not for importance, I thank my daughter, Giulia. She was and is my greatest strength. She is the reason for everything. I thank her for existing and for looking at me every day, every morning as a daughter in love with her mother.

References

1. Siracusa, V., Rocculi, P., Romani, S. & Rosa, M. D. Biodegradable polymers for food packaging: a review. *Trends Food Sci. Technol.* **19**, 634–643 (2008).
2. Cha, D. S. & Chinnan, M. S. Biopolymer-Based Antimicrobial Packaging: A Review. *Crit. Rev. Food Sci. Nutr.* **44**, 223–237 (2004).
3. Idumah, C. I., Hassan, A. & Ihuoma, D. E. Recently emerging trends in polymer nanocomposites packaging materials. *Polym.-Plast. Technol. Mater.* **58**, 1054–1109 (2019).
4. Sapalidis, A. A., Katsaros, F. K., Romanos, G. E., Kakizis, N. K. & Kanellopoulos, N. K. Preparation and characterization of novel poly-(vinyl alcohol)–*Zostera* flakes composites for packaging applications. *Compos. Part B Eng.* **38**, 398–404 (2007).
5. Valdés, A., Mellinas, A. C., Ramos, M., Garrigós, M. C. & Jiménez, A. Natural additives and agricultural wastes in biopolymer formulations for food packaging. *Front. Chem.* **2**, (2014).
6. Bertolino, V. *et al.* Effect of the Biopolymer Charge and the Nanoclay Morphology on Nanocomposite Materials. *Ind. Eng. Chem. Res.* **55**, 7373–7380 (2016).
7. Choi, J. S. & Park, W. H. Effect of biodegradable plasticizers on thermal and mechanical properties of poly(3-hydroxybutyrate). *Polym. Test.* **23**, 455–460 (2004).
8. Vieira, M. G. A., da Silva, M. A., dos Santos, L. O. & Beppu, M. M. Natural-based plasticizers and biopolymer films: A review. *Eur. Polym. J.* **47**, 254–263 (2011).
9. Satyanarayana, K. G., Arizaga, G. G. C. & Wypych, F. Biodegradable composites based on lignocellulosic fibers—An overview. *Prog. Polym. Sci.* **34**, 982–1021 (2009).
10. Jawaid, M. & Abdul Khalil, H. P. S. Cellulosic/synthetic fibre reinforced polymer hybrid composites: A review. *Carbohydr. Polym.* **86**, 1–18 (2011).

11. Saba, N., Tahir, P. & Jawaid, M. A Review on Potentiality of Nano Filler/Natural Fiber Filled Polymer Hybrid Composites. *Polymers* **6**, 2247–2273 (2014).
12. Shen, J., Song, Z., Qian, X., Yang, F. & Kong, F. Nanofillers for papermaking wet end applications. *Bioresources* **5**, 1328–1331 (2010).
13. Uddin, F. Clays, Nanoclays, and Montmorillonite Minerals. *Metall. Mater. Trans. A* **39**, 2804–2814 (2008).
14. Giannelis, E. P. Polymer Layered Silicate Nanocomposites. *Adv. Mater.* **8**, 29–35 (1996).
15. Hsu, S.-W., Rodarte, A. L., Som, M., Arya, G. & Tao, A. R. Colloidal Plasmonic Nanocomposites: From Fabrication to Optical Function. *Chem. Rev.* **118**, 3100–3120 (2018).
16. Tharanathan, R. N. Biodegradable films and composite coatings: past, present and future. *Trends Food Sci. Technol.* **14**, 71–78 (2003).
17. Yu, L., Wang, H., Zhang, Y., Zhang, B. & Liu, J. Recent advances in halloysite nanotube derived composites for water treatment. *Environ. Sci. Nano* **3**, 28–44 (2016).
18. Ezzatahmadi, N. *et al.* Clay-supported nanoscale zero-valent iron composite materials for the remediation of contaminated aqueous solutions: A review. *Chem. Eng. J.* **312**, 336–350 (2017).
19. Ribeiro, L. N. M. *et al.* Pectin-coated chitosan–LDH bionanocomposite beads as potential systems for colon-targeted drug delivery. *Int. J. Pharm.* **463**, 1–9 (2014).
20. Iwata, T. Biodegradable and Bio-Based Polymers: Future Prospects of Eco-Friendly Plastics. *Angew. Chem. Int. Ed.* **54**, 3210–3215 (2015).
21. Santacruz, S., Rivadeneira, C. & Castro, M. Edible films based on starch and chitosan. Effect of starch source and concentration, plasticizer, surfactant's hydrophobic tail and mechanical treatment. *Food Hydrocoll.* **49**, 89–94 (2015).

22. Niazi, M. B. K., Zijlstra, M. & Broekhuis, A. A. Influence of plasticizer with different functional groups on thermoplastic starch. *J. Appl. Polym. Sci.* **132**, n/a-n/a (2015).
23. Alizadeh Asl, S., Mousavi, M. & Labbafi, M. Synthesis and Characterization of Carboxymethyl Cellulose from Sugarcane Bagasse. *J. Food Process. Technol.* **08**, (2017).
24. Celebi, H. & Kurt, A. Effects of processing on the properties of chitosan/cellulose nanocrystal films. *Carbohydr. Polym.* **133**, 284–293 (2015).
25. Karnnet, S., Potiyaraj, P. & Pimpan, V. Preparation and properties of biodegradable stearic acid-modified gelatin films. *Polym. Degrad. Stab.* **90**, 106–110 (2005).
26. Audic, J.-L. & Chaufer, B. Influence of plasticizers and crosslinking on the properties of biodegradable films made from sodium caseinate. *Eur. Polym. J.* **41**, 1934–1942 (2005).
27. Kaewprachu, P., Osako, K. & Rawdkuen, S. Effects of plasticizers on the properties of fish myofibrillar protein film. *J. Food Sci. Technol.* **55**, 3046–3055 (2018).
28. Shit, S. C. & Shah, P. M. Edible Polymers: Challenges and Opportunities. *J. Polym.* **2014**, 1–13 (2014).
29. Tanaka, M., Iwata, K., Sanguandeeikul, R., Handa, A. & Ishizaki, S. Influence of plasticizers on the properties of edible films prepared from fish water-soluble proteins. *Fish. Sci.* **67**, 346–351 (2001).
30. Pommet, M., Redl, A., Morel, M.-H. & Guilbert, S. Study of wheat gluten plasticization with fatty acids. *Polymer* **44**, 115–122 (2003).
31. Pérez-Gago, M. B. & Krochta, J. M. Lipid Particle Size Effect on Water Vapor Permeability and Mechanical Properties of Whey Protein/Beeswax Emulsion Films. *J. Agric. Food Chem.* **49**, 996–1002 (2001).

32. Orliac, O., Rouilly, A., Silvestre, F. & Rigal, L. Effects of various plasticizers on the mechanical properties, water resistance and aging of thermo-moulded films made from sunflower proteins. *Ind. Crops Prod.* **18**, 91–100 (2003).
33. Bertan, L. C., Tanada-Palmu, P. S., Siani, A. C. & Grosso, C. R. F. Effect of fatty acids and ‘Brazilian elemi’ on composite films based on gelatin. *Food Hydrocoll.* **19**, 73–82 (2005).
34. Jeevitha, R. S. J., Bella, G. R. & Booshan, S. A. T. Preparation and Characterization of Micro Crystalline Cellulose Fiber Reinforced Chitosan based Polymer Composites. *Asian J. Res. Chem.* **8**, 453 (2015).
35. Tang, C. *et al.* Preparation and properties of chitosan nanocomposites with nanofillers of different dimensions. *Polym. Degrad. Stab.* **94**, 124–131 (2009).
36. Ravi Kumar, M. N. V. A review of chitin and chitosan applications. *React. Funct. Polym.* **46**, 1–27 (2000).
37. Hong, S. I. *et al.* Effect of shear rate on structural, mechanical, and barrier properties of chitosan/montmorillonite nanocomposite film. *J. Appl. Polym. Sci.* **119**, 2742–2749 (2011).
38. Wang, X., Chung, Y. S., Lyoo, W. S. & Min, B. G. Preparation and properties of chitosan/poly(vinyl alcohol) blend foams for copper adsorption. *Polym. Int.* **55**, 1230–1235 (2006).
39. Yi, H. *et al.* Biofabrication with Chitosan. *Biomacromolecules* **6**, 2881–2894 (2005).
40. Huang, G., Liu, Y. & Chen, L. Chitosan and its derivatives as vehicles for drug delivery. *Drug Deliv.* **24**, 108–113 (2017).
41. Tamura, H., Furuike, T., Nair, S. V. & Jayakumar, R. Biomedical applications of chitin hydrogel membranes and scaffolds. *Carbohydr. Polym.* **84**, 820–824 (2011).

42. Shalumon, K. T. *et al.* Electrospinning of carboxymethyl chitin/poly(vinyl alcohol) nanofibrous scaffolds for tissue engineering applications. *Carbohydr. Polym.* **77**, 863–869 (2009).
43. Shu, X. Z. & Zhu, K. J. A novel approach to prepare tripolyphosphate/chitosan complex beads for controlled release drug delivery. *Int. J. Pharm.* **201**, 51–58 (2000).
44. Jayakumar, R., Prabakaran, M., Sudheesh Kumar, P. T., Nair, S. V. & Tamura, H. Biomaterials based on chitin and chitosan in wound dressing applications. *Biotechnol. Adv.* **29**, 322–337 (2011).
45. Saravanan, S., Leena, R. S. & Selvamurugan, N. Chitosan based biocomposite scaffolds for bone tissue engineering. *Int. J. Biol. Macromol.* **93**, 1354–1365 (2016).
46. Agnihotri, S. A., Mallikarjuna, N. N. & Aminabhavi, T. M. Recent advances on chitosan-based micro- and nanoparticles in drug delivery. *J. Controlled Release* **100**, 5–28 (2004).
47. Kim, I.-Y. *et al.* Chitosan and its derivatives for tissue engineering applications. *Biotechnol. Adv.* **26**, 1–21 (2008).
48. Hajji, S. *et al.* Structural analysis, and antioxidant and antibacterial properties of chitosan-poly (vinyl alcohol) biodegradable films. *Environ. Sci. Pollut. Res.* **23**, 15310–15320 (2016).
49. Jessica D. Schiffman. Fibrous mats containing chitosan nanofibers.
50. Wang, S. & Jing, Y. Effects of formation and penetration properties of biodegradable montmorillonite/chitosan nanocomposite film on the barrier of package paper. *Appl. Clay Sci.* **138**, 74–80 (2017).
51. Tang, C. *et al.* Largely Improved Tensile Properties of Chitosan Film via Unique Synergistic Reinforcing Effect of Carbon Nanotube and Clay. *J. Phys. Chem. B* **112**, 3876–3881 (2008).

52. Yu, P., Bao, R.-Y., Shi, X.-J., Yang, W. & Yang, M.-B. Self-assembled high-strength hydroxyapatite/graphene oxide/chitosan composite hydrogel for bone tissue engineering. *Carbohydr. Polym.* **155**, 507–515 (2017).
53. Meng, D., Dong, L., Wen, Y. & Xie, Q. Effects of adding resorbable chitosan microspheres to calcium phosphate cements for bone regeneration. *Mater. Sci. Eng. C* **47**, 266–272 (2015).
54. Ferreira, N. N. *et al.* A novel pH-responsive hydrogel-based on calcium alginate engineered by the previous formation of polyelectrolyte complexes (PECs) intended to vaginal administration. *Drug Dev. Ind. Pharm.* **43**, 1656–1668 (2017).
55. Tønnesen, H. H. & Karlsen, J. Alginate in Drug Delivery Systems. *Drug Dev. Ind. Pharm.* **28**, 621–630 (2002).
56. George, M. & Abraham, T. E. Polyionic hydrocolloids for the intestinal delivery of protein drugs: Alginate and chitosan — a review. *J. Controlled Release* **114**, 1–14 (2006).
57. El Atouani, S. *et al.* The invasive brown seaweed *Sargassum muticum* as new resource for alginate in Morocco: Spectroscopic and rheological characterization. *Phycol. Res.* **64**, 185–193 (2016).
58. Lee, K. Y. & Mooney, D. J. Alginate: Properties and biomedical applications. *Prog. Polym. Sci.* **37**, 106–126 (2012).
59. Kassem, A. A. *et al.* Development of mucoadhesive microbeads using thiolated sodium alginate for intrapocket delivery of resveratrol. *Int. J. Pharm.* **487**, 305–313 (2015).
60. Qin, Y., Jiang, J., Zhao, L., Zhang, J. & Wang, F. Applications of Alginate as a Functional Food Ingredient. in *Biopolymers for Food Design* 409–429 (Elsevier, 2018). doi:10.1016/B978-0-12-811449-0.00013-X.

61. Nguyen, T. P., Hilal, N., Hankins, N. P. & Novak, J. T. The relationship between cation ions and polysaccharide on the floc formation of synthetic and activated sludge. *Desalination* **227**, 94–102 (2008).
62. Qin, C. *et al.* Convenient one-step approach based on stimuli-responsive sol-gel transition properties to directly build chitosan-alginate core-shell beads. *Food Hydrocoll.* **87**, 253–259 (2019).
63. Augst, A. D., Kong, H. J. & Mooney, D. J. Alginate Hydrogels as Biomaterials. *Macromol. Biosci.* **6**, 623–633 (2006).
64. Siew, C. K., Williams, P. A. & Young, N. W. G. New Insights into the Mechanism of Gelation of Alginate and Pectin: Charge Annihilation and Reversal Mechanism. *Biomacromolecules* **6**, 963–969 (2005).
65. Roger, S., Talbot, D. & Bee, A. Preparation and effect of Ca²⁺ on water solubility, particle release and swelling properties of magnetic alginate films. *J. Magn. Magn. Mater.* **305**, 221–227 (2006).
66. Tan, W.-H. & Takeuchi, S. Monodisperse Alginate Hydrogel Microbeads for Cell Encapsulation. *Adv. Mater.* **19**, 2696–2701 (2007).
67. Kuo, C. K. & Ma, P. X. Ionically crosslinked alginate hydrogels as scaffolds for tissue engineering: Part 1. Structure, gelation rate and mechanical properties. *Biomaterials* **22**, 511–521 (2001).
68. Martinsen, A., Skjåk-Braek, G. & Smidsrød, O. Alginate as immobilization material: I. Correlation between chemical and physical properties of alginate gel beads: ALGINATE AS IMMOBILIZATION MATERIAL. *Biotechnol. Bioeng.* **33**, 79–89 (1989).

69. Finotelli, P. V., Morales, M. A., Rocha-Leão, M. H., Baggio-Saitovitch, E. M. & Rossi, A. M. Magnetic studies of iron(III) nanoparticles in alginate polymer for drug delivery applications. *Mater. Sci. Eng. C* **24**, 625–629 (2004).
70. Kumar, M. & Tamilarasan, R. Kinetics and Equilibrium Studies on the Removal of Victoria Blue Using *Prosopis juliflora* -Modified Carbon/Zn/Alginate Polymer Composite Beads. *J. Chem. Eng. Data* **58**, 517–527 (2013).
71. Ai, L., Li, M. & Li, L. Adsorption of Methylene Blue from Aqueous Solution with Activated Carbon/Cobalt Ferrite/Alginate Composite Beads: Kinetics, Isotherms, and Thermodynamics. *J. Chem. Eng. Data* **56**, 3475–3483 (2011).
72. Cavallaro, G., Gianguzza, A., Lazzara, G., Milioto, S. & Piazzese, D. Alginate gel beads filled with halloysite nanotubes. *Appl. Clay Sci.* **72**, 132–137 (2013).
73. Leung, K. C. M., Chow, T. W., Woo, C. W. & Clark, R. K. F. Tensile, shear and cleavage bond strengths of alginate adhesive. *J. Dent.* **26**, 617–622 (1998).
74. Tal, Y., van Rijn, J. & Nussinovitch, A. Improvement of Structural and Mechanical Properties of Denitrifying Alginate Beads by Freeze-Drying. *Biotechnol. Prog.* **13**, 788–793 (1997).
75. Rhim, J.-W. Physical and mechanical properties of water resistant sodium alginate films. *LWT - Food Sci. Technol.* **37**, 323–330 (2004).
76. Benavides, S., Villalobos-Carvajal, R. & Reyes, J. E. Physical, mechanical and antibacterial properties of alginate film: Effect of the crosslinking degree and oregano essential oil concentration. *J. Food Eng.* **110**, 232–239 (2012).
77. Sousa, M. *et al.* Dynamical Characterization of a Cellulose Acetate Polysaccharide. *J. Phys. Chem. B* **114**, 10939–10953 (2010).
78. Morán, J. I., Alvarez, V. A., Cyras, V. P. & Vázquez, A. Extraction of cellulose and preparation of nanocellulose from sisal fibers. *Cellulose* **15**, 149–159 (2008).

79. Klemm, D., Heublein, B., Fink, H.-P. & Bohn, A. Cellulose: Fascinating Biopolymer and Sustainable Raw Material. *Angew. Chem. Int. Ed.* **44**, 3358–3393 (2005).
80. Ferfera-Harrar, H. & Dairi, N. Green nanocomposite films based on cellulose acetate and biopolymer-modified nanoclays: studies on morphology and properties. *Iran. Polym. J.* **23**, 917–931 (2014).
81. Delhom, C. D., White-Ghoorahoo, L. A. & Pang, S. S. Development and characterization of cellulose/clay nanocomposites. *Compos. Part B Eng.* **41**, 475–481 (2010).
82. Ma, H., Zhou, B., Li, H.-S., Li, Y.-Q. & Ou, S.-Y. Green composite films composed of nanocrystalline cellulose and a cellulose matrix regenerated from functionalized ionic liquid solution. *Carbohydr. Polym.* **84**, 383–389 (2011).
83. Nishino, T., Matsuda, I. & Hirao, K. All-Cellulose Composite. *Macromolecules* **37**, 7683–7687 (2004).
84. Nakamae, K., Nishino, T., Shimizu, Y. & Matsumoto, T. Experimental Determination of the Elastic Modulus of Crystalline Regions of Some Aromatic Polyamides, Aromatic Polyesters, and Aromatic Polyether Ketone. *Polym. J.* **19**, 451–459 (1987).
85. Edgar, K. J. *et al.* Advances in cellulose ester performance and application. *Prog. Polym. Sci.* **26**, 1605–1688 (2001).
86. Heinze, T. & Liebert, T. Unconventional methods in cellulose functionalization. *Prog. Polym. Sci.* **26**, 1689–1762 (2001).
87. Tas, Ç., Özkan, Y., Savaser, A. & Baykara, T. In vitro release studies of chlorpheniramine maleate from gels prepared by different cellulose derivatives. *Il Farm.* **58**, 605–611 (2003).

88. Gorgieva, S. & Kokol, V. Synthesis and application of new temperature-responsive hydrogels based on carboxymethyl and hydroxyethyl cellulose derivatives for the functional finishing of cotton knitwear. *Carbohydr. Polym.* **85**, 664–673 (2011).
89. García, M. A., Ferrero, C., Bértola, N., Martino, M. & Zaritzky, N. Edible coatings from cellulose derivatives to reduce oil uptake in fried products. *Innov. Food Sci. Emerg. Technol.* **3**, 391–397 (2002).
90. Nakagaito, A. N. & Yano, H. The effect of fiber content on the mechanical and thermal expansion properties of biocomposites based on microfibrillated cellulose. *Cellulose* **15**, 555–559 (2008).
91. Guirguis, O. W. & Moselhey, M. T. H. Thermal and structural studies of poly (vinyl alcohol) and hydroxypropyl cellulose blends. *Nat. Sci.* **04**, 57–67 (2012).
92. Mitsuo Narita. Methods for preparing alkali cellulose and cellulose ether.
93. Benslimane, A., Bahlouli, I. M., Bekkour, K. & Hammiche, D. Thermal gelation properties of carboxymethyl cellulose and bentonite-carboxymethyl cellulose dispersions: Rheological considerations. *Appl. Clay Sci.* **132–133**, 702–710 (2016).
94. Mohanty, A. K., Misra, M. & Drzal, L. T. Sustainable Bio-Composites from Renewable Resources: Opportunities and Challenges in the Green Materials World. *J. Polym. Environ.* **10**, 19–26 (2002).
95. Singha, A. S. & Thakur, V. K. Synthesis, Characterisation and Analysis of Hibiscus Sabdariffa Fibre Reinforced Polymer Matrix Based Composites. *Polym. Polym. Compos.* **17**, 189–194 (2009).
96. Ardanuy, M., Claramunt, J. & Toledo Filho, R. D. Cellulosic fiber reinforced cement-based composites: A review of recent research. *Constr. Build. Mater.* **79**, 115–128 (2015).

97. Thakur, V. K. & Singha, A. S. Physicochemical and Mechanical Behavior of Cellulosic Pine Needle-Based Biocomposites. *Int. J. Polym. Anal. Charact.* **16**, 390–398 (2011).
98. Li, X., Tabil, L. G. & Panigrahi, S. Chemical Treatments of Natural Fiber for Use in Natural Fiber-Reinforced Composites: A Review. *J. Polym. Environ.* **15**, 25–33 (2007).
99. Curvelo, A. Thermoplastic starch–cellulosic fibers composites: preliminary results. *Carbohydr. Polym.* **45**, 183–188 (2001).
100. Iwatake, A., Nogi, M. & Yano, H. Cellulose nanofiber-reinforced polylactic acid. *Compos. Sci. Technol.* **68**, 2103–2106 (2008).
101. Bhatnagar, A. & Sain, M. Processing of Cellulose Nanofiber-reinforced Composites. *J. Reinf. Plast. Compos.* **24**, 1259–1268 (2005).
102. Garrison, E. Petrography for Archaeological Geology. in *Techniques in Archaeological Geology* 145–178 (Springer International Publishing, 2016). doi:10.1007/978-3-319-30232-4_6.
103. Hassan, S. B. & Aigbodion, V. S. Effect coal ash on some refractory properties of alumino-silicate (Kankara) clay for furnace lining. *Egypt. J. Basic Appl. Sci.* **1**, 107–114 (2014).
104. Bergaya, F. & Lagaly, G. Chapter 1 General Introduction: Clays, Clay Minerals, and Clay Science. in *Developments in Clay Science* vol. 1 1–18 (Elsevier, 2006).
105. Barrientos-Ramírez, S. *et al.* Use of nanotubes of natural halloysite as catalyst support in the atom transfer radical polymerization of methyl methacrylate. *Microporous Mesoporous Mater.* **120**, 132–140 (2009).
106. Shchukin, D. G., Sukhorukov, G. B., Price, R. R. & Lvov, Y. M. Halloysite Nanotubes as Biomimetic Nanoreactors. *Small* **1**, 510–513 (2005).

107. Abdullayev, E. *et al.* Natural Tubule Clay Template Synthesis of Silver Nanorods for Antibacterial Composite Coating. *ACS Appl Mater Interfaces* **3**, 4040–4046 (2011).
108. Wan, C., Li, M., Bai, X. & Zhang, Y. Synthesis and Characterization of Photoluminescent Eu(III) Coordination Halloysite Nanotube-Based Nanohybrids. *J. Phys. Chem. C* **113**, 16238–16246 (2009).
109. Cavallaro, G., Lazzara, G. & Milioto, S. Dispersions of Nanoclays of Different Shapes into Aqueous and Solid Biopolymeric Matrices. Extended Physicochemical Study. *Langmuir* **27**, 1158–1167 (2011).
110. Cavallaro, G., Donato, D. I., Lazzara, G. & Milioto, S. Films of Halloysite Nanotubes Sandwiched between Two Layers of Biopolymer: From the Morphology to the Dielectric, Thermal, Transparency, and Wettability Properties. *J Phys Chem C* **115**, 20491–20498 (2011).
111. Du, M., Guo, B. & Jia, D. Newly emerging applications of halloysite nanotubes: a review. *Polym. Int.* **59**, 574–582 (2010).
112. Kausar, A. Review on Polymer/Halloysite Nanotube Nanocomposite. *Polym.-Plast. Technol. Eng.* **57**, 548–564 (2018).
113. Vergaro, V. *et al.* Cytocompatibility and Uptake of Halloysite Clay Nanotubes. *Biomacromolecules* **11**, 820–826 (2010).
114. Liu, R., Zhang, B., Mei, D., Zhang, H. & Liu, J. Adsorption of methyl violet from aqueous solution by halloysite nanotubes. *Desalination* **268**, 111–116 (2011).
115. Luo, P. *et al.* Study on the adsorption of Neutral Red from aqueous solution onto halloysite nanotubes. *Water Res.* **44**, 1489–1497 (2010).
116. De Lisi, R., Lazzara, G., Milioto, S. & Muratore, N. Adsorption of a dye on clay and sand. Use of cyclodextrins as solubility-enhancement agents. *Chemosphere* **69**, 1703–1712 (2007).

117. Szczepanik, B. *et al.* The effect of chemical modification on the physico-chemical characteristics of halloysite: FTIR, XRF, and XRD studies. *J. Mol. Struct.* **1084**, 16–22 (2015).
118. Joussein, E. *et al.* Halloysite clay minerals — a review. *Clay Miner.* **40**, 383–426 (2005).
119. Pasbakhsh, P., Churchman, G. J. & Keeling, J. L. Characterisation of properties of various halloysites relevant to their use as nanotubes and microfibre fillers. *Appl. Clay Sci.* **74**, 47–57 (2013).
120. Zhang, L., Wang, T. & Liu, P. Polyaniline-coated halloysite nanotubes via in-situ chemical polymerization. *Appl. Surf. Sci.* **255**, 2091–2097 (2008).
121. Cavallaro, G., Chiappisi, L., Pasbakhsh, P., Gradzielski, M. & Lazzara, G. A structural comparison of halloysite nanotubes of different origin by Small-Angle Neutron Scattering (SANS) and Electric Birefringence. *Appl. Clay Sci.* **160**, 71–80 (2018).
122. Lvov, Y. M., Shchukin, D. G., Mohwald, H. & Price, R. R. Halloysite Clay Nanotubes for Controlled Release of Protective Agents. *ACS Nano* **2**, 814–820 (2008).
123. Abdullayev, E., Joshi, A., Wei, W., Zhao, Y. & Lvov, Y. Enlargement of Halloysite Clay Nanotube Lumen by Selective Etching of Aluminum Oxide. *ACS Nano* **6**, 7216–7226 (2012).
124. Shemesh, R., Krepker, M., Nitzan, N., Vaxman, A. & Segal, E. Active packaging containing encapsulated carvacrol for control of postharvest decay. *Postharvest Biol. Technol.* **118**, 175–182 (2016).
125. Deng, S., Zhang, J., Ye, L. & Wu, J. Toughening epoxies with halloysite nanotubes. *Polymer* **49**, 5119–5127 (2008).

126. Chang, P. R., Xie, Y., Wu, D. & Ma, X. Amylose wrapped halloysite nanotubes. *Carbohydr. Polym.* **84**, 1426–1429 (2011).
127. Jinhua, W. *et al.* Rapid adsorption of Cr (VI) on modified halloysite nanotubes. *Desalination* **259**, 22–28 (2010).
128. K. Krejčová. NANO- A MIKROTUBULY PRO L...ČIVA.
129. Xie, Y., Chang, P. R., Wang, S., Yu, J. & Ma, X. Preparation and properties of halloysite nanotubes/plasticized *Dioscorea opposita* Thunb. starch composites. *Carbohydr. Polym.* **83**, 186–191 (2011).
130. X. Z. Shu, K. J. Zhu. Chitosan/gelatin microspheres prepared by modified emulsification and ionotropic gelation. *J. Microencapsul.* **18**, 237–245 (2001).
131. Rooj, S. *et al.* Preparation and properties of natural nanocomposites based on natural rubber and naturally occurring halloysite nanotubes. *Mater. Des.* **31**, 2151–2156 (2010).
132. Panda, A. K., Mishra, B. G., Mishra, D. K. & Singh, R. K. Effect of sulphuric acid treatment on the physico-chemical characteristics of kaolin clay. *Colloids Surf. Physicochem. Eng. Asp.* **363**, 98–104 (2010).
133. Murray, H. H. Overview — clay mineral applications. *Appl. Clay Sci.* **5**, 379–395 (1991).
134. Papoulis, D., Tsolis-Katagas, P. & Katagas, C. Progressive Stages in the Formation of Kaolin Minerals of Different Morphologies in the Weathering of Plagioclase. *Clays Clay Miner.* **52**, 275–286 (2004).
135. Lazzara, G. *et al.* An assembly of organic-inorganic composites using halloysite clay nanotubes. *Curr. Opin. Colloid Interface Sci.* **35**, 42–50 (2018).

136. Sorrentino, A., Gorrasi, G. & Vittoria, V. Potential perspectives of bio-nanocomposites for food packaging applications. *Trends Food Sci. Technol.* **18**, 84–95 (2007).
137. Alam, A., Zhang, Y., Kuan, H.-C., Lee, S.-H. & Ma, J. Polymer composite hydrogels containing carbon nanomaterials—Morphology and mechanical and functional performance. *Prog. Polym. Sci.* **77**, 1–18 (2018).
138. Alexandre, M. & Dubois, P. Polymer-layered silicate nanocomposites: preparation, properties and uses of a new class of materials. *Mater. Sci. Eng. R Rep.* **28**, 1–63 (2000).
139. Akpan, E. I., Shen, X., Wetzel, B. & Friedrich, K. Design and Synthesis of Polymer Nanocomposites. in *Polymer Composites with Functionalized Nanoparticles* 47–83 (Elsevier, 2019). doi:10.1016/B978-0-12-814064-2.00002-0.
140. Abbasipour, M., Khajavi, R., Yousefi, A. A., Yazdanshenas, M. E. & Razaghian, F. The piezoelectric response of electrospun PVDF nanofibers with graphene oxide, graphene, and halloysite nanofillers: a comparative study. *J. Mater. Sci. Mater. Electron.* **28**, 15942–15952 (2017).
141. Manias, E. *et al.* Polypropylene/Montmorillonite Nanocomposites. Review of the Synthetic Routes and Materials Properties. *Chem. Mater.* **13**, 3516–3523 (2001).
142. Ozkoc, G. & Kemaloglu, S. Morphology, biodegradability, mechanical, and thermal properties of nanocomposite films based on PLA and plasticized PLA. *J. Appl. Polym. Sci.* **114**, 2481–2487 (2009).
143. Kojima, Y. *et al.* Mechanical properties of nylon 6-clay hybrid. *J. Mater. Res.* **8**, 1185–1189 (1993).
144. Gilman, J. W., Kashiwagi, T. & Lichtenhan, J. D. Nanocomposites: A revolutionary new flame retardant approach. in vol. 42 1078–1089 (1997).

145. Gilman, J. W. *et al.* Flammability Properties of Polymer–Layered-Silicate Nanocomposites. Polypropylene and Polystyrene Nanocomposites †. *Chem. Mater.* **12**, 1866–1873 (2000).
146. Yano, K., Usuki, A., Okada, A., Kurauchi, T. & Kamigaito, O. Synthesis and properties of polyimide–clay hybrid. *J. Polym. Sci. Part Polym. Chem.* **31**, 2493–2498 (1993).
147. Kawasumi, M. The discovery of polymer-clay hybrids. *J. Polym. Sci. Part Polym. Chem.* **42**, 819–824 (2004).
148. Lo, C. K. *et al.* Langmuir–Blodgett Thin Films of Diketopyrrolopyrrole-Based Amphiphiles. *ACS Appl. Mater. Interfaces* **10**, 11995–12004 (2018).
149. Breton, M. Formation and Possible Applications of Polymeric Langmuir-Blodgett Films. A Review. *J. Macromol. Sci. Part C* **21**, 61–87 (1981).
150. Hirahara, M. *et al.* Application of electrospray spreading to a modified Langmuir–Blodgett technique for organo-clay hybrid film preparation. *Colloids Surf. Physicochem. Eng. Asp.* **580**, 123714 (2019).
151. Ferreira, A. M., Tonda-Turo, C., Mancuso, E. & Gentile, P. Multilayer nanoscale functionalization to treat disorders and enhance regeneration of bone tissue. *Nanomedicine Nanotechnol. Biol. Med.* **19**, 22–38 (2019).
152. Zhang, L., Zhu, L., Larson, S. R., Zhao, Y. & Wang, X. Layer-by-layer assembly of nanorods on a microsphere *via* electrostatic interactions. *Soft Matter* **14**, 4541–4550 (2018).
153. Chen, S. *et al.* Fabrication and Characterization of Layer-by-Layer Composite Nanoparticles Based on Zein and Hyaluronic Acid for Codelivery of Curcumin and Quercetagenin. *ACS Appl. Mater. Interfaces* **11**, 16922–16933 (2019).

154. Zhen, H., Wang, T., Jia, R., Su, B. & Gao, C. Preparation and performance of antibacterial layer-by-layer polyelectrolyte nanofiltration membranes based on metal–ligand coordination interactions. *RSC Adv.* **5**, 86784–86794 (2015).
155. Carosio, F., Ghanadpour, M., Alongi, J. & Wågberg, L. Layer-by-layer assembled chitosan/phosphorylated nanocellulose as a bio-based and flame protecting nano-exoskeleton on PU foams. (2018).
156. Yang, F., Wang, P., Yang, X. & Cai, Z. Antifogging and Antireflective Coatings by Spin-LbL Assembly of SiO₂ and ZrO₂ Nanoparticles. *Nanosci. Nanotechnol.-Asia* **9**, 109–113 (2018).
157. Arabzadeh, A. *et al.* Superhydrophobic coatings on Portland cement concrete surfaces. *Constr. Build. Mater.* **141**, 393–401 (2017).
158. Makaremi, M. *et al.* Effect of Morphology and Size of Halloysite Nanotubes on Functional Pectin Bionanocomposites for Food Packaging Applications. *ACS Appl. Mater. Interfaces* **9**, 17476–17488 (2017).
159. Lvov, Y., Aerov, A. & Fakhrullin, R. Clay nanotube encapsulation for functional biocomposites. *Adv Colloid Interface Sci* **207**, 189–198 (2014).
160. Fakhrullin, R. F. & Lvov, Y. M. Halloysite clay nanotubes for tissue engineering. *Nanomed.* **11**, 2243–2246 (2016).
161. Finnigan, B., Martin, D., Halley, P., Truss, R. & Campbell, K. Morphology and properties of thermoplastic polyurethane composites incorporating hydrophobic layered silicates. *J. Appl. Polym. Sci.* **97**, 300–309 (2005).
162. Liang, B. *et al.* Ca²⁺ Enhanced Nacre-Inspired Montmorillonite–Alginate Film with Superior Mechanical, Transparent, Fire Retardancy, and Shape Memory Properties. *ACS Appl. Mater. Interfaces* **8**, 28816–28823 (2016).

163. Huang, G., Yang, J., Gao, J. & Wang, X. Thin Films of Intumescent Flame Retardant-Polyacrylamide and Exfoliated Graphene Oxide Fabricated via Layer-by-Layer Assembly for Improving Flame Retardant Properties of Cotton Fabric. *Ind. Eng. Chem. Res.* **51**, 12355–12366 (2012).
164. Burke, S. E. & Barrett, C. J. Swelling Behavior of Hyaluronic Acid/Polyallylamine Hydrochloride Multilayer Films. *Biomacromolecules* **6**, 1419–1428 (2005).
165. YAMASHITA, Y. The Filter for Removing Ethylene Gas by the Enzyme Immobilization. *Trans Mater Res Soc J* **27**, 399–402 (2002).
166. Qiu, X., Leporatti, S., Donath, E. & Möhwald, H. Studies on the Drug Release Properties of Polysaccharide Multilayers Encapsulated Ibuprofen Microparticles. *Langmuir* **17**, 5375–5380 (2001).
167. Kretsis, G. A review of the tensile, compressive, flexural and shear properties of hybrid fibre-reinforced plastics. *Composites* **18**, 13–23 (1987).
168. Decher, G. Fuzzy Nanoassemblies: Toward Layered Polymeric Multicomposites. *Science* **277**, 1232–1237 (1997).
169. Artyukhin, A. B., Bakajin, O., Stroeve, P. & Noy, A. Layer-by-Layer Electrostatic Self-Assembly of Polyelectrolyte Nanoshells on Individual Carbon Nanotube Templates. *Langmuir* **20**, 1442–1448 (2004).
170. Lvov, Y., Price, R., Gaber, B. & Ichinose, I. Thin film nanofabrication via layer-by-layer adsorption of tubule halloysite, spherical silica, proteins and polycations. *Colloids Surf. Physicochem. Eng. Asp.* **198–200**, 375–382 (2002).
171. Nair, L. S. & Laurencin, C. T. Polymers as Biomaterials for Tissue Engineering and Controlled Drug Delivery. in *Tissue Engineering I* (eds. Lee, K. & Kaplan, D.) vol. 102 47–90 (Springer Berlin Heidelberg, 2006).

172. Paul McGee, J. Zero order release of protein from poly(ϵ -lactide-co-glycolide) microparticles prepared using a modified phase separation technique. *J. Controlled Release* **34**, 77–86 (1995).
173. Yang, J. *et al.* Enhanced Therapeutic Efficacy of Doxorubicin for Breast Cancer Using Chitosan Oligosaccharide-Modified Halloysite Nanotubes. *ACS Appl. Mater. Interfaces* **8**, 26578–26590 (2016).
174. Lee, Y., Jung, G.-E., Cho, S. J., Geckeler, K. E. & Fuchs, H. Cellular interactions of doxorubicin-loaded DNA-modified halloysite nanotubes. *Nanoscale* (2013) doi:10.1039/C3NR02665E.
175. Akhtar, N. & Patel, S. Agro-Industrial Discards and Invasive Weed-Based Lignocelluloses as Green Building Materials: A Pertinent Review. in *Ecological Wisdom Inspired Restoration Engineering* (eds. Achal, V. & Mukherjee, A.) 121–130 (Springer Singapore, 2019). doi:10.1007/978-981-13-0149-0_7.
176. Cavallaro, G., Lazzara, G., Milioto, S. & Parisi, F. Hydrophobically Modified Halloysite Nanotubes as Reverse Micelles for Water-in-Oil Emulsion. *Langmuir* **31**, 7472–7478 (2015).
177. Lazzara, G., Massaro, M. & Riela, S. Current Status of Nanoclay Phytotoxicity. in *Phytotoxicity of Nanoparticles* (eds. Faisal, M., Saquib, Q., Alatar, A. A. & Al-Khedhairi, A. A.) 151–174 (Springer International Publishing, 2018).
178. Azizli, M. J. *et al.* Studying the roles of nanoclay and blend composition on the improved properties of natural rubber/chloroprene composites. *Polym. Compos.* **39**, 1562–1574 (2018).
179. Mudhoo, A. *et al.* Green synthesis, activation and functionalization of adsorbents for dye sequestration. *Environ. Chem. Lett.* **17**, 157–193 (2019).

180. Massaro, M. *et al.* Eco-friendly functionalization of natural halloysite clay nanotube with ionic liquids by microwave irradiation for Suzuki coupling reaction. *J Organomet Chem* **749**, 410–415 (2014).
181. Cavallaro, G., Lazzara, G. & Milioto, S. Exploiting the Colloidal Stability and Solubilization Ability of Clay Nanotubes/Ionic Surfactant Hybrid Nanomaterials. *J Phys. Chem. C* **116**, 21932–21938 (2012).
182. Bertolino, V., Cavallaro, G., Lazzara, G., Milioto, S. & Parisi, F. Biopolymer-Targeted Adsorption onto Halloysite Nanotubes in Aqueous Media. *Langmuir* **33**, 3317–3323 (2017).
183. Patrickios, C. S., Hertler, W. R. & Hatton, T. A. Protein complexation with acrylic polyampholytes. *Biotechnol. Bioeng.* **44**, 1031–1039 (1994).
184. Wanjun, T., Cunxin, W. & Donghua, C. Kinetic studies on the pyrolysis of chitin and chitosan. *Polym. Degrad. Stab.* **87**, 389–394 (2005).
185. Rusmirović, J. D. *et al.* Effect of the modified silica Nanofiller on the Mechanical Properties of Unsaturated Polyester Resins Based on Recycled Polyethylene Terephthalate. *Polym. Compos.* **38**, 538–554 (2017).
186. Li, W. *et al.* Polyvinyl chloride as a multimodal tissue-mimicking material with tuned mechanical and medical imaging properties: Polyvinyl chloride as a tissue-mimicking material. *Med. Phys.* **43**, 5577–5592 (2016).
187. Yusoff, R. B., Takagi, H. & Nakagaito, A. N. Tensile and flexural properties of polylactic acid-based hybrid green composites reinforced by kenaf, bamboo and coir fibers. *Ind. Crops Prod.* **94**, 562–573 (2016).
188. Hamad, K., Kaseem, M., Yang, H. W., Deri, F. & Ko, Y. G. Properties and medical applications of polylactic acid: A review. *Express Polym. Lett.* **9**, 435–455 (2015).

189. Liu, M., Zhang, Y., Wu, C., Xiong, S. & Zhou, C. Chitosan/halloysite nanotubes bionanocomposites: Structure, mechanical properties and biocompatibility. *Int. J. Biol. Macromol.* **51**, 566–575 (2012).
190. Bertolino, V., Cavallaro, G., Milioto, S., Parisi, F. & Lazzara, G. Thermal Properties of Multilayer Nanocomposites Based on Halloysite Nanotubes and Biopolymers. *J. Compos. Sci.* **2**, 41 (2018).
191. Umemura, Y. Preparation and application of clay mineral films. in *Developments in Clay Science* vol. 9 377–396 (Elsevier, 2018).
192. Bertolino, V., Cavallaro, G., Lazzara, G., Milioto, S. & Parisi, F. Halloysite nanotubes sandwiched between chitosan layers: novel bionanocomposites with multilayer structures. *New J. Chem.* **42**, 8384–8390 (2018).
193. Farris, S. *et al.* Wetting of Biopolymer Coatings: Contact Angle Kinetics and Image Analysis Investigation. *Langmuir* **27**, 7563–7574 (2011).
194. Cavallaro, G., Lisi, R., Lazzara, G. & Milioto, S. Polyethylene glycol/clay nanotubes composites. *J. Therm. Anal. Calorim.* **112**, 383–389 (2013).
195. Du, M., Guo, B. & Jia, D. Thermal stability and flame retardant effects of halloysite nanotubes on poly(propylene). *Eur. Polym. J.* **42**, 1362–1369 (2006).
196. Massaro, M. *et al.* Halloysite nanotubes for efficient loading, stabilization and controlled release of insulin. *J. Colloid Interface Sci.* **524**, 156–164 (2018).
197. Darder, M. *et al.* Microfibrous Chitosan–Sepiolite Nanocomposites. *Chem. Mater.* **18**, 1602–1610 (2006).
198. *Multilayer thin films: sequential assembly of nanocomposite materials.* (Wiley-VCH, 2003).
199. Elizarova, I. S. & Luckham, P. F. Layer-by-layer adsorption: Factors affecting the choice of substrates and polymers. *Adv. Colloid Interface Sci.* **262**, 1–20 (2018).

200. Zhao, H. C., Wu, X. T., Tian, W. W. & Ren, S. T. Synthesis and Thermal Property of Poly(Allylamine Hydrochloride). *Adv. Mater. Res.* **150–151**, 1480–1483 (2010).
201. Lourenço, J. M. C. *et al.* Counterions in Poly(allylamine hydrochloride) and Poly(styrene sulfonate) Layer-by-Layer Films. *Langmuir* **20**, 8103–8109 (2004).
202. Chien, H.-W., Tan, S.-F., Wei, K.-L. & Tsai, W.-B. Modulation of the functions of osteoblast-like cells on poly(allylamine hydrochloride) and poly(acrylic acid) multilayer films. *Colloids Surf. B Biointerfaces* **88**, 297–303 (2011).
203. Zhou, W., Yu, L., Li, Y., Gao, B. & Wang, Z. Layer by Layer Assembly of Poly (Allylamine Hydrochloride)/Phosphate Ions and Poly (Sodium 4-Styrene Sulfonate) Membrane for Forward Osmosis Application. *J. Ocean Univ. China* **18**, 743–749 (2019).
204. Burdick, J. A. & Prestwich, G. D. Hyaluronic Acid Hydrogels for Biomedical Applications. *Adv. Mater.* **23**, H41–H56 (2011).
205. Toole, B. P. Hyaluronan: from extracellular glue to pericellular cue. *Nat. Rev. Cancer* **4**, 528–539 (2004).
206. Highley, C. B., Prestwich, G. D. & Burdick, J. A. Recent advances in hyaluronic acid hydrogels for biomedical applications. *Curr. Opin. Biotechnol.* **40**, 35–40 (2016).
207. Prestwich, G. D. Hyaluronic acid-based clinical biomaterials derived for cell and molecule delivery in regenerative medicine. *J. Controlled Release* **155**, 193–199 (2011).
208. Zamboni, F., Vieira, S., Reis, R. L., Miguel Oliveira, J. & Collins, M. N. The potential of hyaluronic acid in immunoprotection and immunomodulation: Chemistry, processing and function. *Prog. Mater. Sci.* **97**, 97–122 (2018).
209. Dosio, F., Arpicco, S., Stella, B. & Fattal, E. Hyaluronic acid for anticancer drug and nucleic acid delivery. *Adv. Drug Deliv. Rev.* **97**, 204–236 (2016).

210. Phosphate-buffered saline (PBS): *Cold Spring Harb. Protoc.* **2006**, pdb.rec8247 (2006).
211. Yao, T. & Asayama, Y. Animal-cell culture media: History, characteristics, and current issues. *Reprod. Med. Biol.* **16**, 99–117 (2017).
212. V. Bertolino *et al.* Layer-by-layer systems such as drug delivery.
213. Jiao, G. *et al.* Limitations of MTT and CCK-8 assay for evaluation of graphene cytotoxicity. *RSC Adv.* **5**, 53240–53244 (2015).
214. Janes, K. A., Fresneau, M. P., Marazuela, A., Fabra, A. & Alonso, M. J. Chitosan nanoparticles as delivery systems for doxorubicin. *J. Controlled Release* **73**, 255–267 (2001).
215. V. Bertolino *et al.* Biopolymer/HNTs nanocomposites with smart features.

Curriculum vitae

**FORMATO EUROPEO PER
IL CURRICOLO
VITAE**



INFORMAZIONI PERSONALI

Nome VANESSA RITA BERTOLINO
Indirizzo VIA Cavour 14, 91025- MARSALA (TP)
Telefono Fisso 0923 982335 Mobile +39 320 3094323

E-mail vanessarita.bertolino@unipa.it

Nazionalità Italiana

Data e luogo di nascita 21/05/1987 Marsala

ESPERIENZA LAVORATIVA

• Data 2/08/2010- 30/09/2010
• Nome del datore di lavoro Dott. Vito Falco
• Tipo e indirizzo di azienda ASSESSORATO DELLE RISORSE AGRICOLE E ALIMENTARI (REGIONE SICILIANA) UOS 35,
Centro di Ricerca per l'Innovazione della Filiera Vitivinicola "Ernesto Del Giudice",
C.da Bosco, 421- 91025 Marsala (TP)

• Tipo di impiego Attività di Tirocinio
Utilizzo delle tecniche analitiche di tipo cromatografico (HPLC-GC) e spettrofotometrico (UV-Vis)
per analisi e caratterizzazione uve, moste e vini per finalità di tipizzazione dei vitigni autoctoni
siciliani.

• Data 9/09/2014- 9/09/2015
• Nome del datore di lavoro Responsabile scientifico del progetto Prof. Eugenio Caponetti
• Tipo e indirizzo di azienda UniNetLab-STEBICEF
• Tipo di impiego Contrattista co.co.co
• Principali mansioni e responsabilità Supporto tecnico-scientifico alle attività di ricerca
nell'ambito del progetto "GREEN-CLEAN- OR2"

• Data anno accademico 2016/2017
• Tipo e indirizzo di azienda Università degli Studi di Palermo
• Tipo di impiego Tutor universitario

Principali mansioni e responsabilità Attività di tutorato per scuole di scienze e di base applicate

ISTRUZIONE E FORMAZIONE

- Data 31/10/2015
 - Nome e tipo di istituto di istruzione o formazione Dottorato di Ricerca in Scienza dei Materiali e Nanotecnologie XXXI CICLO (durata 3 anni) (in convenzione UNICT-UNIPA)
Progetto di Ricerca dal titolo:
"Preparazione e studio di films compositi di biopolimeri con *nanofillers* caricati con specie attive"
Tutor di Dottorato Prof. Giuseppe Lazzara
Sede di servizio Università degli Studi di Palermo, Dipartimento di Fisica e Chimica.

- Data Luglio 2014- ABILITAZIONE alla professione di CHIMICO (Sez. A)

- Data 27 Marzo 2013
 - Nome e tipo di istituto di istruzione o formazione Facoltà di Scienze MM. FF. NN - Università degli Studi di Palermo
Corso di Laurea Magistrale in Chimica.
 - Qualifica conseguita Dottore Magistrale in Chimica, classe LM-54.
Titolo della tesi:
"Preparazione e caratterizzazione chimico-fisica di bionanocompositi. Effetto della carica del biopolimero e della morfologia della nanoparticella."
 - Livello nella classificazione nazionale 110 / 110 e Lode

- Data 10 Novembre 2010
 - Nome e tipo di istituto di istruzione o formazione Facoltà di Scienze MM. FF. NN - Università degli Studi di Palermo
Corso di Laurea in Chimica.
 - Qualifica conseguita Dottore in Chimica, classe 21-
CLASSE DELLE LAUREE IN SCIENZE E TECNOLOGIE CHIMICHE.
Titolo tesi: " Caratterizzazione termica e calorimetrica di nanocompositi PEG20000/Allosite "
 - Livello nella classificazione nazionale 110 / 110 e Lode

• Data	12 Luglio 2006
• Nome e tipo di istituto di istruzione o formazione	Liceo Scientifico Statale "P. Ruggieri" di Marsala
• Qualifica conseguita	Diploma di Maturità Scientifica.
• Livello nella classificazione nazionale	100 / 100 e menzione

Seminari, Comunicazioni a Congresso e Pubblicazioni...

Seminari:

1. Presentazione su invito del Prof. Pablo Taboada del proprio progetto di ricerca nell'ambito del dottorato in "Scienza dei Materiali e Nanotecnologie" presso Department of Condensed Matter Physics, Santiago de Compostela, Spagna.

Comunicazioni a congresso:

1. M.L. Saladino, V. Bertolino, P. Colomba, E. Caponetti, "Preparation and physico-chemical characterization of biocomposites based on cellulose derivatives and MCM-41" X Convegno Nazionale INSTM sulla Scienza e Tecnologia dei Materiali, 28 Giugno- 1 Luglio 2015, Favignana (TP) (Italy). **Poster**
2. M.L. Saladino, P. Colomba, V. Bertolino, E. Caponetti, "Mesoporous materials for controlled release of biocides" XV Congresso Divisione di Chimica dell'Ambiente e dei Beni Culturali – Società Chimica Italiana Bergamo, 14 – 18 giugno 2015. **Poster**
3. V. Bertolino, G. Cavallaro, G. Lazzara, S. Milioto, F. Parisi, "Hybrids based on biopolymer/halloysite clay nanotubes for cultural heritage applications" International Confederation for Thermal Analysis and Calorimetry 2016, 14-19 agosto 2016, Orlando (Florida). **Poster**
4. V. Bertolino, G. Cavallaro, G. Lazzara, S. Milioto, F. Parisi, "Physico-chemical characterization of halloysite- polymer systems in aqueous solution" XXXVIII AICAT CONGRESS 2016, 25-28 settembre, Ischia. **Poster**
5. V. Bertolino, G. Cavallaro, G. Lazzara, S. Milioto, F. Parisi, "Effect of Biopolymer Charge on Halloysite Nanotubes Stability in Water" MoDeSt Workshop Nano Materials and BioMaterials for the next Decade, 5-7 Luglio, Pantelleria (Italy). **Oral communication**
6. V. Bertolino, G. Cavallaro, G. Lazzara, S. Milioto, F. Parisi, "Halloysite Biopolymer System in Aqueous Solution: Nano-ITC Investigation" 16th ICC International Clay Conference, 17-21 Luglio Granada, Spagna. **Poster**
7. V. Bertolino, G. Cavallaro, G. Lazzara, S. Milioto, F. Parisi, "Thermal analytical characterization of multilayer and bionanocomposites" 13th Mediterranean Conference on Calorimetry and Thermal Analysis- Medicta 2017, Loano (SV) Italia. **Poster**
8. V. Bertolino, G. Cavallaro, G. Lazzara, S. Milioto, F. Parisi, "Physico-chemical characterization of halloysite (HNTs)- polymer systems in aqueous solution" 17th Course Frontiers in Water Biophysics 2019, Erice (TP) Italia. **Poster**
9. V. Bertolino, G. Lazzara, S. Milioto, S. Barbosa, R. Martínèz-Gonzàles, P. Taboada, "Biopolymer/ HNTs nanocomposites with smart features" CEEC-TAC 5 & MEDICTA 2019 Conference, Roma (RO) Italia. **Poster**

Articoli scientifici :

1. Vanessa Bertolino, Giuseppe Cavallaro, Giuseppe Lazzara, Marcello Merli, Stefana Milioto, Filippo Parisi, Luciana Sciascia; "Effect of the biopolymer charge and the nanoclay morphology on nanocomposite materials", Ind.Eng. Chem. Res. 2016, 55, 7373-7380.
2. Vanessa Bertolino, Giuseppe Cavallaro, Giuseppe Lazzara, Stefana Milioto, Filippo Parisi; "Biopolymer-Targeted Adsorption onto Halloysite Nanotubes in Aqueous Media", Langmuir 2017,33, 3317-3323.
3. Vanessa Bertolino, Giuseppe Cavallaro, Giuseppe Lazzara, Stefana Milioto, Filippo Parisi; "Crystallinity of block copolymer controlled by cyclodextrin", J Therm Anal Calorim 2018, 132, 191-196.
4. Vanessa Bertolino, Giuseppe Cavallaro, Stefana Milioto, Filippo Parisi, Giuseppe Lazzara; "Thermal Properties of Multilayer Nanocomposites Based on Halloysite Nanotubes and Biopolymers", J. Compos. Sci. 2018, 2, 41-52.
5. Vanessa Bertolino, Giuseppe Cavallaro, Giuseppe Lazzara, Stefana Milioto, Filippo Parisi, "Halloysite nanotubes sandwiched between chitosan layers: a novel bionanocomposite with multilayer structure", New J. Chem., DOI:10.1039/C8NJ01161C.
6. Vanessa Bertolino, Giuseppe Cavallaro, Stefana Milioto, Giuseppe Lazzara, "Polysaccharides/Halloysite nanotubes for smart bionanocomposite materials", Carbohydrate Polymers (submitted)

- Corso di formazione
"Occasioni di finanziamento della ricerca e della mobilità in ambito europeo"
Palermo, 9-12 novembre 2015
- 36th Berlin School on Neutron
Scattering Berlino, 25 Febbraio – 4 Marzo 2016
Lise Meitner Campus / Helmholtz-Zentrum Berlin für Materialien und Energie
- SUMMER SCHOOL AND WORKSHOP IN
CALORIMETRY Calorimetry and thermal methods in material
science
Lyon, Francia 19 Giugno - 24 Giugno 2016
- XXXVIII AICAT CONGRESS
Calorimetry, Thermal Analysis and Applied Thermodynamics
Ischia, 25-28 Settembre 2016
Vincitrice di borsa di studio
- STAGE SCIENTIFICO connesso con l'attività di ricerca di Dottorato
sotto la supervisione del Prof. Pablo Taboada
Santiago de Compostela, Spagna 9 Settembre- 21 Dicembre 2016
- MoDeSt Workshop Nano Materials and BioMaterials for the next Decade
Pantelleria (Italy), 5-7 Luglio 2017
Comunicazione orale presentata personalmente
- 16th ICC International Clay Conference,
Granada, Spagna 17-21 Luglio 2017
- 13th Mediterranean Conference on Calorimetry and Thermal Analysis
Medicta Loano, Italia 24-27 Settembre 2017
- 17th Course Frontiers in Water Biophysics,
Erice, Italia
- CEEC-TAC 5 & MEDICTA 2019,
Roma, Italia 27-30 Agosto 2019

CAPACITÀ E COMPETENZE PERSONALI	
MADRELINGUA	ITALIANO
ALTRE LINGUA	INGLESE
<ul style="list-style-type: none"> • Capacità di lettura • Capacità di scrittura • Capacità di espressione orale 	<p>OTTIME</p> <p>OTTIME</p> <p>BUONE</p>
CAPACITÀ E COMPETENZE RELAZIONALI	Flessibilità e spirito di adattamento, entusiasmo e capacità di comunicare. Incline alle pubbliche relazioni e ottime capacità dialettiche.
CAPACITÀ E COMPETENZE ORGANIZZATIVE	Capacità di coordinare, amministrare persone e progetti; capacità di organizzare e disciplinare il lavoro ripartendo in modo equilibrato il proprio tempo.
CAPACITÀ E COMPETENZE TECNICHE	<p>Conoscenza sistemi operativi Windows (95, 98, 2000, XP, Vista)</p> <p>Conoscenza avanzata del pacchetto Microsoft Office.</p> <p>Conoscenza delle applicazioni: Dropbox, Origin, Kaleidagraph, ImageJ, CorelDraw.</p>
PATENTE O PATENTI	Patente B

Autorizzo il trattamento dei dati personali contenuti all'interno del presente curriculum vitae per gli usi consentiti dall'art. 13 del D. Lgs. 196/2003.

Attached Papers

Attached Paper I

Biopolymer-Targeted Adsorption onto Halloysite Nanotubes in Aqueous Media

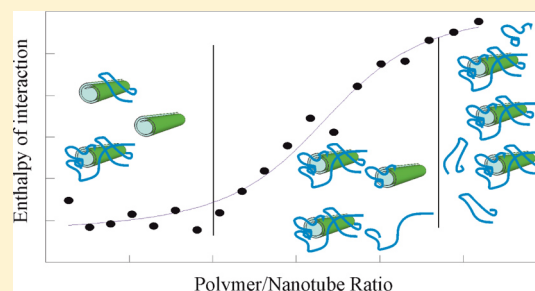
Vanessa Bertolino, Giuseppe Cavallaro, Giuseppe Lazzara,*[✉] Stefana Milioto, and Filippo Parisi

Department of Physics and Chemistry, Università degli Studi di Palermo, Viale delle Scienze, pad. 17, 90128 Palermo, Italy

Supporting Information

ABSTRACT: Studies on the adsorption of biopolymers onto halloysite nanotubes (HNTs) in water were conducted. Three polymers with different charges—anionic (pectin), neutral (hydroxypropyl cellulose), and cationic (chitosan)—were chosen. The thermodynamic parameters for the adsorption of polymers onto the HNT surface were determined by isothermal titration calorimetry (ITC). The experimental data were interpreted based on a Langmuir adsorption model. The standard variations in free energy, enthalpy, and entropy of the process were obtained and discussed. Turbidimetry was used to evaluate the stability of functionalized nanoparticles in water. The ζ -potential clarified the surface charge properties of functionalized nanotubes upon polymer adsorption.

The interaction of modified nanotubes with polymers led to the formation of a colloidal system with tunable stability and surface properties, which offers different perspectives on new applications of these dispersions, such as carriers for substances to be released in response to external stimuli.



INTRODUCTION

In recent years, there has been particular interest in research on nanoclays. They are among the materials considered green¹ and may have different applications.^{2,3} Halloysite clay is a promising nanomaterial because of its versatile properties, such as hollow tubular morphology, a large specific area, tunable surface chemistry, abundance, high mechanical strength, and thermal stability. Halloysite nanotubes (HNTs) are quite polydisperse in nature, with length ranging from 50 to 1500 nm, external diameter ranging from 20 to 150 nm, and lumen ranging from 10 to 15 nm.⁴ The HNT cell unit possesses two water molecules of crystallization that are strongly retained within the rolled structure.^{5,6}

The chemical properties of the outermost surface of the HNTs are similar to the properties of SiO₂, whereas the properties of the inner cylindrical core can be associated with those of Al₂O₃.⁷ This different chemistry determines a positively charged lumen and a negatively charged outer surface in the 2–8 pH interval.¹ Recently, HNTs have been reported to be a new type of additive for polymers such as polypropylene⁸ and polyvinyl alcohol,⁹ and the mechanical and thermal properties of these composites have been found to be better than those of the original¹⁰ polymeric matrix. They are also used in the preparation of polymer systems in the transport and delivery of drugs and in wastewater treatment. Many studies have been conducted on HNTs as entrapment systems for loading, storage, and controlled release of substances^{1,11} such as gas,¹² self-healing agents,¹³ corrosion inhibitors,¹⁴ antimicrobials,^{15–17} drugs,^{18–20} and proteins.^{21,22} Although the biocompatibility of halloysite has been confirmed for cells and microorganisms,^{23–25} its medical use might be restricted to oral

dosing, dermal application, or dental use¹ because of the nonbiodegradability of the aluminosilicate. The numerous applications of HNTs are linked to the possibility to realize selective modifications of HNT surfaces, which can be easily achieved by using anionic and cationic surfactants,^{26–29} γ -methacryloxypropyl trimethoxysilane (MPS),³⁰ octadecylphosphonic acid,³¹ aminosilanes,³² or drug molecules.^{33,34} The HNT modification is an attractive challenge, with the goal being to produce rather stable dispersions for applications where nanocontainers and nanocarriers are required to oppose the sedimentation of pristine HNTs and to direct molecular species into the internal space to fabricate desired nanostructures for the purposes of interest.^{33,35,36} There are different methods for ensuring the aggregative stability of the colloid dispersion. One of these is its steric stabilization by a bonded polymer to a surface of dispersed particles. In this way, in particular, the aggregation of particles because of van der Waals attraction is hindered by the presence of polymer chains on a particle surface. Another strategy for nanoparticle stabilization in aqueous media is enhancing electrostatic repulsions by increasing the surface charge.

In this work, we have characterized aqueous dispersions of HNTs in the presence of biopolymers with different charges. In particular, we have used (1) chitosan, a cationic polysaccharide, because of the presence of protonable amino groups; (2) pectin from citrus, an anionic polysaccharide, because of $-\text{COOH}$ dissociation; and (3) hydroxypropyl cellulose, a neutral

Received: February 21, 2017

Revised: March 8, 2017

Published: March 9, 2017

polymer. Dry films of these biopolymers have already been investigated in combination with HNTs for sustainable packaging applications^{30,37–40} and tissue engineering.^{41–43} On the other hand, the interactions in aqueous media are not well established, although they are strategically correct for the choice of casting parameters in dry film preparation and for applications involving dispersions. ζ -Potential and turbidimetry allowed us to investigate the stability of aqueous dispersions. Isothermal titration calorimetry investigated interactions between components to highlight the thermodynamic properties for the adsorption phenomenon through direct measurements. The hydrophilicity of both the inner and outer surfaces made HNTs dispersible in aqueous biopolyelectrolytes. The interaction site has a profound effect on the properties and stability of dispersions.

MATERIALS AND METHODS

Hydroxypropyl cellulose (HPC; average molecular mass 80 kg mol⁻¹), chitosan (acetylated chitin, poly-D-glucosamine, 75–85% deacetylated, with a low molecular weight of 120 kg mol⁻¹), citrus pectin (degree of methyl esterification 24%, average molecular weight 65 kg mol⁻¹), and halloysite nanoclay are Aldrich products.

Sample Preparation. Aqueous solutions of polymers were prepared according to the literature.⁴⁴ Briefly, the polymer was added to water, and the mixture was kept under stirring for 24 h. After that, the nanotube powder was added to the polymer solution, and the mixture was kept under stirring for another 24 h. For the chitosan–HNT system, given the low solubility of the polymer at neutral pH, it was necessary to adjust the pH to 3.5 by adding 0.1 mol dm⁻³ acetic acid.

Isothermal Titration Calorimetry (ITC). ITC experiments were performed using the ultrasensitive Nano-iTC200 calorimeter (Micro-Cal). Approximately 40 μ L of the water/polymer mixture was injected (2 μ L per injection) into the thermally equilibrated ITC cell (200 μ L) containing the water/HNT dispersion. The experimental protocol (stirring rate, and initial concentrations) required special attention as in the measuring cells at the start of each titration calorimetry, a dispersion of HNT was present. The cell was thermally equilibrated at 25.000 \pm 0.005 $^{\circ}$ C. The calorimeter sensitivity was at least 2 nW. The effects of dilution of the polymer and HNT were measured and then subtracted from the heats of titration to obtain the thermal effects of interaction for the *i*th step (ΔH_i). In the case of the chitosan-based system, three consecutive titrations were carried out to obtain the full titration curve because of the large heat flow signals.

ζ -Potential. ζ -Potential measurements were carried out using a Zetasizer Nano-ZS (Malvern Instruments) at *t* = 25 $^{\circ}$ C. The measurements were taken using a disposable folded capillary cell.

Turbidimetric Experiments. The measurements were carried out at 20.0 \pm 0.1 $^{\circ}$ C using a Beckman spectrophotometer (model DU-640). UV–vis spectra, reported as optical density (*T*) versus wavelength (λ), were registered in the 200–800 nm range, at different times, for a total of 3 days. In such a λ range, both polymer and nanotubes do not absorb, but the optical density value of each dispersion changes over time because there is a sedimentation process of HNT particles. The speed of sedimentation process influences the shape of the curve obtained by plotting the optical density as a function of time. The concentration was 1.0 wt % for HNTs and 0.10 wt % for the polymer.

Viscosity and Density Measurements. Viscosity measurements were carried out using Schoot Gerate AVS 440, an Ubbelohde suspended-level capillary automatic viscometer, which allows us to determine kinematic viscosity by measuring the time it takes for the sample, whose volume is defined by two ring-shaped marks, to flow laminarily through a capillary under the influence of gravity. The capillary was immersed in a thermostated water bath at 20.0 \pm 0.1 $^{\circ}$ C. The flow time was implemented in automatic viscometers, in which additional sensors detect the time it takes for the sample to flow. Density measurements of dispersions were determined at 20 $^{\circ}$ C using

a vibrating tube densimeter (DSA 5000 M Anton Paar). It is possible, by knowing the “time of flow” (*t*) and density values (*d*), to calculate the relative viscosity ($\eta_r = \eta_{\text{solution}}/\eta_{\text{water}}$) of the analyzed dispersions as

$$\eta_{\text{solution}}/\eta_{\text{water}} = (t_{\text{solution}}/t_{\text{water}}) \times (d_{\text{water}}/d_{\text{solution}}) \quad (1)$$

The η_{water} value at the same condition of temperature is 1.001 cP. Polymer concentration was fixed at this value for turbidimetric experiments (0.10 wt %).

RESULTS

Turbidimetric Measurements. The optical density is related to the concentration of nanoparticle in suspension, and therefore its time dependence can be used to investigate the colloidal stability of the HNT dispersion in water.²⁷ The dispersions were prepared at two different pH values to evaluate the influence of the polymer and HNT charge density on the settling process of the nanotubes.

Figure 1 shows the optical density (*T*) values as a function of time for each dispersion.

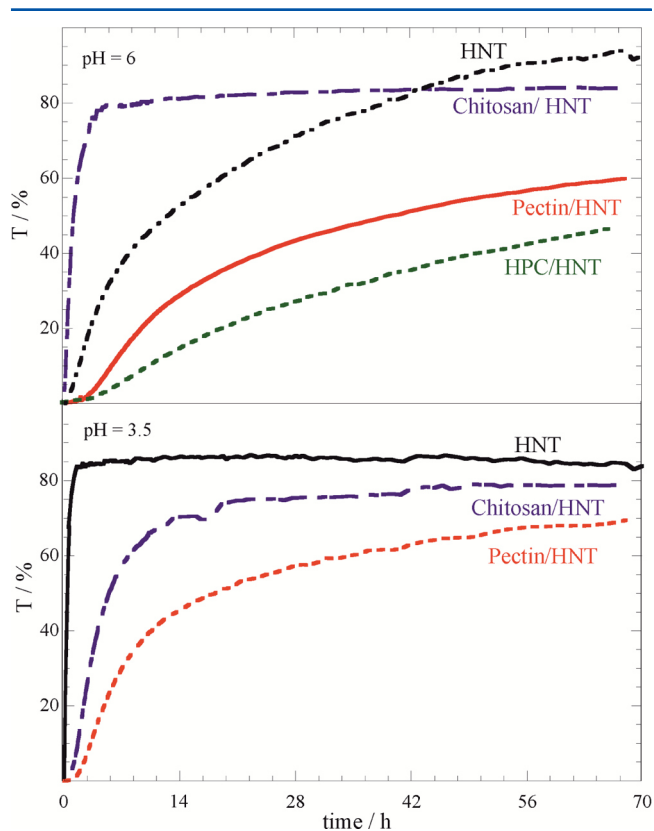


Figure 1. Optical density measured at $\lambda = 800$ nm as a function of time for HNT and polymer/HNT aqueous dispersion at different pH values.

The *T* values increased rather quickly up to 10 min to 2 h, depending on the investigated system. The sedimentation process is influenced by both pH and polymer addition. The *T* versus time curves can be fitted to the empirical exponential expression⁴⁵

$$T = T_{\text{inf}}[1 - \exp(-t/t_0)] \quad (2)$$

where T_{inf} is the level-off value of the optical density, *t* is the time, and t_0 is the characteristic time for the sedimentation process. The exponential function was used because it is a convenient function for calculation and comparison of

sedimentation processes in colloidal systems.⁴⁵ The best fits for all systems are given in the Supporting Information. Table 1 shows parameters (T_{inf} , t_0), calculated by the best fit based on eq 2 for each system.

Table 1. Fit Parameters for HNT Sedimentation Kinetics and Viscosity Values for the Aqueous Polymer Solutions^a

	pH	T_{inf} (%)	t_0 (10^3 s)	η_r
HNT	3.5	85.3 ± 0.1	1.57 ± 0.02	
HNT	6	90.3 ± 0.7	57.0 ± 1.2	
HPC/HNT	6	72.4 ± 1.9	224 ± 9	1.078
pectin/HNT	3.5	66.9 ± 0.5	45.7 ± 0.9	1.445
pectin/HNT	6	64.0 ± 0.6	91.0 ± 1.9	1.044
chitosan/HNT	3.5	77.7 ± 0.4	21.1 ± 0.4	2.850
chitosan/HNT	6	82.0 ± 0.2	5.4 ± 0.1	1.108

^aConcentrations were 1.0 and 0.10 wt % for the HNT and polymer, respectively.

The dispersion stability is dependent on particle dimensions, charge, viscosity of the medium, and interactions between components (HNTs/polymer). These parameters determine the kinetic and thermodynamic stabilities.

Isothermal Titration Calorimetry. ITC measurements were performed to investigate the polymer adsorption onto halloysite nanotubes in aqueous dispersion. The ITC curves show a sigmoidal profile of ΔH_i versus polymer/HNT mass ratio ($R_{P:HNT}$). A similar trend was observed for other nanoparticle/polymer systems, and it was discussed in terms of polymer adsorption.^{46,47} The ΔH_i versus $R_{P:HNT}$ profiles were analyzed based on a simple Langmuir-type adsorption model that was suitable for the adsorption of HPC onto discoidal nanoclay in water.⁴⁷ Briefly, it is assumed that a nanoparticle can be saturated by a certain amount of polymer and, therefore, the halloysite possesses a total concentration of adsorption sites S_t equal to

$$S_t = ZA_{sp}C_{HNT} \quad (3)$$

where Z is the maximum weight (in grams) of polymer adsorbed per surface unit of nanoparticle, A_{sp} is the specific surface area for HNT ($60 \text{ m}^2 \text{ g}^{-1}$), and C_{HNT} is the concentration of HNT (g dm^{-3}).

The equilibrium constant of the adsorption process (K_{ads}) can be defined as

$$K_{ads} = X_{ads}/(X_f S_f) \quad (4)$$

in which X_{ads} and X_f are the fraction of adsorbed and free polymer, respectively, and S_f is the concentration of free adsorption sites onto HNT. The injection heat for the i th titration step is given by

$$Q_i = Q_j - Q_{j-1} + (Q_j + Q_{j-1})V_a/2V_c \quad (5)$$

For the j th and $(j - 1)$ th states before and after the i th addition step, the corresponding Q_j and Q_{j-1} are

$$Q_j = C_{P,j}V_c\Delta H_{ads}^\circ X_{ads,j} \quad (6)$$

$$Q_{j-1} = C_{P,j-1}V_c\Delta H_{ads}^\circ X_{ads,j-1} \quad (7)$$

where $C_{P,j-1}$ and $C_{P,j}$ are the polymer concentrations before and after the injection, ΔH_{ads}° is the enthalpy of adsorption, V_c is the cell volume, and X_{ads} is the fraction of adsorbed polymer related to the equilibrium constant. The third term on the right hand side of eq 5 is the correction for the cell-displaced volume.⁴⁸

The experimental data were successfully fitted by eqs 3–7 and provided K_{ads} , Z , and ΔH_{ads}° (Table 2). Figure 2 shows the fitting results. The minimization procedure was performed by means of the nonlinear least-squares fitting based on the Levenberg–Marquardt algorithm.

The standard free energy (ΔG_{ads}°) and entropy (ΔS_{ads}°) for the adsorption process were calculated as

$$\Delta G_{ads}^\circ = -RT \ln K_{ads} \quad T\Delta S_{ads}^\circ = \Delta H_{ads}^\circ - \Delta G_{ads}^\circ \quad (8)$$

ζ -Potential Measurements. The ζ -potential was measured for aqueous dispersions of HNTs/polymer dispersions as a function of $R_{P:HNT}$ (Figure 3). The polymer concentration was varied from approximately 2×10^{-6} to 2×10^{-1} wt %, whereas the concentration of HNT was kept constant at 1 wt %.

The ζ -potential values of approximately -20 mV is observed at a low polymer concentration for all cases, in agreement with the expected value for bare HNT (-19.4 mV).²⁷ As expected for the nonionic polymer, the addition of HPC hardly alters the ζ -potential values. On the other hand, the addition of charged biopolymers shifted the ζ -potential values toward negative and positive values for pectin and chitosan, respectively. It should be noted that although the HNT/chitosan mixture can approach very high ζ -potential values, the largest in absolute value, a null charge is interpolated for $R_{P:HNT} \approx 4 \times 10^{-4}$.

For $R_{P:HNT} = 0.1$ and at constant ionic strength (NaCl 0.01 M), the effect of pH was monitored for HNT/charged polymer systems (Figure 4).

The trends of ζ -potential values for both HNT/chitosan and HNT/pectin dispersions showed that the ζ -potential decreases with pH. The presence of pectin moves the ζ -potential values toward slightly more negative values than the bare HNT. Such a difference is reduced at acidic pH when the pectin is expected to be protonated and therefore uncharged. On the other hand, chitosan presents the maximum positive charge density at acidic pH because of the protonation of the amino groups. Therefore, the changes induced in the ζ -potential values reflect the protonation equilibria of the biopolymer.

DISCUSSION

The stability of nanoclays in aqueous dispersion is controlled by several parameters such as surface charge, particle size, and solvent viscosity. The addition of a polymer can certainly play a role at the solid/liquid interface, contributing to the colloidal stability. Therefore, it is crucial to investigate the polymer adsorption and the corresponding equilibrium parameters to highlight the mechanism of formation and to find out the

Table 2. Adsorption Parameters from ITC Measurements for Polymer–HNT Dispersions

	K_{ads} ($\text{dm}^3 \text{ g}^{-1}$)	Z (g m^{-2})	ΔH_{ads}° (10^3 kJ mol^{-1})	ΔG_{ads}° (kJ mol^{-1})	ΔS_{ads}° ($\text{kJ mol}^{-1} \text{ K}^{-1}$)
chitosan	10.2 ± 1.5	$(2.6 \pm 0.1) \times 10^{-4}$	-47.0 ± 1.6	-19.8 ± 0.4	-157.8 ± 0.1
pectin	12 ± 2	$(2.5 \pm 0.1) \times 10^{-4}$	-0.73 ± 0.03	-20.2 ± 0.4	-2.40 ± 0.02
HPC	393 ± 92	$(5.15 \pm 0.08) \times 10^{-3}$	-2.17 ± 0.07	-28.9 ± 0.6	-7.17 ± 0.03

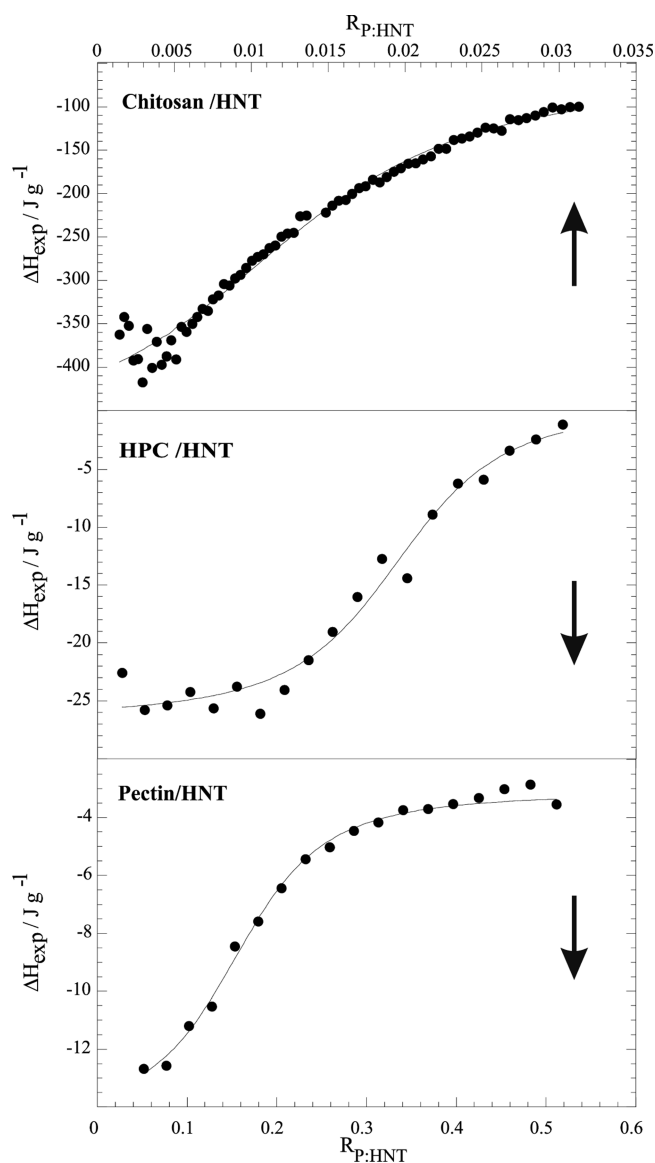


Figure 2. ITC data for HNT titration with chitosan, pectin, and HPC. Lines are best fits according to eqs 3–7.

amount of adsorbed macromolecule that can lead to steric/electrostatic stabilization of the nanoparticle dispersions.

ITC data provided direct access to the thermodynamic characterization of the investigated system. The $\Delta G_{\text{ads}}^{\circ}$ values (Table 2) show that the nonionic HPC has a stronger tendency to adsorb onto HNT whereas chitosan and pectin have a comparable affinity toward the nanoclay. Besides the largest affinity, HPC presents the largest loading amount at saturation onto the HNT nanotubes (Z values are approximately 1 order of magnitude larger, Table 2). It should be noted that the largest amount of HPC adsorbed per unit surface onto HNT is approximately twice as much as that of laponite nanodisks ($Z = 1.9 \times 10^{-3} \text{ g m}^{-2}$)⁴⁷ that, actually, have smaller characteristic sizes.

The adsorption mechanism/driving force can be highlighted by the enthalpy/entropy contributions. Although ΔH can be obtained by the correlation of $\Delta G_{\text{ads}}^{\circ}$ to temperature through the classical van't Hoff equation, this approach might be inappropriate because of the presence of supramolecular interactions, which might be largely influenced by the

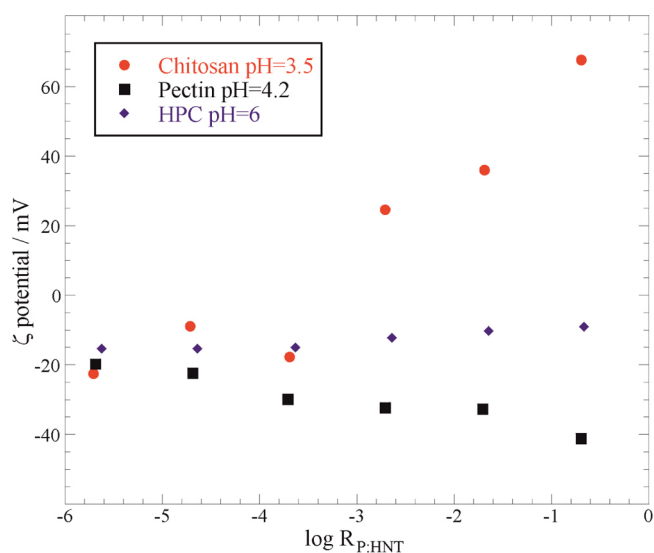


Figure 3. ζ -Potential values as a function of $R_{\text{P:HNT}}$ for HNT/polymer dispersions.

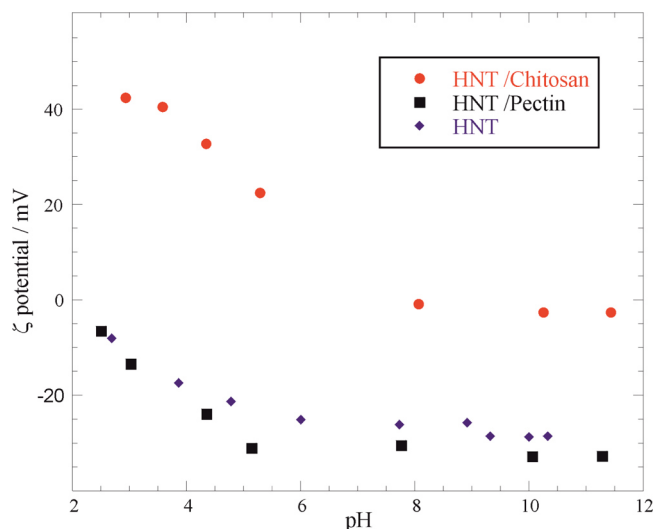


Figure 4. ζ -Potential values as a function of pH for HNT/chitosan and HNT/pectin citrus dispersions. Both systems had a HNT/polymer ratio of 10:1.

temperature variation. For instance, the eventual stoichiometry changes make the classical van't Hoff equation invalid for supramolecular equilibria.^{49,50} It is straightforward that only the calorimetric experiments provide direct and unambiguous insights into the heat exchange occurring during a given process, and this is particularly important for supramolecular associative processes in solution.^{50–52}

From ITC experiments, we find out that in all cases, $\Delta H_{\text{ads}}^{\circ}$ is strongly negative. This indicates that the polymer–nanoparticle interactions are favored as the driving forces for the adsorption phenomena. Our findings agree with reports on the adsorption of HPC on laponite nanoclay.⁴⁷ The entropic contribution for the polymer adsorption is always negative, demonstrating the loss of configuration freedom of the polymer in the adsorbed state. Another contribution to the entropy change for the adsorption phenomenon is related to the release of counterions and hydration water from polymer and/or nanoparticle surface. This contribution is expected to be positive, and in our case it is

not the dominant entropic factor. Such a peculiarity was observed for the polymer adsorbed onto nanoparticles where low curvature regions are present (i.e., disklike shape) as also evidenced by neutron-scattering experiments.^{47,53} On the other hand, polyelectrolytes/ionic micelle interactions are typically driven by entropic factors due to counterion release.⁵⁴

The colloidal stability of HNT in the presence of biopolymers can be discussed in light of the thermodynamics of the adsorption. Provided that the stability of dispersed particles in solution was not correlated to a change in the water/polymer solution viscosity (see [Supporting Information](#)), it is possible to speculate on the effect of polymer/HNT particle interactions. The level-off value of the optical density obtained from turbidimetric experiments reflects the amount of nanoparticles left in the solvent after equilibration. All of the investigated polymers generate T_{inf} values lower than that for the corresponding HNT aqueous dispersion, proving the enhancement of the HNT stability in water. As regards the timescale to approach the dispersion equilibrium, HPC is the more efficient polymer in retarding the sedimentation. The ζ -potential trends for chitosan- and pectin-based mixtures show that an electrostatic mechanism of nanotube stabilization exists. As a general feature, chitosan is efficient in stabilizing HNT dispersions under acidic pH, whereas pectin is recommended for the same purpose at basic pH values. The obtained results are consistent with the protonation equilibrium expected for both biopolyelectrolytes generating electrostatic interaction, which are strong enough to ensure a certain amount of polysaccharide “bound” on halloysite surfaces. In particular, pectin should adsorb within the HNT lumen onto the positively charged surface of alumina, altering the overall HNT charge toward more negative values. The opposite occurs for chitosan, which is selectively adsorbed on the outer silica surface. It is intriguing to follow the charge variation in HNT as a function of chitosan addition. In particular, a null charge is extrapolated at a chitosan/HNT ratio corresponding to $6.6 \times 10^{-6} \text{ g m}^{-2}$. This value is much smaller than the maximum loading ability (Z in [Table 2](#)) at which the halloysite charge inversion is observed. As regards the nonionic HPC, a nearly constant ζ -potential is obtained. On the other hand, turbidimetric studies evidenced that HPC is the most efficient polymer to stabilize HNTs in water. To compare the efficacy of a steric stabilization mechanism due to a polymer layer adsorbed onto HNT, some insights into the attached polymer configuration are needed. A similar approach was used to interpret the effect of poly(*N*-isopropylacrylamide) adsorption on the steric stabilization of HNT in water.³⁶ The reduced tethered density (Σ) of a polymer can be calculated as⁵⁵

$$\Sigma = \sigma\pi R_g^2 \quad (9)$$

where σ is the grafting density (chain/area) and R_g is the polymer gyration radius. The σ values are obtained from ITC data (Z values in [Table 2](#)), whereas $R_g = 15$, 60, and 39.5 nm were used for pectin,⁵⁶ chitosan,⁵⁷ and HPC,⁵⁸ respectively. On the basis of the Σ values, the polymer configuration at the solid/liquid interface is identified as (1) weakly interacting ($\Sigma < 1$), (2) mushroom-to-brush transition ($1 < \Sigma < 5$), and (3) highly stretched regime ($\Sigma > 5$). We calculated the Σ values to be 1.6, 14, and 190 for pectin, chitosan, and HPC, respectively. These results indicate that HPC is in a stretched conformation at the interface, and therefore its adsorption could be

considered very efficient in creating a steric barrier around the nanotubes against agglomeration and precipitations.

CONCLUSIONS

We studied the thermodynamic and surface properties of the nanotube HNT dispersed in aqueous solutions of chitosan, pectin, and hydroxypropyl cellulose. Thermodynamic properties were obtained through ITC measurements. The experimental data were interpreted on the basis of a model of adsorption of the polymer on the nanoparticle and allowed the calculation of the standard variation in free energy, enthalpy, and entropy of the process. The stability of the dispersions is controlled by the interactions (electrostatic and steric) between the dispersed particles.

When repulsion is the dominant factor as in the case of the HNT/HPC system, the system remains stable and in a dispersed state as shown by turbidimetric kinetics. Modified nanotubes through interactions with polymers may lead to the formation of colloidal systems with controlled stability, which offers different perspectives of new applications (in cosmetics and medical implants) of these dispersions such as good carriers of substances to be released in response to external stimuli such as pH.

ASSOCIATED CONTENT

Supporting Information

The Supporting Information is available free of charge on the ACS Publications website at DOI: [10.1021/acs.langmuir.7b00600](https://doi.org/10.1021/acs.langmuir.7b00600).

Best fits for turbidimetric data ([PDF](#))

AUTHOR INFORMATION

Corresponding Author

*E-mail: giuseppe.lazzara@unipa.it.

ORCID

Giuseppe Lazzara: [0000-0003-1953-5817](https://orcid.org/0000-0003-1953-5817)

Notes

The authors declare no competing financial interest.

ACKNOWLEDGMENTS

The work was financially supported by the University of Palermo, FIRB 2012 (prot. RBFR12ETLS) and PON-TECLA (PON03PE_00214_1).

REFERENCES

- (1) Lvov, Y. M.; Shchukin, D. G.; Möhwald, H.; Price, R. R. Halloysite Clay Nanotubes for Controlled Release of Protective Agents. *ACS Nano* **2008**, *2*, 814–820.
- (2) Ruiz-Hitzky, E.; Aranda, P.; Darder, M.; Rytwo, G. Hybrid Materials Based on Clays for Environmental and Biomedical Applications. *J. Mater. Chem.* **2010**, *20*, 9306–9321.
- (3) Viseras, C.; Cerezo, P.; Sanchez, R.; Salcedo, I.; Aguzzi, C. Current Challenges in Clay Minerals for Drug Delivery. *Appl. Clay Sci.* **2010**, *48*, 291–295.
- (4) Pasbakhsh, P.; Churchman, G. J.; Keeling, J. L. Characterisation of Properties of Various Halloysites Relevant to Their Use as Nanotubes and Microfibre Fillers. *Appl. Clay Sci.* **2013**, *74*, 47–57.
- (5) Duce, C.; Cipriotti, S. V.; Ghezzi, L.; Ierardi, V.; Tinè, M. R. Thermal Behavior Study of Pristine and Modified Halloysite Nanotubes. *J. Therm. Anal. Calorim.* **2015**, *121*, 1011–1019.
- (6) Joussein, E.; Petit, S.; Churchman, G.; Theng, B.; Righi, D.; Delvaux, B. Halloysite Clay Minerals—A Review. *Clay Miner.* **2005**, *40*, 383–426.

- (7) Shchukin, D. G.; Sukhorukov, G. B.; Price, R. R.; Lvov, Y. M. Halloysite Nanotubes as Biomimetic Nanoreactors. *Small* **2005**, *1*, 510–513.
- (8) Du, M.; Guo, B.; Liu, M.; Jia, D. Preparation and Characterization of Polypropylene Grafted Halloysite and Their Compatibility Effect to Polypropylene/Halloysite Composite. *Polym. J.* **2006**, *38*, 1198–1204.
- (9) Liu, M.; Guo, B.; Du, M.; Jia, D. Drying Induced Aggregation of Halloysite Nanotubes in Polyvinyl Alcohol/Halloysite Nanotubes Solution and Its Effect on Properties of Composite Film. *Appl. Phys. A* **2007**, *88*, 391–395.
- (10) Siracusa, V.; Blanco, I.; Romani, S.; Tylewicz, U.; Rocculi, P.; Rosa, M. D. Poly(lactic Acid)-Modified Films for Food Packaging Application: Physical, Mechanical, and Barrier Behavior. *J. Appl. Polym. Sci.* **2012**, *125*, E390–E401.
- (11) Rabea, E. I.; Badawy, M. E.-T.; Stevens, C. V.; Smagghe, G.; Steurbaut, W. Chitosan as Antimicrobial Agent: Applications and Mode of Action. *Biomacromolecules* **2003**, *4*, 1457–1465.
- (12) Cavallaro, G.; Lazzara, G.; Milioto, S.; Palmisano, G.; Parisi, F. Halloysite Nanotube with Fluorinated Lumen: Non-Foaming Nanocapsule for Storage and Controlled Release of Oxygen in Aqueous Media. *J. Colloid Interface Sci.* **2014**, *417*, 66–71.
- (13) Abdullayev, E.; Abbasov, V.; Tursunbayeva, A.; Portnov, V.; Ibrahimov, H.; Mukhtarova, G.; Lvov, Y. Self-Healing Coatings Based on Halloysite Clay Polymer Composites for Protection of Copper Alloys. *ACS Appl. Mater. Interfaces* **2013**, *5*, 4464–4471.
- (14) Shchukin, D. G.; Lamaka, S. V.; Yasakau, K. A.; Zheludkevich, M. L.; Ferreira, M. G. S.; Möhwald, H. Active Anticorrosion Coatings with Halloysite Nanocapsules. *J. Phys. Chem. C* **2008**, *112*, 958–964.
- (15) Shi, Y.-F.; Tian, Z.; Zhang, Y.; Shen, H.-B.; Jia, N.-Q. Functionalized Halloysite Nanotube-Based Carrier for Intracellular Delivery of Antisense Oligonucleotides. *Nanoscale Res. Lett.* **2011**, *6*, 608.
- (16) Jana, S.; Kondakova, A. V.; Shevchenko, S. N.; Sheval, E. V.; Gonchar, K. A.; Timoshenko, V. Y.; Vasiliev, A. N. Halloysite Nanotubes with Immobilized Silver Nanoparticles for Anti-Bacterial Application. *Colloids Surf., B* **2017**, *151*, 249–254.
- (17) Viseras, M. T.; Aguzzi, C.; Cerezo, P.; Viseras, C.; Valenzuela, C. Equilibrium and Kinetics of 5-Aminosalicylic Acid Adsorption by Halloysite. *Microporous Mesoporous Mater.* **2008**, *108*, 112–116.
- (18) Liu, M.; Zhang, Y.; Wu, C.; Xiong, S.; Zhou, C. Chitosan/Halloysite Nanotubes Bionanocomposites: Structure, Mechanical Properties and Biocompatibility. *Int. J. Biol. Macromol.* **2012**, *51*, 566–575.
- (19) Dzamukova, M. R.; Naumenko, E. A.; Lvov, Y. M.; Fakhrullin, R. F. Enzyme-Activated Intracellular Drug Delivery with Tubule Clay Nanoformulation. *Sci. Rep.* **2015**, *5*, 10560.
- (20) Lvov, Y.; Aerov, A.; Fakhrullin, R. Clay Nanotube Encapsulation for Functional Biocomposites. *Adv. Colloid Interface Sci.* **2014**, *207*, 189–198.
- (21) Tully, J.; Yendluri, R.; Lvov, Y. Halloysite Clay Nanotubes for Enzyme Immobilization. *Biomacromolecules* **2016**, *17*, 615–621.
- (22) Porta, V. D.; Bramanti, E.; Campanella, B.; Tiné, M. R.; Duce, C. Conformational Analysis of Bovine Serum Albumin Adsorbed on Halloysite Nanotubes and Kaolinite: A Fourier Transform Infrared Spectroscopy Study. *RSC Adv.* **2016**, *6*, 72386–72398.
- (23) Fakhrullina, G. I.; Akhatova, F. S.; Lvov, Y. M.; Fakhrullin, R. F. Toxicity of Halloysite Clay Nanotubes in Vivo: A *Caenorhabditis elegans* Study. *Environ. Sci.: Nano* **2015**, *2*, 54–59.
- (24) Shutava, T. G.; Fakhrullin, R. F.; Lvov, Y. M. Spherical and Tubule Nanocarriers for Sustained Drug Release. *Curr. Opin. Pharmacol.* **2014**, *18*, 141–148.
- (25) Wei, W.; Minullina, R.; Abdullayev, E.; Fakhrullin, R.; Mills, D.; Lvov, Y. Enhanced Efficiency of Antiseptics with Sustained Release from Clay Nanotubes. *RSC Adv.* **2014**, *4*, 488–494.
- (26) Cavallaro, G.; Lazzara, G.; Milioto, S.; Parisi, F.; Sanzillo, V. Modified Halloysite Nanotubes: Nanoarchitectures for Enhancing the Capture of Oils from Vapor and Liquid Phases. *ACS Appl. Mater. Interfaces* **2014**, *6*, 606–612.
- (27) Cavallaro, G.; Lazzara, G.; Milioto, S. Exploiting the Colloidal Stability and Solubilization Ability of Clay Nanotubes/Ionic Surfactant Hybrid Nanomaterials. *J. Phys. Chem. C* **2012**, *116*, 21932–21938.
- (28) Cavallaro, G.; Lazzara, G.; Milioto, S.; Parisi, F. Hydrophobically Modified Halloysite Nanotubes as Reverse Micelles for Water-in-Oil Emulsion. *Langmuir* **2015**, *31*, 7472–7478.
- (29) Owoseni, O.; Nyankson, E.; Zhang, Y.; Adams, S. J.; He, J.; McPherson, G. L.; Bose, A.; Gupta, R. B.; John, V. T. Release of Surfactant Cargo from Interfacially-Active Halloysite Clay Nanotubes for Oil Spill Remediation. *Langmuir* **2014**, *30*, 13533–13541.
- (30) Pasbakhsh, P.; Ismail, H.; Fauzi, M. N. A.; Bakar, A. A. EPDM/Modified Halloysite Nanocomposites. *Appl. Clay Sci.* **2010**, *48*, 405–413.
- (31) Yah, W. O.; Takahara, A.; Lvov, Y. M. Selective Modification of Halloysite Lumen with Octadecylphosphonic Acid: New Inorganic Tubular Micelle. *J. Am. Chem. Soc.* **2012**, *134*, 1853–1859.
- (32) Barrientos-Ramírez, S.; de Oca-Ramírez, G. M.; Ramos-Fernández, E. V.; Sepúlveda-Escribano, A.; Pastor-Blas, M. M.; González-Montiel, A. Surface Modification of Natural Halloysite Clay Nanotubes with Aminosilanes. Application as Catalyst Supports in the Atom Transfer Radical Polymerization of Methyl Methacrylate. *Appl. Catal., A* **2011**, *406*, 22–33.
- (33) Massaro, M.; Amorati, R.; Cavallaro, G.; Guernelli, S.; Lazzara, G.; Milioto, S.; Noto, R.; Poma, P.; Riela, S. Direct Chemical Grafted Curcumin on Halloysite Nanotubes as Dual-Responsive Prodrug for Pharmacological Applications. *Colloids Surf., B* **2016**, *140*, 505–513.
- (34) Massaro, M.; Colletti, C. G.; Noto, R.; Riela, S.; Poma, P.; Guernelli, S.; Parisi, F.; Milioto, S.; Lazzara, G. Pharmaceutical Properties of Supramolecular Assembly of Co-Loaded Cardanol/Triazole-Halloysite Systems. *Int. J. Pharm.* **2015**, *478*, 476–485.
- (35) Cavallaro, G.; Lazzara, G.; Massaro, M.; Milioto, S.; Noto, R.; Parisi, F.; Riela, S. Biocompatible Poly(*N*-isopropylacrylamide)-Halloysite Nanotubes for Thermoresponsive Curcumin Release. *J. Phys. Chem. C* **2015**, *119*, 8944–8951.
- (36) Cavallaro, G.; Lazzara, G.; Milioto, S.; Parisi, F. Steric Stabilization of Modified Nanoclays Triggered by Temperature. *J. Colloid Interface Sci.* **2016**, *461*, 346–351.
- (37) Biddeci, G.; Cavallaro, G.; Di Blasi, F.; Lazzara, G.; Massaro, M.; Milioto, S.; Parisi, F.; Riela, S.; Spinelli, G. Halloysite Nanotubes Loaded with Peppermint Essential Oil as Filler for Functional Biopolymer Film. *Carbohydr. Polym.* **2016**, *152*, 548–557.
- (38) Gorrasi, G. Dispersion of Halloysite Loaded with Natural Antimicrobials into Pectins: Characterization and Controlled Release Analysis. *Carbohydr. Polym.* **2015**, *127*, 47–53.
- (39) Gorrasi, G.; Pantani, R.; Murariu, M.; Dubois, P. PLA/Halloysite Nanocomposite Films: Water Vapor Barrier Properties and Specific Key Characteristics. *Macromol. Mater. Eng.* **2014**, *299*, 104–115.
- (40) Bertolino, V.; Cavallaro, G.; Lazzara, G.; Merli, M.; Milioto, S.; Parisi, F.; Sciascia, L. Effect of the Biopolymer Charge and the Nanoclay Morphology on Nanocomposite Materials. *Ind. Eng. Chem. Res.* **2016**, *55*, 7373–7380.
- (41) Liu, M.; Wu, C.; Jiao, Y.; Xiong, S.; Zhou, C. Chitosan-Halloysite Nanotubes Nanocomposite Scaffolds for Tissue Engineering. *J. Mater. Chem. B* **2013**, *1*, 2078–2089.
- (42) Naumenko, E. A.; Guryanov, I. D.; Yendluri, R.; Lvov, Y. M.; Fakhrullin, R. F. Clay Nanotube-Biopolymer Composite Scaffolds for Tissue Engineering. *Nanoscale* **2016**, *8*, 7257–7271.
- (43) Fakhrullin, R. F.; Lvov, Y. M. Halloysite Clay Nanotubes for Tissue Engineering. *Nanomedicine* **2016**, *11*, 2243–2246.
- (44) Cavallaro, G.; Donato, D. I.; Lazzara, G.; Milioto, S. Films of Halloysite Nanotubes Sandwiched between Two Layers of Biopolymer: From the Morphology to the Dielectric, Thermal, Transparency, and Wettability Properties. *J. Phys. Chem. C* **2011**, *115*, 20491–20498.
- (45) Patrickios, C. S.; Hertler, W. R.; Hatton, T. A. Protein Complexation with Acrylic Polyampholytes. *Biotechnol. Bioeng.* **1994**, *44*, 1031–1039.
- (46) McFarlane, N. L.; Wagner, N. J.; Kaler, E. W.; Lynch, M. L. Calorimetric Study of the Adsorption of Poly(ethylene oxide) and

Poly(vinyl pyrrolidone) onto Cationic Nanoparticles. *Langmuir* **2010**, *26*, 6262–6267.

(47) Cavallaro, G.; Lazzara, G.; Milioto, S. Aqueous Phase/Nanoparticles Interface: Hydroxypropyl Cellulose Adsorption and Desorption Triggered by Temperature and Inorganic Salts. *Soft Matter* **2012**, *8*, 3627–3633.

(48) Tellinghuisen, J. Calibration in Isothermal Titration Calorimetry: Heat and Cell Volume from Heat of Dilution of NaCl(aq). *Anal. Biochem.* **2007**, *360*, 47–55.

(49) Holtzer, A.; Holtzer, M. F. Use of the Van't Hoff Relation in Determination of the Enthalpy of Micelle Formation. *J. Phys. Chem.* **1974**, *78*, 1442–1443.

(50) De Lisi, R.; Lazzara, G.; Milioto, S. Temperature-Controlled Poly(propylene) Glycol Hydrophobicity on the Formation of Inclusion Complexes with Modified Cyclodextrins. A DSC and ITC Study. *Phys. Chem. Chem. Phys.* **2011**, *13*, 12571–12577.

(51) Terekhova, I. V.; Romanova, A. O.; Kumeev, R. S.; Fedorov, M. V. Selective Na⁺/K⁺ Effects on the Formation of α -Cyclodextrin Complexes with Aromatic Carboxylic Acids: Competition for the Guest. *J. Phys. Chem. B* **2010**, *114*, 12607–12613.

(52) Taboada, P.; Mosquera, V.; Attwood, D.; Yang, Z.; Booth, C. Enthalpy of Micellisation of a Diblock Copoly(oxyethylene/oxypropylene) by Isothermal Titration Calorimetry. Comparison with the Van't Hoff Value. *Phys. Chem. Chem. Phys.* **2003**, *5*, 2625–2627.

(53) Nelson, A.; Cosgrove, T. A Small-Angle Neutron Scattering Study of Adsorbed Poly(ethylene oxide) on Laponite. *Langmuir* **2004**, *20*, 2298–2304.

(54) Chiappisi, L.; Gradzielski, M. Co-Assembly in Chitosan–Surfactant Mixtures: Thermodynamics, Structures, Interfacial Properties and Applications. *Adv. Colloid Interface Sci.* **2015**, *220*, 92–107.

(55) Peng, S.; Bhushan, B. Smart Polymer Brushes and Their Emerging Applications. *RSC Adv.* **2012**, *2*, 8557.

(56) Fishman, M. L.; El-Atawy, Y. S.; Sondey, S. M.; Gillespie, D. T.; Hicks, K. B. Component and Global Average Radii of Gyration of Pectins from Various Sources. *Carbohydr. Polym.* **1991**, *15*, 89–104.

(57) Morariu, S.; Brunchi, C.-E.; Bercea, M. The Behavior of Chitosan in Solvents with Different Ionic Strengths. *Ind. Eng. Chem. Res.* **2012**, *51*, 12959–12966.

(58) Martins, R. M.; da Silva, C. A.; Becker, C. M.; Samios, D.; Christoff, M.; Bica, C. I. D. Anionic Surfactant Aggregation with (Hydroxypropyl)Cellulose in the Presence of Added Salt. *J. Braz. Chem. Soc.* **2006**, *17*, 944–953.

Attached Paper II

Effect of the Biopolymer Charge and the Nanoclay Morphology on Nanocomposite Materials

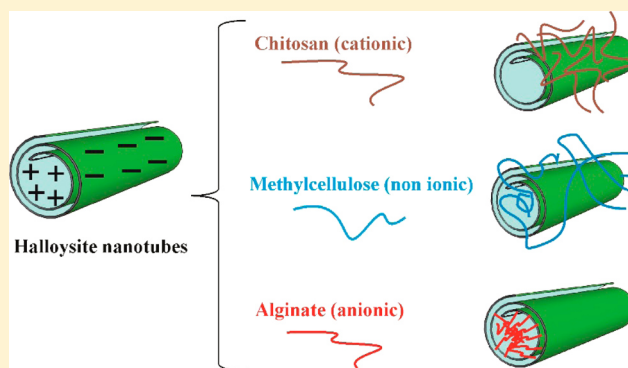
Vanessa Bertolino,[†] Giuseppe Cavallaro,[†] Giuseppe Lazzara,^{*,†} Marcello Merli,[‡] Stefana Milioto,[†] Filippo Parisi,[†] and Luciana Sciascia[‡]

[†]Dipartimento di Fisica e Chimica, Università degli Studi di Palermo, Viale delle Scienze pad. 17, Palermo I-90128, Italy

[‡]Dipartimento di Scienze della Terra e del Mare, Università degli Studi di Palermo, via Archirafi 36, Palermo I-90123, Italy

S Supporting Information

ABSTRACT: This work represents a contribution to the design, preparation, and characterization of nanocomposite materials based on biocompatible components. The effects of composition, filler geometry, and polymer charge were highlighted, and their role on the final properties of the nanocomposites was revealed. We combined some biopolymers (methylcellulose, alginate, chitosan) with two nanoclays (kaolinite sheets and halloysite nanotubes) to prepare nanocomposites by means of the casting method from water. The thermal stability, the surface wettability, and the mechanical properties of the obtained films were studied. SEM micrographs highlighted the surface morphology of the biocomposite materials. X-ray data allowed us to correlate the mesoscopic structure to the properties of these nanocomposites.



INTRODUCTION

Petrochemical-based plastics are widely used as packaging materials because of their large availability at relatively low cost and good mechanical performance. Nowadays, their use has to be restricted because they are not biodegradable and so pose serious ecological problems.¹ The growing environmental attention requires packaging films with both user-friendly and eco-friendly features. Examples of these packaging materials include biobased polymers, bioplastic or biopolymer packaging products made of raw materials originating from agricultural or marine sources.² The main issue related to the use of these biopolymers is the strong hydrophilic character, high degradation, and inadequate mechanical properties in moist environments.³⁴ The biopolymer functionality can be tuned through its combination with additives, such as plasticizers and nanoparticles.^{5–7} Nanocomposites represent an alternative to conventional technologies for improving polymer properties, by adding particles for which at least one dimension is in the nanometer range.⁸ The entity of the interactions is strongly affected by the nature of the dispersed phase; it is maximized passing from isodimensional particles to nanotubes.⁹ These nanocomposites may exhibit markedly improved mechanical, thermal, optical, and physicochemical properties compared to those of the pure polymer or conventional (microscale) composites as first demonstrated by Kojima and co-workers¹⁰ for nylon–clay nanocomposites. As examples, an enhancement of the mechanical performances (Young modulus and stress at breaking) and heat resistance as well as a decrease of gas permeability and flammability were observed.^{11–13} Due to the

large surface/volume ratio of the reinforcing phase, low content of nanofillers (<5–6% wt) might cause a significant improvement of some physicochemical properties.^{9,10,14,15} In this work, halloysite nanotubes (HNT) and kaolinite (Kao) were used as natural nanofillers. Their suitability is primarily due to the ecocompatibility and nontoxicity. Although halloysite ($\text{Al}_2\text{Si}_2\text{O}_5(\text{OH})_4 \cdot 2\text{H}_2\text{O}$) and kaolinite ($\text{Al}_2\text{Si}_2\text{O}_5(\text{OH})_4$) have similar chemistry, they possess different morphology.¹⁶ HNT has a characteristic spiral shape, forming hollow tubular nanoparticles.^{17–19} The HNT cavity is suitable for the encapsulation of active molecules with antioxidant and antimicrobial capacity.^{20,21} Biocompatibility of halloysite has been proved for yeast,²² bacteria,²³ nematodes,²⁴ and human cell cultures.²⁵ Kao is an aluminosilicate mineral characterized by a sheet-like geometry. The morphology of HNT provides a different chemistry at the inner and outer surfaces of the nanotube. Such a peculiarity endowed selective modification protocols based on electrostatic interactions^{26–29} or specific chemical reactions.^{30–32} As concerns the biopolymers, we used methylcellulose, alginate, and chitosan, which are nonionic, anionic, and cationic polymers, respectively. They are nontoxic, biocompatible, and biodegradable, and are widely used for the development of systems for release of drugs,^{33–36} tissue engineering,³⁷ decontamination,^{38,39} and food additives.⁴⁰

Received: May 11, 2016

Revised: June 24, 2016

Accepted: June 24, 2016

Published: June 24, 2016

This paper contributes to the knowledge of the sustainable nanocomposite perspective for industrial applications, such as packaging, because of their chemical and engineering properties (mechanical performances, thermal stability, and wettability), which can be properly controlled by the specific biopolymer/nanoclay interactions.

MATERIALS AND METHODS

Methylcellulose (av Mw ca. 14 kg mol⁻¹, 27.5–31.5 wt % methoxy), sodium alginate (Mw = 70–100 kg mol⁻¹), chitosan (75–85% deacetylated, Mw = 50–190 kg mol⁻¹), glacial acetic acid, and halloysite (HNT) are from Sigma. Kaolinite (Kao) is a Fluka product. All of the products were used without further purification.

Nanocomposite Preparation. Biopolymer/clay nanocomposites were prepared by means of the aqueous casting method as described elsewhere.⁴¹ Briefly, we prepared a 2 wt % aqueous solution of each biopolymer (methylcellulose, chitosan, and alginate) under stirring at 70 °C for ca. 2 h. The glacial acetic acid was used to solubilize chitosan in water, given the low solubility of polymer at neutral pH. Then, an appropriate amount of filler (HNT or Kao) was added to the biopolymer solutions and kept under stirring overnight. The well-dispersed biopolymer/filler mixtures were poured into glass Petri dishes at 40 °C for ca. 24 h to evaporate water. The obtained films were easily removed from the supports and stored in a desiccator at room temperature. The filler concentration (C_f) expressed as weight percent (grams of filler/100 g of nanocomposites) was systematically changed.

Thermogravimetric Analysis. Thermogravimetric (TG) measurements were conducted by using a Q5000 IR apparatus (TA Instruments) under a nitrogen flow of 25 and 10 cm³ min⁻¹ for the sample and the balance, respectively. The weight of each sample was ca. 5 mg. Experiments were performed by heating the sample from room temperature to 900 °C with a rate of 10 °C min⁻¹ in a platinum crucible. For each sample we determined the polymer degradation temperature (T_d), the moisture loss (MD₁₂₀), and the percentage of residual matter at 900 °C (MR₉₀₀). MD₁₂₀ and MR₉₀₀ values were obtained by the dependence of the mass loss to the temperature (TG curves), while T_d values were estimated at the maximum of the temperature dependence of the first-order derivative functions of the mass loss percentage (DTG curves).

Scanning Electron Microscopy. The morphology of the nanocomposites was studied by using a microscope ESEM FEI QUANTA 200F. Before each experiment, the sample surface was coated with gold in argon by means of an Edwards sputter coater s150a to minimize charging under electron beam.

Dynamic-Mechanical Analysis. Dynamic-mechanical measurements (DMA) were performed using a DMA Q800 apparatus (TA Instruments). The samples were films of rectangular shape (10.00 × 6.00 × 0.060 mm³). Tensile tests were carried out with a stress ramp of 1 MPa min⁻¹ at 26.0 ± 0.5 °C. The analysis of the stress versus strain curves allowed us to determine the elastic modulus (E), the tensile strength (σ_r), and the elongation at breaking point ($\varepsilon\%$).

DMA experiments were also carried out in the oscillatory regime (frequency of 1.0 Hz) by heating the sample from 100 °C to film deterioration with a rate of 4 °C min⁻¹.

Contact Angle. Contact angle measurements were performed through an optical contact angle apparatus (OCA 20, Data Physics Instruments) equipped with a CCD camera with high resolution power. SCA 20 software (Data Physics

Instruments) was used for data acquisition. The water contact angle just after the deposition (Φ_i) was measured by the method by placing a droplet of 5.0 ± 0.5 μL onto the sample surface. Both the support and the injecting syringe were kept at 25.0 ± 0.1 °C.

Each sample was analyzed five times, and the average values are reported.

X-ray Diffraction. X-ray diffraction (XRD) analysis was performed by means of a Philips PW 1729 diffractometer (model RX) in Bragg–Brentano geometry using Ni-filtered Cu K α radiation ($\lambda = 1.5406 \text{ \AA}$, 40 kV, 40 mA). Diffractograms were registered in the range of scattering angles $2\theta = 4\text{--}60^\circ$, with a scan increment of 0.01°/s.

RESULTS AND DISCUSSIONS

Thermal Properties. TG analysis is a proper method to highlight the thermal stability of polymers,^{42,43} and nanocomposites.^{7,44} Moreover, the TG method was reported for investigating dehydration and dehydroxylation of nanoclays.⁴⁵ MD₁₂₀ values (Table 1) provided evidence that the water content of methylcellulose (nonionic) is much lower with respect to those of alginate (anionic) and chitosan (cationic).

Table 1. Degradation Temperature and Water Content for Biopolymers^a

polymer	$T_d/^\circ\text{C}$	MD ₁₂₀ /wt %
alginate	251.1	15.3
chitosan	304.6	11.2
methylcellulose	360.2	3.5

^aThe error estimated by standard deviation on at least three independent measurements is ±0.5 °C for T_d and ±0.1 wt % for MD₁₂₀.

Filling polymers with clay nanoparticles (HNT and Kao) shaped the thermal behavior of bioplastics. T_d values showed that the filler morphology affected the polymers' degradation (Figure 1).

For the bionanocomposites based on methylcellulose and chitosan, nanoclays generate a slight T_d decrease. Alginate was thermally stabilized by the addition of HNT, while an opposite effect was observed in the presence of kaolinite. These results could be explained by taking into account the different clay morphology, which influences the specific polymer/filler interactions. As reported in literature studies,⁴⁶ HNT can entrap polymers within their tubular cavity, determining an increase of their thermal stability;⁴⁷ such a phenomenon cannot be observed for flat kaolinite. Moreover, the homogeneous dispersion of HNT into the anionic matrix⁴⁸ generates an efficient barrier effect on the volatile products.⁷ The thermal stability is a consequence of the preferential interactions between inner and outer HNT surfaces and biopolymers (Scheme 1).

Accordingly, one has to consider that methylcellulose is neutral, chitosan is cationic, and alginate is anionic. Furthermore, in solution the inner and outer surfaces of the tubular structure of the HNT particles have different charges,¹⁹ being that the inner surface is positively charged, while the external one is negatively charged. This view was confirmed by the DTG curves of the nanocomposites at $C_f = 50 \text{ wt \%}$ (Figure 2), which showed a peculiar effect in the high temperature range.

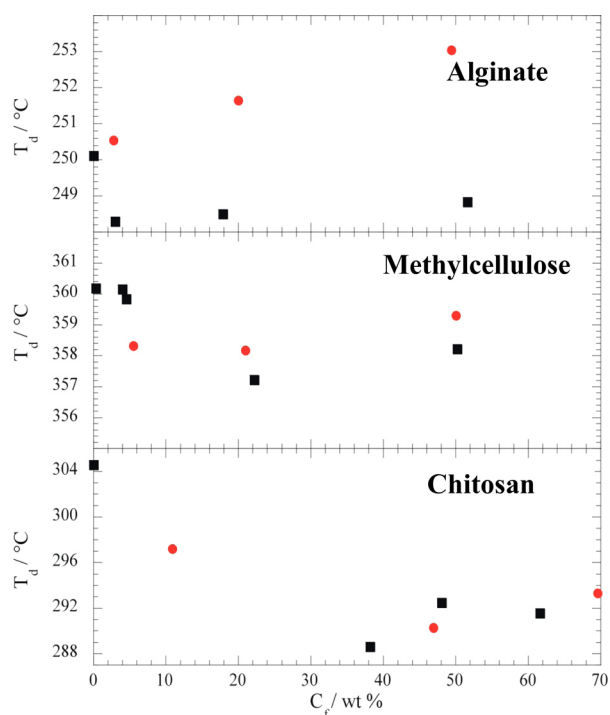


Figure 1. Degradation temperatures as functions of concentration of nanofiller (●, HNT; ■, kaolinite). The error estimated by standard deviation on at least three independent measurements is ± 0.5 °C for T_d .

Scheme 1. Mechanisms of Polymer/HNT Interaction Based on Electrostatic Interactions

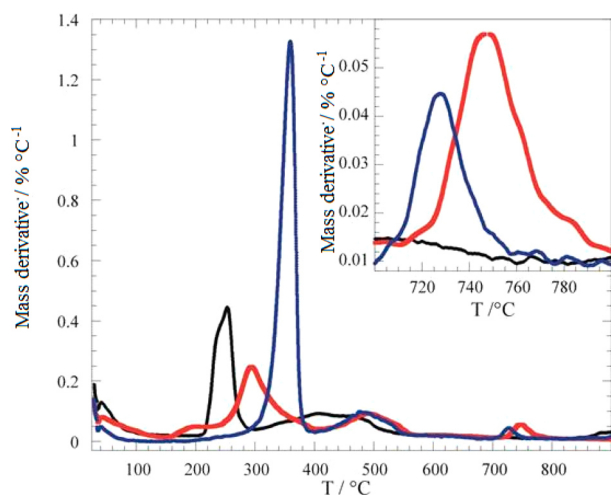
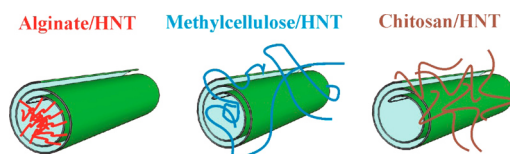


Figure 2. DTG curves of the polymers (blue for methylcellulose, black for alginate, red for chitosan) containing 50 wt % of HNT.

We observed DTG peaks for chitosan and methylcellulose nanocomposites between 700 and 800 °C, which are similar to those of pristine HNT. These peaks are attributed to the dehydroxylation of alumina groups of the HNT lumen.⁴⁵ On

the contrary, the DTG curve of alginate/HNT does not show the dehydroxylation process, in agreement with the specific interaction between the polymer and HNT inner surface. Namely, the ionic exchange involving alginate COO^- groups and Al–OH groups generates significant structural changes that cancel out the weight loss at 700–800 °C due to dehydroxylation of alumina groups.

Thermograms were also collected on the same samples at variable heating rates (β) to determine the activation energy (E_a) of degradation. A larger filler concentration was chosen. The Friedman's method was used to calculate E_a without making any assumption on the reaction mechanism. The following equation was used

$$\ln(\beta \, d\alpha/dT) = \ln[Af(\alpha)] - E_a/RT \quad (1)$$

where $d\alpha/dT$ is the first derivative of α with respect to temperature and $f(\alpha)$ is a function of the extent of conversion (α) that depends on the degradation mechanism. In this case the E_a values, at each α value, are obtained from the slopes of the $\ln(\beta \, d\alpha/dT)$ versus $1/T$ plot.

For all of the investigated nanocomposites, E_a does not depend on α , and therefore the average values are provided in Table 2.

Table 2. Activation Energy Values for Biopolymers and Nanocomposites

material	$E_a/\text{kJ mol}^{-1}$
alginate	236 ± 12
alginate/HNT	400 ± 30
alginate/Kao	250 ± 20
methylcellulose	191 ± 8
methylcellulose/HNT	209 ± 3
methylcellulose/Kao	193 ± 3
chitosan	197 ± 25
chitosan/HNT	212 ± 24
chitosan/Kao	266 ± 20

The E_a data provide evidence for the effect of filler and its morphology on polymer thermal stability. In particular, HNT generated a strong enhancement of the energetic barrier to the degradation process of alginate, according to the proposed model of interaction (Scheme 1). Such an effect was not observed for Kao. On the contrary, the filler morphology does not influence the E_a value for methylcellulose.

Mechanical Properties. An example of the stress versus strain curve for the investigated biofilms is presented in Figure 3.

As concerns the pristine biopolymers, we found that alginate possesses the best mechanical performance (Table 3), with the elastic modulus and breaking stress having the largest values within the investigated systems.

The E and σ_r values measured for pristine polymers are comparable to the mechanical properties of petrochemical-based plastics used as packaging materials, such as polyethylene terephthalate (PET) ($E = 2000$ MPa)⁴⁹ and polyvinyl chloride (PVC) ($E = 800$ MPa),⁵⁰ and comparable to the mechanical properties of other biopolymers, such as polylactic acid (PLA) ($E = 3550$ MPa).^{51,52}

For both methylcellulose and chitosan, the nanofiller addition did not affect the elastic modulus as well as the tensile strength (Figure 4). On the other hand, the presence of HNT into alginate matrix determined an increase of the elastic

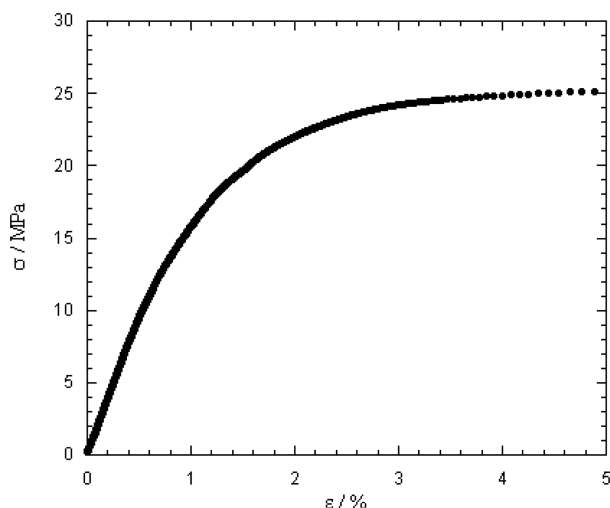


Figure 3. Stress–strain curve for methylcellulose–HNT nanocomposite ($C_f = 13$ wt %).

Table 3. Elastic Modulus and Breaking Stress for the Biopolymers

polymer	E/MPa	σ_r/MPa
alginate	1602	24
chitosan	1172	14
methylcellulose	1487	16

modulus, while the opposite effect was observed for alginate/Kao nanocomposites, showing a decreasing σ_r versus C_f trend as well. Filling alginate with HNT generated an increase of the tensile strength for $C_f < 30$ wt %, whereas at very high C_f the σ_r value is lower compared to that of pristine polymer. Similar results were observed for HNT/pectin nanocomposites.⁷ These results highlight the important role of electrostatic interactions

and morphology on the mechanical performances of the nanocomposites. DMA measurements in the oscillatory regime as a function of temperature endowed to estimate the glass transition of polymers, which was determined at the maximum of $\tan \phi$ versus T function.

It should be noted that alginate as well as alginate-based films did not show any significant variation of the $\tan \phi$ versus T curve because they did not undergo either structural changes or phase transitions up to the degradation of polymer matrix (see the Supporting Information). On the contrary, chitosan and its nanocomposites showed peaks in the $\tan \phi$ versus T curve at ca. 180 °C, while methylcellulose-based films evidenced a peak on $\tan \phi$ versus T curve at ca. 200 °C. The addition of low molecular weight additives, which can act as plasticizers, can significantly change the T_g .^{53,54} As illustrated in Figure 5, for all bionanocomposites a reduction of the peak intensity was observed by increasing the filler concentration; this finding could be attributed to a higher capacity of the pure polymer to dissipate energy as viscous response at elevated temperature.⁵⁵ The T_g values of nanocomposites showed very small changes upon increasing the filler content; this evidence is attributed to interactions between the polymer and the filler.⁵⁵ For magnetic nanocomposites in epoxy resin the increase of T_g due to the addition of nanoparticles is attributed to reduced mobility of macromolecular chains.⁵⁶

Wettability and Morphology. Potential applications of bionanocomposite materials are strongly influenced by the films' wettability. This parameter reflects the structure and the chemical composition of the surface affecting several properties, such as the biocompatibility, adhesion, and selective adsorption on a solid surface.⁵⁷ The wettability is strictly correlated to the water contact angle (θ_i) of a drop just deposited on the film surface. Table 4 collects θ_i values for pristine biopolymers and bionanocomposites based on HNT at very high filler concentration.

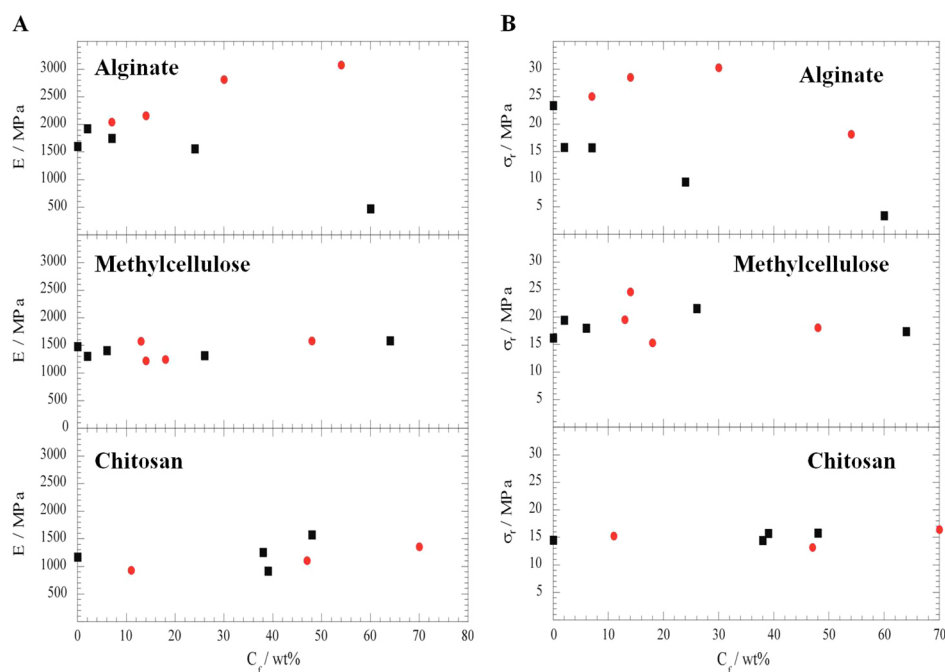


Figure 4. (A) Young's modulus of the polymer films as a function of the nanofiller amount (●, HNT; ■, kaolinite). (B) Tensile strength of the polymer films as a function of the nanofiller amount (●, HNT; ■, kaolinite).

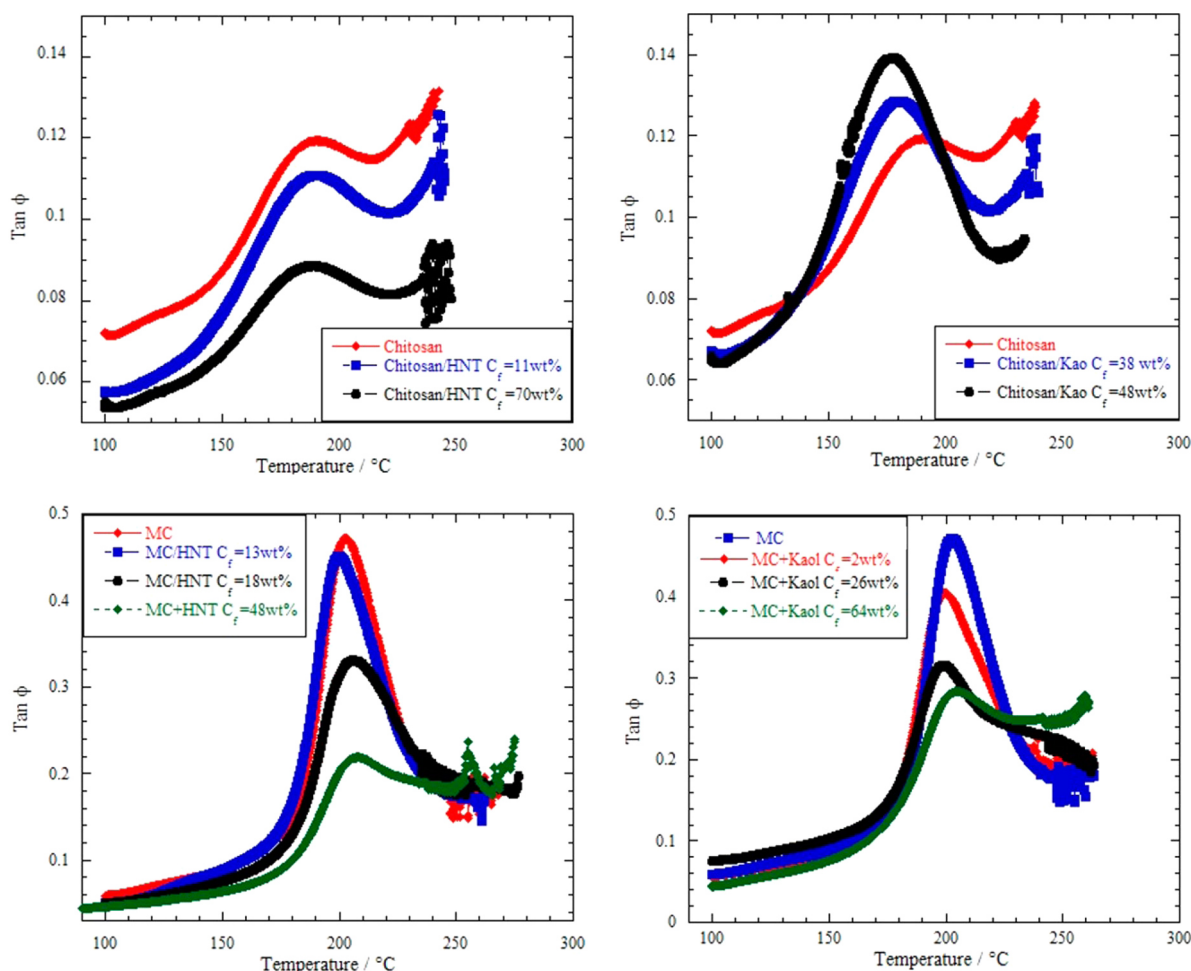


Figure 5. Variation of $\tan \phi$ as a function of temperature for pristine polymers and nanocomposites.

Table 4. θ_i Values of Drop at Deposition on the Polymer and Nanocomposite Films Containing HNT or Kao^a

C_f /wt %	filler	θ_i /deg
0	Alginate	67
54	HNT	61
60	Kao	61
0	Methylcellulose	54
48	HNT	61
64	Kao	66
0	Chitosan	90
47	HNT	65
39	Kao	74

^aThe estimated error of at least three independent measurements is $\pm 1^\circ$.

θ_i data showed that chitosan possesses the strongest hydrophobic character (Table 4), which is reduced by the addition of HNT. This result can be attributed to the enrichment of HNT unto the film interface as evidenced by SEM micrographs (Figure 6). Namely, hydrophilic HNT particles induced a decrease of the θ_i value. SEM images highlighted that HNT particles are uniformly dispersed on alginate surface determining a slight decrease of the θ_i value. As

concerns the methylcellulose/HNT composite, we observed that the addition of the filler induces an enhancement of the surface toughness (Figure 6). Accordingly, θ_i value of the nanocomposite is larger with respect to that of pristine methylcellulose indicating an increase of the surface hydrophobicity.

Figure 7 illustrates XRD spectra for alginate-HNTs, methylcellulose-HNTs nanocomposites, and HNT. Literature⁵⁸ reports of XRD data on chitosan/HNT composites provide evidence for the intercalation of polymer into nanotube interlayers.

As reported in the literature,^{59,60} pure HNT showed a peak at 12.4° (2θ) corresponding to a (001) basal spacing of 7.15 Å. The peaks at 8.4 and 10.0 Å of alginate/HNT and methylcellulose/HNT, respectively, could be due to a partial intercalation of the polymers with consequent increase of the HNT interlayer spacing. Both composites provided also an XRD peak at ca. 7 Å indicating the coexistence of two phases: HNT with intercalated polymer (interlayer > 7 Å) and HNT with no intercalation (interlayer ca. 7 Å). Similar results were observed for the intercalation of the antibiotic metronidazole⁶¹ and the surfactant⁶² Tween 20 into the K10-montmorillonite clay.

CONCLUSION

Nanocomposites based on polymers (methylcellulose, alginate, or chitosan) and nanoclays (halloysite nanotubes and kaolinite)

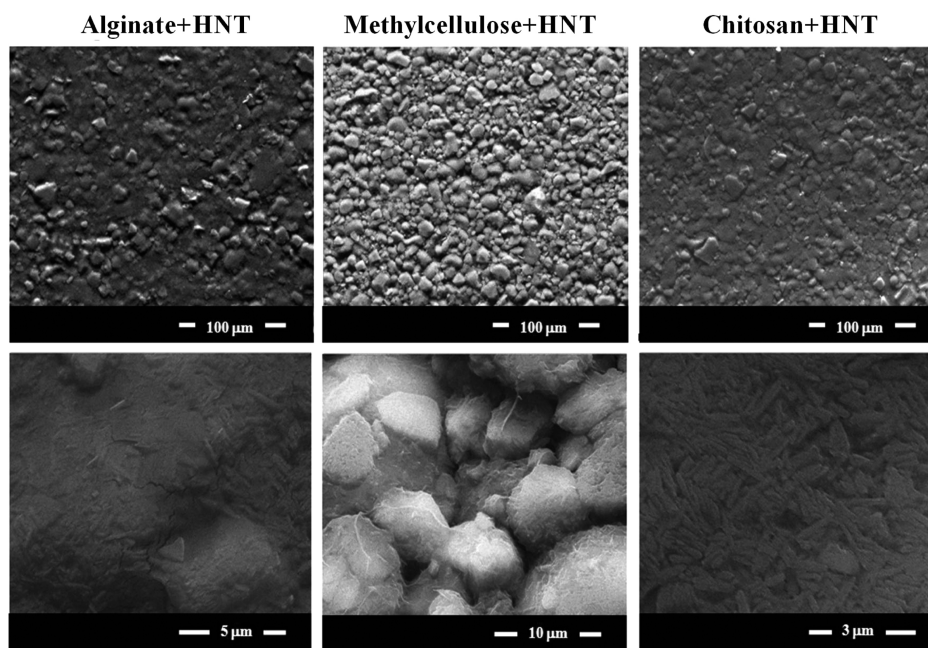


Figure 6. SEM images of nanocomposites at $C_f = 50$ wt %.

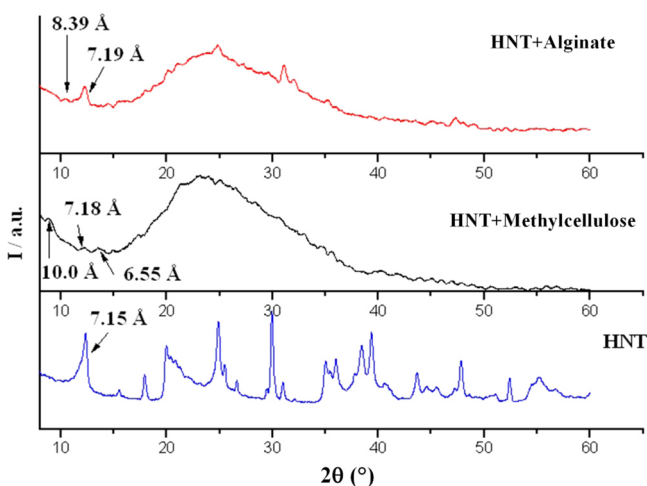


Figure 7. Diffractograms of HNT, HNT + methylcellulose ($C_f = 18$ wt %), and HNT + alginate ($C_f = 30$ wt %).

have been prepared. The concentration of nanoclay was systematically varied for each nanocomposite, and a compact film was always obtained. Thermal degradation process has highlighted the key role of the morphology of the nanoclay and the specific interaction of biopolymers with the inside and/or outside surface of the nanotubes. In particular, the interaction of the cationic polymer (chitosan) could occur with the negative outer surface of the nanotube and that of the anionic alginate with the inner surface of the cavity (positive charge), while the methylcellulose, a nonionic polymer, could interact without specificity with the surfaces of halloysite nanotubes. The mechanical properties of nanocomposites are strongly connected to the interactions between biopolymer and nanofiller. The alginate encapsulation into the nanotube cavity improved tensile properties of the nanocomposites. The data of the surface wettability of the films were correctly interpreted on the basis of the roughness and the surface composition (presence or absence of nanoparticles) by means of SEM

micrographs. X-ray data indicated the coexistence of two phases in nanocomposites with HNT nanotubes, namely, HNT with partially intercalated polymer and HNT with no intercalation.

In general, the investigated physicochemical characteristics of the bionanocomposite films are affected by the filler morphology as well as the biopolymer nature. Controlling the biopolymer/nanoclay interactions can open the route to generate smart nanomaterials with interesting technological properties, such as reliable thermal stability, hydrophobicity surface, and relevant mechanical performances.

■ ASSOCIATED CONTENT

📄 Supporting Information

The Supporting Information is available free of charge on the ACS Publications website at DOI: 10.1021/acs.iecr.6b01816.

DMA data for alginate film (PDF)

■ AUTHOR INFORMATION

Corresponding Author

*E-mail: giuseppe.lazzara@unipa.it.

Notes

The authors declare no competing financial interest.

■ ACKNOWLEDGMENTS

The work was financially supported by the University of Palermo, FIRB 2012 (prot. RBF12ETLS), and PON-TECLA (PON03PE_00214_1). This contribution was identified by Session Chair Dr. Pilar Aranda (Instituto de Ciencia de Materiales de Madrid (Spain), CSIC) as the Best Presentation in the session "PMSE" of the 2016 ACS Spring National Meeting in San Diego, CA.

■ REFERENCES

- (1) Siracusa, V.; Rocculi, P.; Romani, S.; Rosa, M. D. Biodegradable Polymers for Food Packaging: A Review. *Trends Food Sci. Technol.* 2008, 19 (12), 634.

- (2) Cha, D. S.; Chinnan, M. S. Biopolymer-Based Antimicrobial Packaging: A Review. *Crit. Rev. Food Sci. Nutr.* **2004**, *44* (4), 223.
- (3) Tharanathan, R. N. Biodegradable Films and Composite Coatings: Past, Present and Future. *Trends Food Sci. Technol.* **2003**, *14* (3), 71.
- (4) Mlčoch, T.; Kučerík, J. Hydration and Drying of Various Polysaccharides Studied Using DSC. *J. Therm. Anal. Calorim.* **2013**, *113*, 1177.
- (5) De Silva, R.; Pasbakhsh, P.; Goh, K.; Chai, S.-P.; Chen, J. Synthesis and Characterisation of Poly (Lactic Acid)/halloysite Bionanocomposite Films. *J. Compos. Mater.* **2014**, *48*, 3705.
- (6) Gorrasi, G.; Pantani, R.; Murariu, M.; Dubois, P. PLA/Halloysite Nanocomposite Films: Water Vapor Barrier Properties and Specific Key Characteristics. *Macromol. Mater. Eng.* **2014**, *299* (1), 104.
- (7) Cavallaro, G.; Lazzara, G.; Milioto, S. Dispersions of Nanoclays of Different Shapes into Aqueous and Solid Biopolymeric Matrices. Extended Physicochemical Study. *Langmuir* **2011**, *27* (3), 1158.
- (8) Ruiz-Hitzky, E.; Aranda, P.; Darder, M.; Rytwo, G. Hybrid Materials Based on Clays for Environmental and Biomedical Applications. *J. Mater. Chem.* **2010**, *20* (42), 9306.
- (9) LeBaron, P. Polymer-Layered Silicate Nanocomposites: An Overview. *Appl. Clay Sci.* **1999**, *15* (1–2), 11.
- (10) Kojima, Y.; Usuki, A.; Kawasumi, M.; Okada, A.; Fukushima, Y.; Kurauchi, T.; Kamigaito, O. Mechanical Properties of Nylon 6-Clay Hybrid. *J. Mater. Res.* **1993**, *8* (5), 1185.
- (11) Guin, T.; Krecker, M.; Milhorn, A.; Hagen, D. A.; Stevens, B.; Grunlan, J. C. Exceptional Flame Resistance and Gas Barrier with Thick Multilayer Nanobrick Wall Thin Films. *Adv. Mater. Interfaces* **2015**, *2* (11), 201500214.
- (12) Alexandre, M.; Dubois, P. Polymer-Layered Silicate Nanocomposites: Preparation, Properties and Uses of a New Class of Materials. *Mater. Sci. Eng., R* **2000**, *28* (1–2), 1.
- (13) Du, M.; Guo, B.; Jia, D. Thermal Stability and Flame Retardant Effects of Halloysite Nanotubes on Poly(propylene). *Eur. Polym. J.* **2006**, *42* (6), 1362.
- (14) Blanco, I.; Abate, L.; Bottino, F. A.; Bottino, P. Thermal Behaviour of a Series of Novel Aliphatic Bridged Polyhedral Oligomeric Silsesquioxanes (POSSs)/polystyrene (PS) Nanocomposites: The Influence of the Bridge Length on the Resistance to Thermal Degradation. *Polym. Degrad. Stab.* **2014**, *102* (0), 132.
- (15) Blanco, I.; Bottino, F. A. Thermal Study on Phenyl, Hepta Isobutyl-Polyhedral Oligomeric Silsesquioxane/polystyrene Nanocomposites. *Polym. Compos.* **2013**, *34* (2), 225.
- (16) Joussein, E.; Petit, S.; Churchman, G. J.; Theng, B.; Righi, D.; Delvaux, B. Halloysite Clay Minerals — a Review. *Clay Miner.* **2005**, *40* (4), 383.
- (17) Pasbakhsh, P.; Churchman, G. J.; Keeling, J. L. Characterisation of Properties of Various Halloysites Relevant to Their Use as Nanotubes and Microfibre Fillers. *Appl. Clay Sci.* **2013**, *74*, 47.
- (18) Lvov, Y. M.; Price, R. R. Halloysite Nanotubes, a Novel Substrate for the Controlled Delivery of Bioactive Molecules. In *Bio-Inorganic Hybrid Nanomaterials*; Ruiz-Hitzky, E., Ariga, K., Lvov, Y. M., Eds.; Wiley-VCH Verlag GmbH & Co. KGaA: Weinheim, Germany, 2007; pp 419–441.
- (19) Lvov, Y. M.; Shchukin, D. G.; Mohwald, H.; Price, R. R. Halloysite Clay Nanotubes for Controlled Release of Protective Agents. *ACS Nano* **2008**, *2* (5), 814.
- (20) Shemesh, R.; Krepker, M.; Nitzan, N.; Vaxman, A.; Segal, E. Active Packaging Containing Encapsulated Carvacrol for Control of Postharvest Decay. *Postharvest Biol. Technol.* **2016**, *118*, 175.
- (21) Abdullayev, E.; Sakakibara, K.; Okamoto, K.; Wei, W.; Ariga, K.; Lvov, Y. Natural Tubule Clay Template Synthesis of Silver Nanorods for Antibacterial Composite Coating. *ACS Appl. Mater. Interfaces* **2011**, *3* (10), 4040.
- (22) Konnova, S. A.; Sharipova, I. R.; Demina, T. A.; Osin, Y. N.; Yarullina, D. R.; Ilinskaya, O. N.; Lvov, Y. M.; Fakhrullin, R. F. Biomimetic Cell-Mediated Three-Dimensional Assembly of Halloysite Nanotubes. *Chem. Commun.* **2013**, *49* (39), 4208.
- (23) Wei, W.; Minullina, R.; Abdullayev, E.; Fakhrullin, R.; Mills, D.; Lvov, Y. Enhanced Efficiency of Antiseptics with Sustained Release from Clay Nanotubes. *RSC Adv.* **2014**, *4* (1), 488.
- (24) Fakhrullina, G. I.; Akhatova, F. S.; Lvov, Y. M.; Fakhrullin, R. F. Toxicity of Halloysite Clay Nanotubes in Vivo: A Caenorhabditis Elegans Study. *Environ. Sci.: Nano* **2015**, *2* (1), 54.
- (25) Dzamukova, M. R.; Naumenko, E. A.; Lvov, Y. M.; Fakhrullin, R. F. Enzyme-Activated Intracellular Drug Delivery with Tubule Clay Nanof ormulation. *Sci. Rep.* **2015**, *5*, 10560.
- (26) Cavallaro, G.; Lazzara, G.; Milioto, S.; Parisi, F.; Sanzillo, V. Modified Halloysite Nanotubes: Nanoarchitectures for Enhancing the Capture of Oils from Vapor and Liquid Phases. *ACS Appl. Mater. Interfaces* **2014**, *6* (1), 606.
- (27) Cavallaro, G.; Lazzara, G.; Milioto, S.; Palmisano, G.; Parisi, F. Halloysite Nanotube with Fluorinated Lumen: Non-Foaming Nanocontainer for Storage and Controlled Release of Oxygen in Aqueous Media. *J. Colloid Interface Sci.* **2014**, *417* (0), 66.
- (28) Cavallaro, G.; Lazzara, G.; Milioto, S.; Parisi, F. Hydrophobically Modified Halloysite Nanotubes as Reverse Micelles for Water-in-Oil Emulsion. *Langmuir* **2015**, *31* (27), 7472.
- (29) Tully, J.; Yendluri, R.; Lvov, Y. Halloysite Clay Nanotubes for Enzyme Immobilization. *Biomacromolecules* **2016**, *17* (2), 615.
- (30) Yah, W. O.; Takahara, A.; Lvov, Y. M. Selective Modification of Halloysite Lumen with Octadecylphosphonic Acid: New Inorganic Tubular Micelle. *J. Am. Chem. Soc.* **2012**, *134* (3), 1853.
- (31) Yah, W. O.; Xu, H.; Soejima, H.; Ma, W.; Lvov, Y.; Takahara, A. Biomimetic Dopamine Derivative for Selective Polymer Modification of Halloysite Nanotube Lumen. *J. Am. Chem. Soc.* **2012**, *134* (29), 12134.
- (32) Massaro, M.; Piana, S.; Colletti, C. G.; Noto, R.; Riela, S.; Baiamonte, C.; Giordano, C.; Pizzolanti, G.; Cavallaro, G.; Milioto, S.; Lazzara, G. Multicavity Halloysite-Amphiphilic Cyclodextrin Hybrids for Co-Delivery of Natural Drugs into Thyroid Cancer Cells. *J. Mater. Chem. B* **2015**, *3* (19), 4074.
- (33) Liu, M.; Zhang, Y.; Wu, C.; Xiong, S.; Zhou, C. Chitosan/halloysite Nanotubes Bionanocomposites: Structure, Mechanical Properties and Biocompatibility. *Int. J. Biol. Macromol.* **2012**, *51* (4), 566.
- (34) Alcantara, A. C. S.; Aranda, P.; Darder, M.; Ruiz-Hitzky, E. Bionanocomposites Based on Alginate-Zein/layered Double Hydroxide Materials as Drug Delivery Systems. *J. Mater. Chem.* **2010**, *20* (42), 9495.
- (35) Cavallaro, G.; Lazzara, G.; Konnova, S.; Fakhrullin, R.; Lvov, Y. Composite Films of Natural Clay Nanotubes with Cellulose and Chitosan. *Green Mater.* **2014**, *2* (4), 232.
- (36) Viseras, M. T.; Aguzzi, C.; Cerezo, P.; Viseras, C.; Valenzuela, C. Equilibrium and Kinetics of 5-Aminosalicylic Acid Adsorption by Halloysite. *Microporous Mesoporous Mater.* **2008**, *108* (1–3), 112.
- (37) Liu, M.; Wu, C.; Jiao, Y.; Xiong, S.; Zhou, C. Chitosan-Halloysite Nanotubes Nanocomposite Scaffolds for Tissue Engineering. *J. Mater. Chem. B* **2013**, *1* (15), 2078.
- (38) Cataldo, S.; Gianguzza, A.; Pettignano, A.; Villaescusa, I. Mercury(II) Removal from Aqueous Solution by Sorption onto Alginate, Pectate and Polygalacturonate Calcium Gel Beads. A Kinetic and Speciation Based Equilibrium Study. *React. Funct. Polym.* **2013**, *73* (1), 207.
- (39) Cataldo, S.; Muratore, N.; Orecchio, S.; Pettignano, A. Enhancement of Adsorption Ability of Calcium Alginate Gel Beads towards Pd(II) Ion. A Kinetic and Equilibrium Study on Hybrid Laponite and Montmorillonite-alginate Gel Beads. *Appl. Clay Sci.* **2015**, *118*, 162.
- (40) Ravi Kumar, M. N. V. A Review of Chitin and Chitosan Applications. *React. Funct. Polym.* **2000**, *46* (1), 1.
- (41) Kuila, B. K.; Nandi, A. K. Physical, Mechanical, and Conductivity Properties of Poly(3-hexylthiophene)-Montmorillonite Clay Nanocomposites Produced by the Solvent Casting Method. *Macromolecules* **2004**, *37* (23), 8577.

- (42) Rotaru, A.; Nicolaescu, I.; Rotaru, P.; Neaga, C. Thermal Characterization of Humic Acids and Other Components of Raw Coal. *J. Therm. Anal. Calorim.* **2008**, *92* (1), 297.
- (43) Kučerík, J.; Průšová, A.; Rotaru, A.; Flimel, K.; Janeček, J.; Conte, P. DSC Study on Hyaluronan Drying and Hydration. *Thermochim. Acta* **2011**, *523* (1–2), 245.
- (44) Cavallaro, G.; Donato, D. I.; Lazzara, G.; Milioto, S. Films of Halloysite Nanotubes Sandwiched between Two Layers of Biopolymer: From the Morphology to the Dielectric, Thermal, Transparency, and Wettability Properties. *J. Phys. Chem. C* **2011**, *115* (42), 20491.
- (45) Duce, C.; Vecchio Cipriotti, S.; Ghezzi, L.; Ierardi, V.; Tinè, M. R. Thermal Behavior Study of Pristine and Modified Halloysite Nanotubes. *J. Therm. Anal. Calorim.* **2015**, *121* (3), 1011.
- (46) Arcudi, F.; Cavallaro, G.; Lazzara, G.; Massaro, M.; Milioto, S.; Noto, R.; RIELA, S. Selective Functionalization of Halloysite Cavity by Click Reaction: Structured Filler for Enhancing Mechanical Properties of Bionanocomposite Films. *J. Phys. Chem. C* **2014**, *118* (27), 15095.
- (47) Du, M.; Guo, B.; Jia, D. Thermal Stability and Flame Retardant Effects of Halloysite Nanotubes on Poly(propylene). *Eur. Polym. J.* **2006**, *42* (6), 1362.
- (48) Cavallaro, G.; Lazzara, G.; Milioto, S. Exploiting the Colloidal Stability and Solubilization Ability of Clay Nanotubes/Ionic Surfactant Hybrid Nanomaterials. *J. Phys. Chem. C* **2012**, *116* (41), 21932.
- (49) Torres, N.; Robin, J. J.; Boutevin, B. Study of Thermal and Mechanical Properties of Virgin and Recycled Poly(ethylene Terephthalate) before and after Injection Molding. *Eur. Polym. J.* **2000**, *36* (10), 2075.
- (50) Vadukumpully, S.; Paul, J.; Mahanta, N.; Valiyaveetil, S. Flexible Conductive Graphene/poly(vinyl Chloride) Composite Thin Films with High Mechanical Strength and Thermal Stability. *Carbon* **2011**, *49* (1), 198.
- (51) Perego, G.; Cella, G. D.; Bastioli, C. Effect of Molecular Weight and Crystallinity on Poly(lactic Acid) Mechanical Properties. *J. Appl. Polym. Sci.* **1996**, *59* (1), 37.
- (52) Kim, I.-H.; Jeong, Y. G. Polylactide/exfoliated Graphite Nanocomposites with Enhanced Thermal Stability, Mechanical Modulus, and Electrical Conductivity. *J. Polym. Sci., Part B: Polym. Phys.* **2010**, *48* (8), 850.
- (53) Hancock, B. C.; Zografi, G. The Relationship Between the Glass Transition Temperature and the Water Content of Amorphous Pharmaceutical Solids. *Pharm. Res.* **1994**, *11* (4), 471.
- (54) Schubnell, M.; Schawe, J. E. K. Quantitative Determination of the Specific Heat and the Glass Transition of Moist Samples by Temperature Modulated Differential Scanning Calorimetry. *Int. J. Pharm.* **2001**, *217* (1–2), 173.
- (55) Liu, M.; Zhang, Y.; Wu, C.; Xiong, S.; Zhou, C. Chitosan/halloysite Nanotubes Bionanocomposites: Structure, Mechanical Properties and Biocompatibility. *Int. J. Biol. Macromol.* **2012**, *51* (4), 566.
- (56) Zhu, J.; Wei, S.; Ryu, J.; Sun, L.; Luo, Z.; Guo, Z. Magnetic Epoxy Resin Nanocomposites Reinforced with Core–Shell Structured Fe@FeO Nanoparticles: Fabrication and Property Analysis. *ACS Appl. Mater. Interfaces* **2010**, *2* (7), 2100.
- (57) Zhou, Q.; Pramoda, K. P.; Lee, J.-M.; Wang, K.; Loo, L. S. Role of Interface in Dispersion and Surface Energetics of Polymer Nanocomposites Containing Hydrophilic POSS and Layered Silicates. *J. Colloid Interface Sci.* **2011**, *355* (1), 222.
- (58) Deen, I.; Pang, X.; Zhitomirsky, I. Electrophoretic Deposition of Composite Chitosan–halloysite Nanotube–hydroxyapatite Films. *Colloids Surf., A* **2012**, *410*, 38.
- (59) Rooj, S.; Das, A.; Thakur, V.; Mahaling, R. N.; Bhowmick, A. K.; Heinrich, G. Preparation and Properties of Natural Nanocomposites Based on Natural Rubber and Naturally Occurring Halloysite Nanotubes. *Mater. Eng.* **2010**, *31* (4), 2151.
- (60) Xie, Y.; Qian, D.; Wu, D.; Ma, X. Magnetic Halloysite Nanotubes/iron Oxide Composites for the Adsorption of Dyes. *Chem. Eng. J.* **2011**, *168* (2), 959.
- (61) Calabrese, I.; Cavallaro, G.; Scialabba, C.; Licciardi, M.; Merli, M.; Sciascia, L.; Turco Liveri, M. L. Montmorillonite Nanodevices for the Colon Metronidazole Delivery. *Int. J. Pharm.* **2013**, *457* (1), 224.
- (62) Calabrese, I.; Cavallaro, G.; Lazzara, G.; Merli, M.; Sciascia, L.; Turco Liveri, M. L. Preparation and Characterization of Bio-Organoclay Using Nonionic Surfactant. *Adsorption* **2016**, *22* (2), 105.

Attached Paper III



Article

Thermal Properties of Multilayer Nanocomposites Based on Halloysite Nanotubes and Biopolymers

Vanessa Bertolino, Giuseppe Cavallaro * , Stefana Milioto, Filippo Parisi and Giuseppe Lazzara

Dipartimento di Fisica e Chimica, Università degli Studi di Palermo, Viale delle Scienze, pad. 17, 90128 Palermo, Italy; vanessarita.bertolino@unipa.it (V.B.); stefana.milioto@unipa.it (S.M.); filippo.parisi@unipa.it (F.P.); giuseppe.lazzara@unipa.it (G.L.)

* Correspondence: giuseppe.cavallaro@unipa.it; Tel.: +39-091-23897962

Received: 22 June 2018; Accepted: 9 July 2018; Published: 12 July 2018



Abstract: This paper reports a novel procedure to fabricate multilayer composite biofilms based on halloysite nanotubes (HNTs) and sustainable polymers. Among the biopolymers, the non-ionic (hydroxypropyl cellulose) and cationic (chitosan) molecules were selected. The nanocomposites were prepared by the sequential casting of ethanol solutions of hydroxypropyl cellulose and aqueous dispersions of chitosan/HNTs. The composition of the bio-nanocomposites was systematically changed in order to investigate the effect of the hydroxypropyl cellulose/HNTs ratio on the thermal properties of the films, which were investigated by differential scanning calorimetry (DSC) and thermogravimetry (TG). DSC studies were conducted in the static air (oxidative atmosphere), while TG measurements were carried out under nitrogen flow (inert atmosphere). The analysis of DSC data provided the enthalpy and the temperature for the oxidative degradation of the bio-nanocomposites. These results were helpful to estimate the efficacy of the well-compacted middle layer of HNTs as a flame retardant. TG experiments were performed at a variable heating rate and the collected data were analyzed by the Friedman's method (non-isothermal thermogravimetric approach) with the aim of studying the kinetics of the hydroxypropyl cellulose degradation in the multilayer nanocomposites. This work represents an advanced contribution for designing novel sustainable nanocomposites with excellent thermal behavior as a consequence of their peculiar multilayer structure.

Keywords: halloysite nanotubes; multilayer nanocomposites; biopolymers; hydroxypropyl cellulose; thermogravimetry; differential scanning calorimetry

1. Introduction

Halloysite is an emerging nanofiller for the fabrication of smart nanocomposites with specific functionalities useful for several technological purposes, such as anti-corrosion coatings [1–3], food packaging [4–6], remediation [7–11], catalysis [12–15], tissue engineering [16–18], preservation of art-works [19–21], and antimicrobial protection [22,23]. Recent biological studies (by means of both in vivo and vitro tests) proved that halloysite exhibits a low toxicity [24–26]. The chemical formula of halloysite is $\text{Al}_2\text{Si}_2\text{O}_5(\text{OH})_4 \cdot 2\text{H}_2\text{O}$. From the mineralogical viewpoint, halloysite is a phyllosilicate 1:1, which means that each composed layer is formed of one octahedral sheet of alumina and one tetrahedral sheet of silica [27]. This mineral possesses a hollow tubular shape with a large polydispersity in sizes on the dependence of the geological setting [28]. The length interval is between 50 and 1500 nm, while the external and internal diameters range between 20–150 and 10–15 nm [28]. The chemical composition of the halloysite surfaces is different, being that the inner one is composed of SiO_2 groups while the external shell is formed by Al_2O_3 groups. Consequently, in the pH 2–8, the cavity possesses a positive net charge, whereas the shell is negatively charged [29]. This peculiarity allows for a

selective modification of the halloysite surfaces by means of ionic molecules that can be exploited to control its colloidal stability and rheological properties as requested for the numerous applications on tubular nanoparticles [30–33]. Within this, the specific electrostatic interactions between ionic polymers and halloysite affect the thermal and mechanical behaviors of the corresponding nanocomposites prepared by the aqueous casting method [34]. The addition of halloysite nanotubes (HNTs) within anionic polymers represents an efficient strategy to enhance the thermal stability of the biomaterials because the polymeric chains are entrapped within the HNTs lumen [4,34]. This effect was detected for pectin/HNTs [4,35] and alginate/HNTs nanocomposites [34]. Biocomposites based on cationic chitosan and halloysite evidenced suitable performances as scaffolds for tissue engineering [18,23,36] and hydrogel for medical purposes [37]. The literature reports that HNTs are efficient reinforcing fillers for chitosan matrix [38,39]. The high dispersibility of halloysite into hydrophilic polymers generated nanocomposite materials with a large wettability and excellent tensile performances in terms of stress at breaking point and elasticity [34]. Nanocomposites based on halloysite and polylactic acid (PLA) showed enhanced barrier properties with respect to the pure biopolymer [40]. Our recent work evidenced that the confinement of HNTs between chitosan layers generated composite biofilms with a relevant flame resistance [41]. It should be noted that the specific functionalities and the physicochemical characteristics of polymer/HNTs nanocomposites are strongly influenced by their mesoscopic structure [42]. Here, we prepared multilayer nanocomposite films formed by three components: two biopolymers (hydroxypropyl cellulose and chitosan) and halloysite (inorganic filler). An intermediate layer of chitosan/HNT was confined between hydroxypropyl cellulose by using a sequential casting procedure performed in different solvents (water and ethanol). The thermal properties of the nanocomposites were investigated by two techniques: thermogravimetry (TG) and differential scanning calorimetry (DSC). The combination of TG and DSC can provide an exhaustive description of the thermal behavior of hybrid systems, including supramolecular complexes [43–45] and polymer/nanofiller composite materials [41,46,47]. Moreover, the mentioned thermal methods are useful within a cultural heritage for the diagnostics [48] and the treatment [20] of artworks. As reported in this paper, TG experiments performed at variable heating rates allow for the determination of the activation energy of the polymer degradation in composite systems [5,49,50]. On the other hand, DSC measurements are helpful to investigate the flame retardant action of nanofillers dispersed in a polymeric matrix [41,51].

This paper reports a novel protocol to generate biopolymers/halloysite nanocomposites with a peculiar sandwich-like shape. The promising thermal properties in the inert atmosphere were investigated by thermogravimetric experiments using a non-isothermal approach, while differential scanning calorimetry measurements in static air revealed that the multilayer morphology confers a fire resistance to the nanocomposites. This study provides a contribution to the fabrication of bio-nanocomposites with a controlled structure that can be exploited for engineering and biological applications.

2. Materials and Methods

2.1. Materials

Chitosan (75–85% deacetylated, $M_w = 50\text{--}190 \text{ kg}\cdot\text{mol}^{-1}$), hydroxypropyl cellulose (HPC, $M_w = 80 \text{ kg}\cdot\text{mol}^{-1}$), ethanol, and glacial acetic acid are Aldrich products (Sigma-Aldrich, St. Louis, MO, USA). Halloysite nanotubes (HNTs; $M_w = 294.19 \text{ g}\cdot\text{mol}^{-1}$) are from Imerys Ceramics New Zealand Limited (Kerikeri, New Zealand). The specific surface of halloysite is $28.64 \text{ m}^2\cdot\text{g}^{-1}$ [28].

2.2. Preparation of Multilayer Nanocomposites

The multilayer nanocomposites were prepared through a sequential casting method. Firstly, we prepared the solutions of chitosan and HPC in two different solvents (water and ethanol, respectively)

and an aqueous dispersion of halloysite. The concentrations and the solvent media used for the biopolymer solution are reported in Table 1.

Table 1. The concentration and solvent medium for the biopolymer solutions.

Material	Solvent	Concentration (wt %)
Hydroxypropyl cellulose (HPC)	ethanol	2.01
Chitosan	water (pH = 3.5)	1.02

Stable polymer solutions were obtained by stirring overnight at 30 °C. As concerns chitosan, the pH of the solution was fixed at 3.5 by adding dropwise 0.1 mol·dm⁻³ acetic acid because of the very low solubility of the biopolymer at neutral pH [29]. Then, halloysite was dispersed in the chitosan solution by sonication and subsequent magnetically stirring overnight at 30 °C. The concentration of halloysite dispersion was 5 wt %. Consequently, the chitosan/HNTs ratio was fixed at 0.2. Chitosan acted as the stabilizing agent of the HNT's aqueous dispersions.

The nanocomposite films with the multilayer structure (a layer of chitosan/HNTs between two layers of HPC) were obtained through the subsequent deposition of the HPC solution and the chitosan/HNTs dispersion as follows: (1) HPC; (2) chitosan/HNTs; (3) HPC.

In detail, the first layer of the nanocomposite was obtained by pouring the HPC solution into a glass Petri dish at 30 °C to evaporate ethanol until the weight was constant. Then, the chitosan/HNTs aqueous dispersion was deposited on the HPC dried film and kept at 30 °C to evaporate water and, consequently, we obtained the second layer. Finally, the casting of the HPC was conducted on the chitosan/HNTs layer allowing to fabricate a sandwich-like structure. It should be noted that the very low solubility of chitosan in ethanol ensures to obtain nanocomposites with a multilayer morphology.

The composition of the nanocomposites was systematically varied by changing the amounts of HPC solutions and chitosan/HNTs used in the sequential casting procedure (Table 2). The variable composition of the nanocomposites was expressed by the weight ratio ($R_{(C+H)/HPC}$) between the middle layer (chitosan + HNTs) and outer layers (HPC).

Table 2. The composition of the nanocomposites and the corresponding amounts of hydroxypropyl cellulose (HPC) solutions and chitosan/halloysite nanotubes (HNTs) dispersions used in the sequential casting.

$R_{(C+H)/HPC}$	Amount of HPC Solution (First Layer)/g	Amount of Chitosan/HNTs Dispersion (Second Layer)/g	Amount of HPC Solution (Third Layer)/g
0.92	8.18	4.96	8.02
1.89	8.15	10.24	8.07
2.81	8.05	15.03	8.00

2.3. Methods

2.3.1. Thermogravimetry

The Q5000 IR apparatus (TA Instruments, New Castle, DE, USA) was employed to perform thermogravimetry (TG) measurements, which were carried out under a nitrogen flows of 25 and 10 cm³·min⁻¹ for the sample and the balance, respectively. The sample (ca. 5 mg) was loaded in a platinum crucible and heated from room temperature to 900 °C at variable heating rates (β), which were 5, 10, 15, and 20 °C·min⁻¹. The analysis of TG data allowed for the determination of the activation energy (E_a) of HPC degradation. The Curie temperatures of standards (nickel, cobalt, and their alloys) were considered for the temperature calibration.

2.3.2. Differential Scanning Calorimetry

The DSC 2920 CE apparatus (TA Instruments) was used to conduct Differential scanning calorimetry (DSC) measurements. The apparatus was calibrated using the melting enthalpy of standard indium ($28.71 \text{ J}\cdot\text{g}^{-1}$). Both the temperature and the power calibration were estimated at variable heating rates in agreement with the recent IUPAC technical report [52]. The sample (ca. 2 mg) was loaded in an aluminum pan. The measurements were performed in the static air from 0 to $600 \text{ }^\circ\text{C}$ at the heating rate of $10 \text{ }^\circ\text{C}\cdot\text{min}^{-1}$.

2.3.3. Scanning Electron Microscopy

A microscope ESEM FEI QUANTA 200F (Hillsboro, OR, USA) was used to investigate the morphological characteristics of the nanocomposite, which were previously coated with gold in argon by means of an Edwards Sputter Coater S150A (Edwards, Burgess Hill, UK) to avoid charging under the electron beam. The measurements were conducted in a high vacuum ($<6 \times 10^{-4} \text{ Pa}$), while the energy of the beam and the working distance were set at 25 kV and 10 mm, respectively.

3. Results and Discussion

3.1. Multilayer Structure the Nanocomposites

Figure 1 shows the schematic representation and the scanning electron microscope (SEM) image for the prepared multilayer nanocomposites.

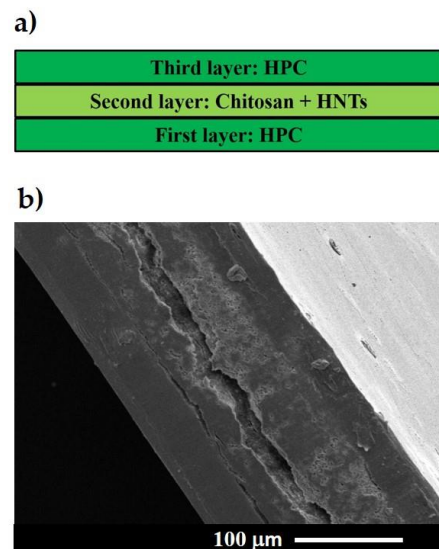


Figure 1. The sketch of the multilayer structure of the nanocomposites (a) and the scanning electron microscope (SEM) image for the composite materials with $R_{(\text{C+H})/\text{HPC}} = 2.81$ (b).

The thickness of the outer HPC layers was kept constant, while the intermediate layer of the chitosan/HNTs was systematically changed. Regarding the HPC layers, the thickness ($h_{(\text{HPC})}$) was calculated as

$$h_{(\text{HPC})} = m_{\text{HPC}} / (\delta_{\text{HPC}} \cdot \pi \cdot r^2), \quad (1)$$

where r is the radius of the Petri dish used for the preparation of the nanocomposites, while m_{HPC} and δ_{HPC} are the mass and the density of HPC, respectively. The thickness of the intermediate layer composed by chitosan and HNTs ($h_{(\text{C+H})}$) was determined by the equations

$$h^*_{(\text{C+H})} = h_{(\text{C})} + h_{(\text{H})}, \quad (2)$$

$$h_{(C)} = m_C / (\delta_C \cdot \pi \cdot r^2), \tag{3}$$

$$h_{(H)} = m_H / (\delta_H \cdot \pi \cdot r^2), \tag{4}$$

where m_C and δ_C are the mass and the density of chitosan, respectively, and m_H and δ_H are the mass and the density of halloysite, respectively. It should be noted that the described approach (Equations (2)–(4)) assumes that the densities of chitosan and halloysite are not altered by their reciprocal interactions. The sum of the calculated thicknesses for each composed layers is in agreement with the total thickness (experimentally determined by a micrometer) of the nanocomposite film. Table 3 collects the thickness values for the prepared nanocomposites.

Table 3. The thicknesses of the films, the outer HPC layers, and intermediate chitosan/HNT layer for the prepared nanocomposites.

$R_{(C+H)/HPC}$	$h_{(HPC)}$ (First Layer)/ μm	$h_{(HPC)}$ (Third Layer)/ μm	h_{C+H} (Middle Layer)/ μm	Nanocomposite Thickness/ μm
0.92	71.2	69.8	2.67	144
1.89	70.9	70.3	5.52	147
2.81	70.1	69.7	8.11	149

3.2. Thermal Properties of the Nanocomposites

3.2.1. Thermogravimetric Analysis: Thermal Behavior under Inert Atmosphere

Figure 2 shows the thermogravimetric curve (determined at $\beta = 10 \text{ }^\circ\text{C}\cdot\text{min}^{-1}$) of the nanocomposite at variable compositions.

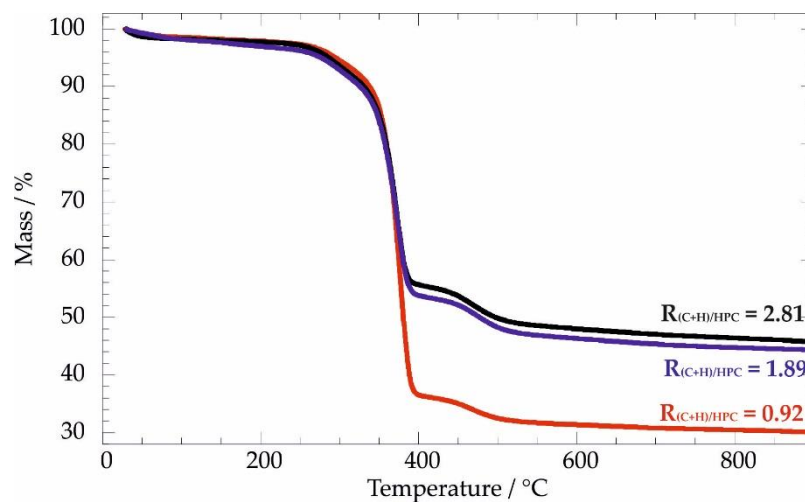


Figure 2. The thermogravimetric curves for the nanocomposites at variable compositions.

We observed three different mass losses: (1) the first mass loss (ML_{150}) occurs in the temperature range between 25 and 150 °C as a consequence of the evaporation of the water physically adsorbed on the materials; (2) the second mass loss (ML_{400}) takes place at the temperature interval 200–400 °C because of the decomposition of the organic moieties; (3) the third mass loss (ML_{550}) occurs in a temperature range of 420–550 °C. As reported in the literature [34], the latter is due to the expulsion of the two water molecules that are present in the halloysite interlayer. Table 4 compares the mass losses for the nanocomposite materials with those for pure hydroxypropyl cellulose.

Table 4. The mass losses and residual masses at 900 °C for pure HPC and nanocomposites determined by thermogravimetry (TG) measurements at $\beta = 10 \text{ }^\circ\text{C}\cdot\text{min}^{-1}$.

$R_{(C+H)/HPC}$	ML ₁₅₀ /%	ML ₄₀₀ /%	ML ₆₀₀ /%	MR ₉₀₀ /%	T _{CHIT} /°C	T _{HPC} /°C
0	0.65	92.4	/	4.07	289.2	369.7
0.92	1.74	61.3	4.28	30.1	290.2	376.4
1.89	1.83	43.2	6.33	44.8	291.6	373.4
2.81	2.31	42.1	6.49	45.8	286.5	374.5

The presence of the intermediate layer composed of chitosan and HNT generated an increase of the ML₁₅₀ indicating an enhancement of the affinity towards water due to the hydrophilic nature of halloysite. As expected, the ML₄₀₀ value was reduced in the nanocomposites, while the opposite effect was detected for ML₆₀₀ results. Compared with neat HPC, MR₉₀₀ is much larger in the composite materials because of the inorganic clay nanotubes, which do not undergo through a complete decomposition even at very high temperatures [34]. The analysis of the differential thermogravimetric (DTG) curves (Figure 3) provided a clearer description of the several degradation steps occurring in the nanocomposites.

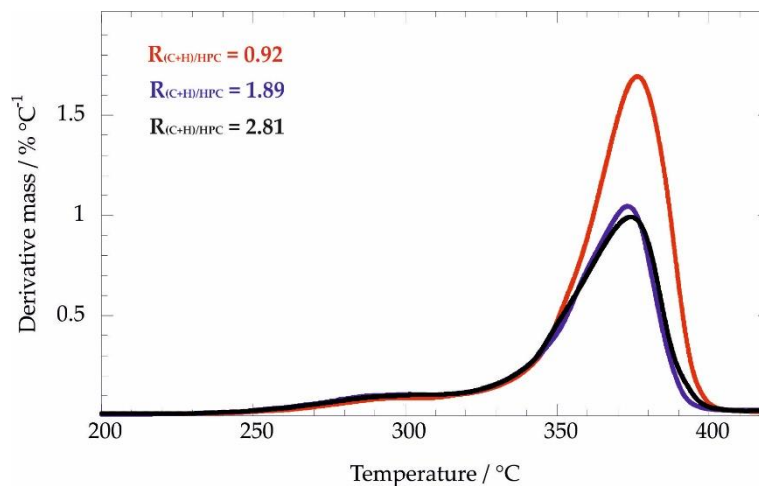


Figure 3. The differential thermogravimetric curves for the nanocomposites at variable compositions.

In the range 200–400 °C, DTG curves showed a shoulder (centered at ca. 290 °C) and a peak (centered at ca. 370 °C) that can be mostly attributed to the thermal degradation of chitosan and HPC, respectively. Accordingly, we determined the HPC degradation temperature (T_{HPC}) from the maximum of the DTG peaks, while the chitosan degradation temperature (T_{CHIT}) was estimated from the maximum of the DTG shoulders. As evidenced in Table 4, a slight thermal stabilization of HPC was observed in the multilayer nanocomposites. Generally, an increase of the polymer resistance to thermal degradation in nanocomposite systems is ascribed to the barrier effect of the nanofillers towards the volatile products generated by the polymer decomposition [34,46]. Regarding chitosan, the degradation temperatures are similar to that of pure chitosan (290.2 °C).

The kinetic aspects of the polymer degradation were studied by using a non-isothermal thermogravimetric method. To this purpose, we performed TG measurements at variable heating rates and the obtained data in the range 200–400 °C were analyzed by means of the Friedman approach, which can be expressed by the equation

$$\ln\left(\frac{\beta d\alpha}{dT}\right) = \ln[Af(\alpha)] - \frac{E_a}{RT} \quad (5)$$

where α is the conversion degree, while A and R represent the pre-exponential factor and the gas constant, respectively. Moreover, $f(\alpha)$ is the function that relates the specific degradation mechanism with the conversion degree. Based on Equation (5), the activation energy (E_a) can be determined by the slope of the $\ln(\beta d\alpha/dT)$ vs. the $1/T$ trends. As a general result, we observed that E_a is constant with α for all of the investigated materials. On this basis, we calculated the average E_a values, which are presented in Figure 4. In general, the presence of the intermediate layer did not significantly affect the kinetics of HPC degradation.

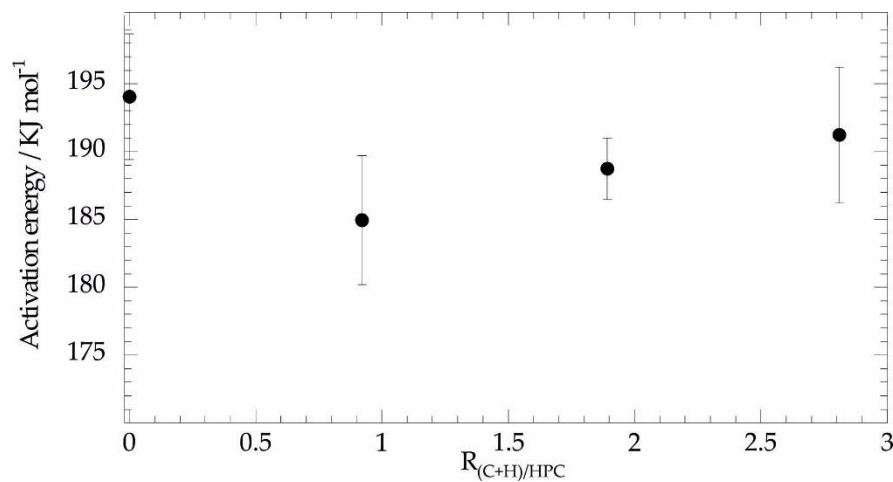


Figure 4. The average activation energy of hydroxypropyl cellulose (HPC) degradation as a function of the weight ratio between the middle layer (chitosan + halloysite nanotubes (HNTs)) and the outer layers (HPC).

3.2.2. Oxidative Degradation of Nanocomposites by Differential Scanning Calorimetry

The oxidative degradation of the nanocomposite materials was investigated by means of DSC measurements conducted statically. As shown in Figure 5, the DSC curves of the multilayer systems present an exothermic reaction due to the degradation of organic components under the oxidative conditions.

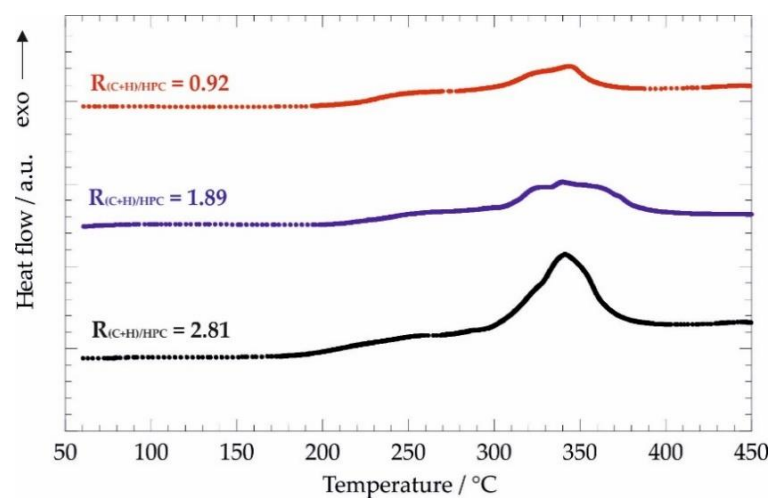


Figure 5. The differential scanning calorimetry (DSC) curves for nanocomposites at variable compositions.

The analysis of the DSC peaks allowed for the exploration of the thermodynamics of the oxidative degradation. In particular, we determined the temperature (T_{ox}) and the enthalpy variation (ΔH_{ox}) of the oxidative degradation by the maximum and the integration of the exothermic peaks. Figure 6 displays the dependence of both T_{ox} and ΔH_{ox} on the weight ratio between the middle layer (chitosan + HNTs) and the outer layers (HPC).

Compared with pure HPC, the nanocomposites gave evidence to the reduction of both parameters. The ΔH_{ox} decrease indicates that the presence of the middle layer composed of chitosan and halloysite lowered the quantity of the heat released during the exothermic process, which is represented by the oxidative degradation. This result gives evidence that the addition of chitosan/HNTs between the HPC layers produces a fire retardant action as expected for well-defined multilayer materials.

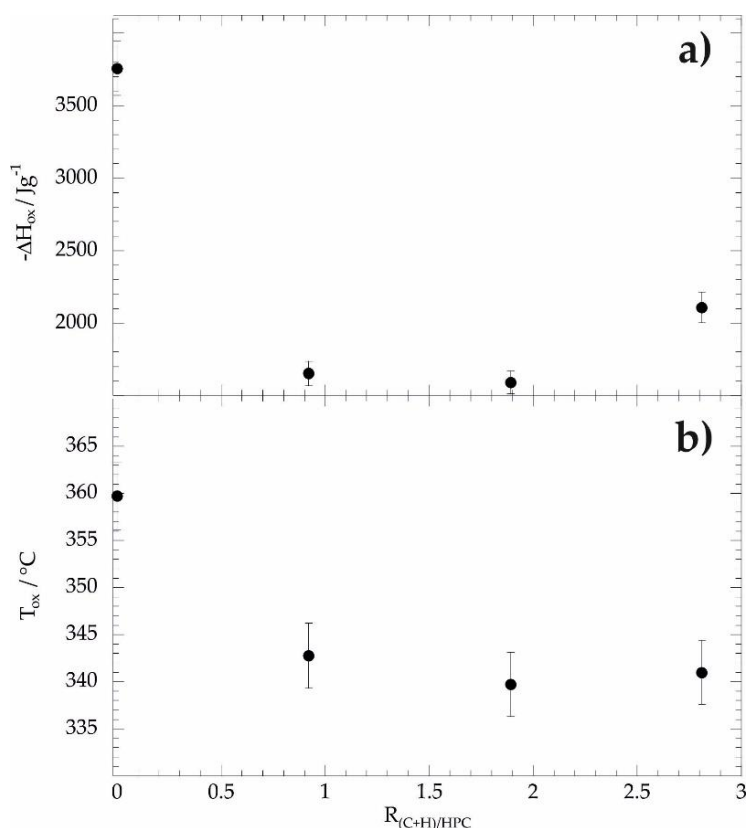


Figure 6. The enthalpy variation (a) and temperature (b) of oxidative degradation as functions of the weight ratio between the middle layer (chitosan + HNTs) and outer layers (HPC).

4. Conclusions

Nanocomposites with a multilayer structure were successfully prepared by the sequential casting of ethanol solutions of HPC and the aqueous dispersion of chitosan/halloysite. The composition of the nanocomposites was systematically varied in order to control the thickness of the intermediate layer composed of chitosan and halloysite nanotubes (HNTs). The thermal properties of the nanocomposites were affected by the peculiar multilayer structure of the biocomposite films. Thermogravimetry (TG) measurements performed under an inert atmosphere gave evidence to a slight increase of the HPC thermal stability in the nanocomposites. TG data collected at variable heating rates were analyzed by the non-isothermal Friedman method, which showed that the activation energy of the HPC degradation is not significantly affected by the addition of the chitosan/HNT layer.

The oxidative degradation of the nanocomposites was studied by Differential Scanning Calorimetry (DSC), which highlighted a reduction in the temperature, as well as the enthalpy variation

for the investigated exothermic process in the multilayer systems. Interestingly, the decrease of the enthalpy change indicates that the chitosan/halloysite layer generates a flame retardant action on the biomaterials. In conclusion, this work describes an easy strategy to fabricate multilayer bio-nanocomposites with promising thermal characteristics.

Author Contributions: G.L., and S.M. conceived and directed the project. G.C. analysed the data and wrote the paper. V.B. and F.P. prepared the nanocomposites and conducted TGA/DSC experiments.

Acknowledgments: The work was financially supported by the University of Palermo.

Conflicts of Interest: The authors declare no conflict of interest.

References

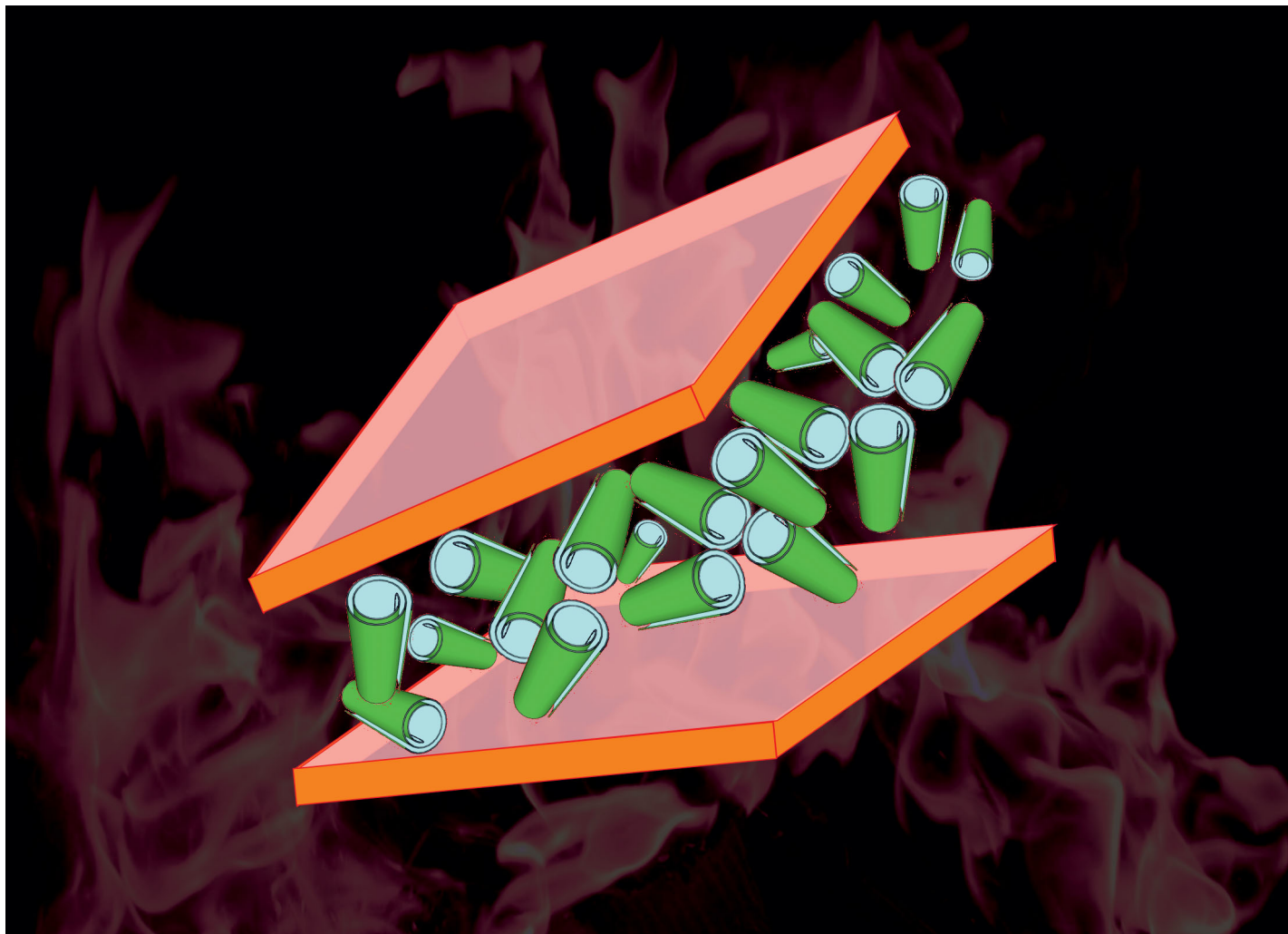
1. Fix, D.; Andreeva, D.V.; Lvov, Y.M.; Shchukin, D.G.; Möhwald, H. Application of inhibitor-loaded halloysite nanotubes in active anti-corrosive coatings. *Adv. Funct. Mater.* **2009**, *19*, 1720–1727. [[CrossRef](#)]
2. Lvov, Y.; Aerov, A.; Fakhrullin, R. Clay nanotube encapsulation for functional biocomposites. *Adv. Colloid Interface Sci.* **2014**, *207*, 189–198. [[CrossRef](#)] [[PubMed](#)]
3. Joshi, A.; Abdullayev, E.; Vasiliev, A.; Volkova, O.; Lvov, Y. interfacial modification of clay nanotubes for the sustained release of corrosion inhibitors. *Langmuir* **2013**, *29*, 7439–7448. [[CrossRef](#)] [[PubMed](#)]
4. Cavallaro, G.; Donato, D.I.; Lazzara, G.; Milioto, S. Films of halloysite nanotubes sandwiched between two layers of biopolymer: From the morphology to the dielectric, thermal, transparency, and wettability properties. *J. Phys. Chem. C* **2011**, *115*, 20491–20498. [[CrossRef](#)]
5. Makaremi, M.; Pasbakhsh, P.; Cavallaro, G.; Lazzara, G.; Aw, Y.K.; Lee, S.M.; Milioto, S. Effect of morphology and size of halloysite nanotubes on functional pectin bionanocomposites for food packaging applications. *ACS Appl. Mater. Interfaces* **2017**, *9*, 17476–17488. [[CrossRef](#)] [[PubMed](#)]
6. Du, M.; Guo, B.; Jia, D. Newly emerging applications of halloysite nanotubes: A review. *Polym. Int.* **2010**, *59*, 574–582. [[CrossRef](#)]
7. Zhao, Y.; Abdullayev, E.; Vasiliev, A.; Lvov, Y. Halloysite nanotubule clay for efficient water purification. *J. Colloid Interface Sci.* **2013**, *406*, 121–129. [[CrossRef](#)] [[PubMed](#)]
8. Zhao, M.; Liu, P. Adsorption behavior of methylene blue on halloysite nanotubes. *Microporous Mesoporous Mater.* **2008**, *112*, 419–424. [[CrossRef](#)]
9. Owoseni, O.; Nyankson, E.; Zhang, Y.; Adams, S.J.; He, J.; McPherson, G.L.; Bose, A.; Gupta, R.B.; John, V.T. Release of surfactant cargo from interfacially-active halloysite clay nanotubes for oil spill remediation. *Langmuir* **2014**, *30*, 13533–13541. [[CrossRef](#)] [[PubMed](#)]
10. Panchal, A.; Swientoniewski, L.T.; Omarova, M.; Yu, T.; Zhang, D.; Blake, D.A.; John, V.; Lvov, Y.M. Bacterial proliferation on clay nanotube Pickering emulsions for oil spill bioremediation. *Colloids Surf. B Biointerfaces* **2018**, *164*, 27–33. [[CrossRef](#)] [[PubMed](#)]
11. Cavallaro, G.; Gianguzza, A.; Lazzara, G.; Milioto, S.; Piazzese, D. Alginate gel beads filled with halloysite nanotubes. *Appl. Clay Sci.* **2013**, *72*, 132–137. [[CrossRef](#)]
12. Liu, Y.; Guan, H.; Zhang, J.; Zhao, Y.; Yang, J.-H.; Zhang, B. Polydopamine-coated halloysite nanotubes supported AgPd nanoalloy: An efficient catalyst for hydrolysis of ammonia borane. *Int. J. Hydrog. Energy* **2018**, *43*, 2754–2762. [[CrossRef](#)]
13. Liu, Y.; Zhang, J.; Guan, H.; Zhao, Y.; Yang, J.-H.; Zhang, B. Preparation of bimetallic Cu-Co nanocatalysts on poly(diallyldimethylammonium chloride) functionalized halloysite nanotubes for hydrolytic dehydrogenation of ammonia borane. *Appl. Surf. Sci.* **2018**, *427*, 106–113. [[CrossRef](#)]
14. Wang, Q.; Wang, Y.; Zhao, Y.; Zhang, B.; Niu, Y.; Xiang, X.; Chen, R. Fabricating roughened surfaces on halloysite nanotubes via alkali etching for deposition of high-efficiency Pt nanocatalysts. *CrystEngComm* **2015**, *17*, 3110–3116. [[CrossRef](#)]
15. Sadjadi, S.; Hosseinnajad, T.; Malmir, M.; Heravi, M.M. Cu@furfural imine-decorated halloysite as an efficient heterogeneous catalyst for promoting ultrasonic-assisted A³ and KA² coupling reactions: A combination of experimental and computational study. *New J. Chem.* **2017**, *41*, 13935–13951. [[CrossRef](#)]
16. Chang, C.W.; van Spreeuwel, A.; Zhang, C.; Varghese, S. PEG/clay nanocomposite hydrogel: A mechanically robust tissue engineering scaffold. *Soft Matter* **2010**, *6*, 5157–5164. [[CrossRef](#)]

17. Fakhruddin, R.F.; Lvov, Y.M. Halloysite clay nanotubes for tissue engineering. *Nanomedicine* **2016**, *11*, 2243–2246. [[CrossRef](#)] [[PubMed](#)]
18. Liu, M.; Wu, C.; Jiao, Y.; Xiong, S.; Zhou, C. Chitosan-halloysite nanotubes nanocomposite scaffolds for tissue engineering. *J. Mater. Chem. B* **2013**, *1*, 2078–2089. [[CrossRef](#)]
19. Cavallaro, G.; Danilushkina, A.A.; Evtugyn, V.G.; Lazzara, G.; Milioto, S.; Parisi, F.; Rozhina, E.V.; Fakhruddin, R.F. Halloysite nanotubes: Controlled access and release by smart gates. *Nanomaterials* **2017**, *7*, 199. [[CrossRef](#)] [[PubMed](#)]
20. Cavallaro, G.; Lazzara, G.; Milioto, S.; Parisi, F.; Sparacino, V. Thermal and dynamic mechanical properties of beeswax-halloysite nanocomposites for consolidating waterlogged archaeological woods. *Polym. Degrad. Stab.* **2015**, *120*, 220–225. [[CrossRef](#)]
21. Cavallaro, G.; Lisi, R.; Lazzara, G.; Milioto, S. Polyethylene glycol/clay nanotubes composites. *J. Therm. Anal. Calorim.* **2013**, *112*, 383–389. [[CrossRef](#)]
22. Gorrasi, G.; Bugatti, V.; Vittoria, V. Pectins filled with LDH-antimicrobial molecules: Preparation, characterization and physical properties. *Carbohydr. Polym.* **2012**, *89*, 132–137. [[CrossRef](#)] [[PubMed](#)]
23. Cavallaro, G.; Lazzara, G.; Konnova, S.; Fakhruddin, R.; Lvov, Y. Composite films of natural clay nanotubes with cellulose and chitosan. *Green Mater.* **2014**, *2*, 232–242. [[CrossRef](#)]
24. Kryuchkova, M.; Danilushkina, A.; Lvov, Y.; Fakhruddin, R. Evaluation of toxicity of nanoclays and graphene oxide in vivo: A Paramecium caudatum study. *Environ. Sci. Nano* **2016**, *3*, 442–452. [[CrossRef](#)]
25. Wang, X.; Gong, J.; Rong, R.; Gui, Z.; Hu, T.; Xu, X. Halloysite nanotubes-induced al accumulation and fibrotic response in lung of mice after 30-day repeated oral administration. *J. Agric. Food Chem.* **2018**, *66*, 2925–2933. [[CrossRef](#)] [[PubMed](#)]
26. Lvov, Y.; Wang, W.; Zhang, L.; Fakhruddin, R. Halloysite clay nanotubes for loading and sustained release of functional compounds. *Adv. Mater.* **2016**, *28*, 1227–1250. [[CrossRef](#)] [[PubMed](#)]
27. Joussein, E.; Petit, S.; Churchman, G.J.; Theng, B.; Righi, D.; Delvaux, B. Halloysite clay minerals—A review. *Clay Miner.* **2005**, *40*, 383–426. [[CrossRef](#)]
28. Cavallaro, G.; Chiappisi, L.; Pasbakhsh, P.; Gradzielski, M.; Lazzara, G. A structural comparison of halloysite nanotubes of different origin by Small-angle neutron scattering (SANS) and electric birefringence. *Appl. Clay Sci.* **2018**, *160*, 71–80. [[CrossRef](#)]
29. Bertolino, V.; Cavallaro, G.; Lazzara, G.; Milioto, S.; Parisi, F. Biopolymer-targeted adsorption onto halloysite nanotubes in aqueous media. *Langmuir* **2017**, *33*, 3317–3323. [[CrossRef](#)] [[PubMed](#)]
30. Kalay, S.; Stetsyshyn, Y.; Lobaz, V.; Harhay, K.; Ohar, H.; Çulha, M. Water-dispersed thermo-responsive boron nitride nanotubes: Synthesis and properties. *Nanotechnology* **2016**, *27*, 035703. [[CrossRef](#)] [[PubMed](#)]
31. Zhao, Y.; Cavallaro, G.; Lvov, Y. Orientation of charged clay nanotubes in evaporating droplet meniscus. *J. Colloid Interface Sci.* **2015**, *440*, 68–77. [[CrossRef](#)] [[PubMed](#)]
32. Liu, M.; Huo, Z.; Liu, T.; Shen, Y.; He, R.; Zhou, C. Self-assembling halloysite nanotubes into concentric ring patterns in a sphere-on-flat geometry. *Langmuir* **2017**, *33*, 3088–3098. [[CrossRef](#)] [[PubMed](#)]
33. Cavallaro, G.; Grillo, I.; Gradzielski, M.; Lazzara, G. Structure of hybrid materials based on halloysite nanotubes filled with anionic surfactants. *J. Phys. Chem. C* **2016**, *120*, 13492–13502. [[CrossRef](#)]
34. Bertolino, V.; Cavallaro, G.; Lazzara, G.; Merli, M.; Milioto, S.; Parisi, F.; Sciascia, L. Effect of the biopolymer charge and the nanoclay morphology on nanocomposite materials. *Ind. Eng. Chem. Res.* **2016**, *55*, 7373–7380. [[CrossRef](#)]
35. Gorrasi, G. Dispersion of halloysite loaded with natural antimicrobials into pectins: Characterization and controlled release analysis. *Carbohydr. Polym.* **2015**, *127*, 47–53. [[CrossRef](#)] [[PubMed](#)]
36. De Silva, R.T.; Pasbakhsh, P.; Goh, K.L.; Chai, S.-P.; Ismail, H. Physico-chemical characterisation of chitosan/halloysite composite membranes. *Polym. Test.* **2013**, *32*, 265–271. [[CrossRef](#)]
37. Ali, A.; Ahmed, S. A review on chitosan and its nanocomposites in drug delivery. *Int. J. Biol. Macromol.* **2018**, *109*, 273–286. [[CrossRef](#)] [[PubMed](#)]
38. Liu, M.; Zhang, Y.; Wu, C.; Xiong, S.; Zhou, C. Chitosan/halloysite nanotubes bionanocomposites: Structure, mechanical properties and biocompatibility. *Int. J. Biol. Macromol.* **2012**, *51*, 566–575. [[CrossRef](#)] [[PubMed](#)]
39. Huang, B.; Liu, M.; Zhou, C. Chitosan composite hydrogels reinforced with natural clay nanotubes. *Carbohydr. Polym.* **2017**, *175*, 689–698. [[CrossRef](#)] [[PubMed](#)]
40. Gorrasi, G.; Pantani, R.; Murariu, M.; Dubois, P. PLA/Halloysite nanocomposite films: water vapor barrier properties and specific key characteristics. *Macromol. Mater. Eng.* **2014**, *299*, 104–115. [[CrossRef](#)]

41. Bertolino, V.; Cavallaro, G.; Lazzara, G.; Milioto, S.; Parisi, F. Halloysite nanotubes sandwiched between chitosan layers: Novel bionanocomposites with multilayer structures. *New J. Chem.* **2018**, *42*, 8384–8390. [[CrossRef](#)]
42. Lvov, Y.; Abdullayev, E. Functional polymer–clay nanotube composites with sustained release of chemical agents. *Prog. Polym. Sci.* **2013**, *38*, 1690–1719. [[CrossRef](#)]
43. Terekhova, I.V. Comparative thermodynamic study on complex formation of native and hydroxypropylated cyclodextrins with benzoic acid. *Thermochim. Acta* **2011**, *526*, 118–121. [[CrossRef](#)]
44. Terekhova, I.V.; Romanova, A.O.; Kumeev, R.S.; Fedorov, M.V. Selective Na⁺/K⁺ effects on the formation of α -cyclodextrin complexes with aromatic carboxylic acids: competition for the guest. *J. Phys. Chem. B* **2010**, *114*, 12607–12613. [[CrossRef](#)] [[PubMed](#)]
45. Blanco, I.; Abate, L.; Bottino, F.A.; Bottino, P. Thermal behaviour of a series of novel aliphatic bridged polyhedral oligomeric silsesquioxanes (POSSs)/polystyrene (PS) nanocomposites: The influence of the bridge length on the resistance to thermal degradation. *Polym. Degrad. Stab.* **2014**, *102*, 132–137. [[CrossRef](#)]
46. Du, M.; Guo, B.; Jia, D. Thermal stability and flame retardant effects of halloysite nanotubes on poly(propylene). *Eur. Polym. J.* **2006**, *42*, 1362–1369. [[CrossRef](#)]
47. Blanco, I.; Abate, L.; Bottino, F.A.; Bottino, P. Thermal degradation of hepta cyclopentyl, mono phenyl-polyhedral oligomeric silsesquioxane (hcp-POSS)/polystyrene (PS) nanocomposites. *Polym. Degrad. Stab.* **2012**, *97*, 849–855. [[CrossRef](#)]
48. Budrugaec, P.; Cucos, A.; Miu, L. The use of thermal analysis methods for authentication and conservation state determination of historical and/or cultural objects manufactured from leather. *J. Therm. Anal. Calorim.* **2011**, *104*, 439–450. [[CrossRef](#)]
49. Vyazovkin, S.; Dranca, I.; Fan, X.; Advincula, R. Degradation and relaxation kinetics of polystyrene—Clay nanocomposite prepared by surface initiated polymerization. *J. Phys. Chem. B* **2004**, *108*, 11672–11679. [[CrossRef](#)]
50. Vyazovkin, S.; Chrissafis, K.; Di Lorenzo, M.L.; Koga, N.; Pijolat, M.; Roduit, B.; Sbirrazzuoli, N.; Suñol, J.J. ICTAC Kinetics Committee recommendations for collecting experimental thermal analysis data for kinetic computations. *Thermochim. Acta* **2014**, *590*, 1–23. [[CrossRef](#)]
51. Palacios, A.; De Gracia, A.; Haurie, L.; Cabeza, L.F.; Fernández, A.I.; Barreneche, C. Study of the thermal properties and the fire performance of flame retardant-organic PCM in bulk form. *Materials* **2018**, *11*, 117. [[CrossRef](#)] [[PubMed](#)]
52. Lee, H.; Fasulo, P.D.; Rodgers, W.R.; Paul, D.R. TPO based nanocomposites. Part 2. Thermal expansion behavior. *Polymer* **2006**, *47*, 3528–3539. [[CrossRef](#)]



Attached Paper IV



Showcasing research conducted by Dr Giuseppe Cavallaro from Department of Physics and Chemistry at University of Palermo, Italy.

Halloysite nanotubes sandwiched between chitosan layers: novel bionanocomposites with multilayer structures

A multilayer bionanocomposite based on chitosan and halloysite nanotubes was prepared by a sequential casting procedure driven by pH. The peculiar sandwich-like morphology conferred flame retardant properties to the hybrid biofilms.

As featured in:






See Giuseppe Cavallaro *et al.*,
New J. Chem., 2018, 42, 8384.



Cite this: *New J. Chem.*, 2018, 42, 8384

Halloysite nanotubes sandwiched between chitosan layers: novel bionanocomposites with multilayer structures†

Vanessa Bertolino, Giuseppe Cavallaro, * Giuseppe Lazzara,  Stefana Milioto and Filippo Parisi 

This work is a contribution to the design of multilayer biocomposites based on halloysite nanotubes (HNTs) and chitosan. Both the polymer and nanotubular inorganic additive have been selected among easily available green materials. An innovative preparation procedure based on the sequential casting of chitosan and HNTs has been proposed in order to obtain multilayer composite biofilms. A physico-chemical investigation (contact angle measurements, differential scanning calorimetry, thermogravimetry) has been conducted to characterize the bionanocomposites. As evidenced by scanning electron microscopy, the nanocomposites possess an intermediate halloysite layer between the chitosan ones. The multilayer morphology of the prepared chitosan/HNT nanocomposites has been confirmed by water contact angle measurements, which revealed that the hybrid films present a hydrophobic surface. The peculiar sandwich-like morphology of the chitosan/HNT hybrid materials has been correlated to their thermal behavior under inert and oxidative atmospheres. The kinetic aspects of chitosan degradation have been studied by a non-isothermal thermogravimetric approach (Friedman's method), while the suitability of HNTs as flame retardant fillers of multilayer nanocomposites has been estimated by the thermodynamic parameters of oxidative degradation. According to the thermogravimetric data, the formation of a well-compacted middle layer of HNTs has induced a reliable decrease in the activation energy of the degradation of chitosan. Differential scanning calorimetry experiments showed that the nanocomposites possess an enhanced ignition temperature compared with pure chitosan. This paper opens new sustainable prospects for the preparation of novel nanocomposites with layered structures that can be strategic for packaging, tissue engineering, and pharmaceutical applications.

Received 9th March 2018,
Accepted 9th April 2018

DOI: 10.1039/c8nj01161c

rsc.li/njc

1. Introduction

In recent years, nanocomposite materials based on natural resources have attracted growing interest because of their excellent properties coupled with their sustainability and low cost. The combination of sustainable polymers and inorganic fillers facilitates the fabrication of composite materials alternative to petrochemical-based plastics for several purposes within packaging,^{1,2} biotechnology^{3–5} and engineering^{6–10} applications. Ruiz-Hitzky *et al.*¹¹ highlighted that filling polymeric matrices with clay nanoparticles can improve the thermal and mechanical behavior of the pristine polymers. The addition of modified montmorillonite¹² and halloysite nanotubes (HNTs)¹³ into polylactic acid (PLA) allowed the fabrication of biofilms with

enhanced barrier properties that are useful for packaging. The high surface/volume ratio of nanoparticles facilitates polymer/filler interactions, which induce the improvement of the thermal stability of nanocomposites.¹⁴ Moreover, the tensile, thermal and wettability properties of biocomposite films are affected by their mesoscopic structure.^{15,16} Within this, hybrid materials with a multilayer morphology exhibited specific characteristics and functionalities that were not detected in nanocomposites with a uniform filler distribution into a polymeric matrix.^{16,17} The literature reports that an intermediate clay layer between the polymers promotes a flame retardant action on well-ordered nanocomposites.¹⁷ Alginate/montmorillonite nanocomposites with a multilayer structure showed excellent flame and fire shielding property.¹⁸ The layer-by-layer assembly of polyacrylamide and graphene oxide allowed the fabrication of fire retardant coatings for cotton fabric.¹⁹ The layer-by-layer (LBL) method represents an easy and successful strategy for the manufacture of thin films with a multilayer structure. This approach presents several advantages with respect to the

Dipartimento di Fisica e Chimica, Università degli Studi di Palermo,
Viale delle Scienze, pad. 17, 90128 Palermo, Italy. E-mail: giuseppe.cavallaro@unipa.it
† Electronic supplementary information (ESI) available. See DOI: 10.1039/c8nj01161c

traditional Langmuir–Blodgett (LB) technique, which is restricted to amphiphilic molecules capable of forming monolayers at the liquid–vapor interface.²⁰ In addition, the LB method requires special instrumentation²¹ and presents several limitations on the shape/size of the substrate as well as on the stability and quality of the films.²²

The preparation of multilayer materials through the LBL method can be driven by electrostatic attractions between oppositely charged molecules²² and hydrophobic interactions.²³ Besides ionic and hydrophobic forces, charge transfer interactions can determine the formation of multilayer films.²⁴ The LBL preparation of multilayer assemblies can be achieved through several deposition procedures including spin-coating, spray-coating, co-extrusion and solvent-casting.²⁵

Here, we prepared chitosan/halloysite composites with a multilayer morphology by using a novel method based on the water casting procedure. The sequential deposition of each layer was controlled by pH conditions.

Both chitosan and halloysite are nontoxic and eco-compatible materials.^{7,26} The biocompatibility of halloysite was demonstrated by several *in vitro* and *in vivo* experiments.^{27–29} Accordingly, halloysite was widely investigated as a nanocarrier for the controlled release of drugs,^{26,30} tissue engineering,^{6,7} wastewater decontamination,^{31–34} catalytic support,^{35–38} and filler for food packaging.^{2,39–41} Halloysite possesses a hollow tubular morphology generated by the rolling of flat kaolinite sheets.⁴² The sizes of halloysite nanotubes (HNTs) are quite polydisperse on the dependence of their geological deposit.⁴³ The length of HNTs ranges between 50 and 1500 nm, while the intervals for the external and internal diameters are 20–150 and 10–15 nm, respectively.⁴³ The surfaces of HNTs possess opposite charges in a wide pH range (between 2 and 8) as a consequence of their different chemical composition. In detail, the SiO₂ based outer surface is negatively charged, while the HNT lumen composed of Al₂O₃ presents a positive charge.⁴⁴ This peculiarity affects the interactions between ionic biopolymers and halloysite and, consequently, the properties of the corresponding bionanocomposite systems.^{15,16,45} It was observed that the encapsulation of anionic alginate within the cavity of HNTs determines the formation of nanocomposites with a higher thermal stability than that of the pure biopolymer.¹⁵ On the other hand, chitosan/HNT nanocomposites prepared by the classic casting method did not reveal any thermal stabilization effect in agreement with the adsorption of a positive biopolymer on the halloysite external surface.¹⁵ The combination of chitosan and HNTs was investigated to prepare composite biofilms for packaging,^{15,26} hydrogels for biomedical applications⁴⁶ and nanocomposite scaffolds for tissue engineering.^{7,47} As evidenced in a recent review,⁴⁸ the filling of chitosan with clay nanoparticles represents a successful strategy for the fabrication of biocompatible hybrid systems that are suitable as drug carriers, electrochemical sensors, and sustainable packaging.

In this work, the sequential casting method was proposed for the preparation of chitosan/halloysite nanocomposites with multilayer morphology. Studies on the morphology and surface properties of the prepared films were conducted to estimate the

efficiency of the preparation method. The flammability and the thermal properties of the multilayer films were determined by differential scanning calorimetry and thermogravimetry measurements performed under both inert and oxidative atmospheres. The attained knowledge can be useful to fabricate composites with a sandwich-like structure that hold potential for several technological purposes.

This paper contributes to the development of sustainable nanocomposites with promising properties for industrial applications because their engineering properties (thermal performances, flammability, and wettability) can be properly controlled by their specific mesoscopic structure.

2. Results and discussion

2.1 Morphology and surface properties

SEM images of chitosan/HNT nanocomposites with variable ratios between the HNTs and the total amount of chitosan ($R_{\text{HNTs:CHIT}}$) are presented in Fig. 1. As designed, the films showed a sandwich-like morphology with the nanotubes confined in the intermediate layer (Fig. 1).

Accordingly, HNTs were not observed on both surfaces of the nanocomposites, while the cross-section view of the SEM images evidenced the presence of nanotubes in the middle region, which is between the outer layers of chitosan. The analysis of the SEM images allowed us to estimate the thickness of the intermediate HNT layer, which was compared to that of the film (Fig. 2). As sketched in Fig. 2, the volume fraction of the middle layer in the nanocomposite depends on $R_{\text{HNTs:CHIT}}$.

The three-layer morphology of chitosan/HNT nanocomposites was confirmed by water contact angle measurements, which allowed us to investigate the surface properties of the films. The contact angle (θ) of a water drop deposited on the surface of the film was measured as a function of time (t). Examples of the water drop images collected just after the deposition of water on the film surface are presented in the ESI.† As a general result, θ decreases over time as a consequence of the adsorption and spreading processes. The θ vs. t trends were fitted by means of a semi-quantitative approach expressed as⁴⁹

$$\theta(t) = \theta_i \cdot \exp(-kt^n) \quad (1)$$

where θ_i is the water contact angle just after the deposition of the drop on the film surface, while k and n are the kinetic constant and the exponential parameter, respectively. It should be noted that n can assume values between 0 (pure adsorption) and 1 (pure spreading). The fitting parameters data (Table 1) highlighted that both adsorption and spreading occur for all materials with n ranging between 0.64 (pristine chitosan) and 0.80 (chitosan/HNT composite with $R_{\text{HNT:CHIT}} = 1.27$). In addition, the k values evidenced that the HNT layer does not strongly affect the kinetics of the adsorption/spreading processes.

As shown in Table 1, the presence of nanotubes induced a slight decrease in θ_i , indicating that the relevant hydrophobicity of the chitosan surfaces was preserved in the bionanocomposites. This finding agrees with the absence of HNTs on the

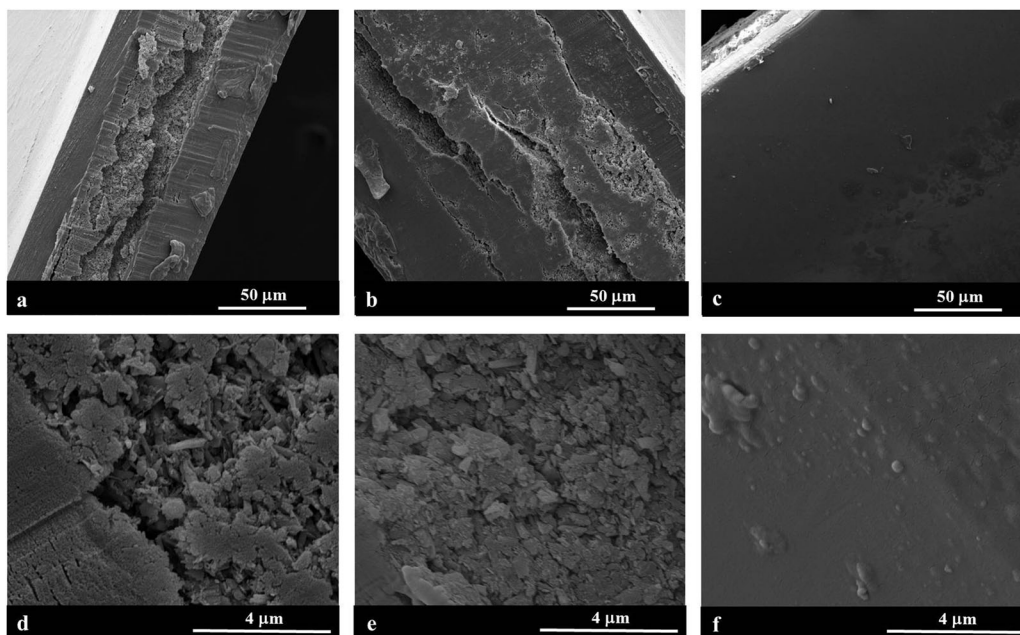


Fig. 1 SEM images of the cross section of chitosan/HNT nanocomposites with $R_{\text{HNT:CHIT}} = 0.62$ (a and d) and $R_{\text{HNT:CHIT}} = 1.27$ (b and e). SEM images of the surface of chitosan/HNT nanocomposites with $R_{\text{HNT:CHIT}} = 1.27$ (c and f).

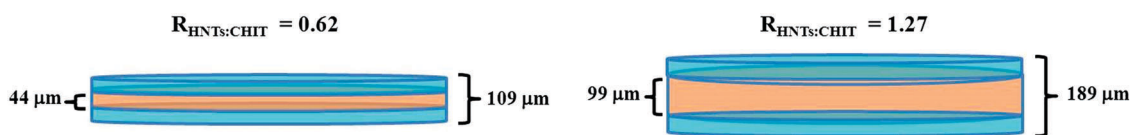


Fig. 2 Schematic representation of the thicknesses of the layers determined from the SEM images of the chitosan/HNT films with variable $R_{\text{HNT:CHIT}}$.

Table 1 Initial water contact angle, exponential parameter and kinetic constant obtained by the fitting of $\theta_{\text{vs.}t}$ trends for the chitosan/HNT nanocomposites with variable composition

$R_{\text{HNT:CHIT}}$	$\theta_{\text{i}}/^\circ$	N	k/s^{-1}
0	86 ± 3	0.641 ± 0.004	0.0078 ± 0.0001
0.33	79 ± 3	0.63 ± 0.01	0.0046 ± 0.0001
0.48	74 ± 4	0.78 ± 0.01	0.0085 ± 0.0001
0.62	84 ± 4	0.62 ± 0.01	0.0038 ± 0.0001
0.94	78 ± 5	0.78 ± 0.01	0.0013 ± 0.0003
1.27	75 ± 4	0.80 ± 0.01	0.0032 ± 0.0001

surface of the film evidenced by the SEM images (Fig. 1). In contrast, the homogeneous filling of chitosan with halloysite showed a significant reduction in θ_{i} (from 90 to 65°) due to the presence of the hydrophilic nanotubes on the film surface.¹⁵ Among the nanocomposites, the film with $R_{\text{HNT:CHIT}} = 0.62$ showed the most hydrophobic surface as evidenced by the largest θ_{i} value. This result indicated that the HNT inner layer is well confined between the chitosan ones.

2.2 Thermal properties of layered chitosan/HNT nanocomposites

2.2.1 Thermal degradation of chitosan. Thermogravimetry represents an established technique to investigate the effect of filler addition on the thermal stability of polymers.^{14,50}

The ESI† reports some examples of thermogravimetric curves for nanocomposites with variable composition. We determined the water content of both pure chitosan and chitosan/HNT composites using their mass losses in the temperature range between 25 and 150 °C (see the ESI†). It should be noted that the nanocomposites with a large HNT content exhibited a mass loss at ca. 500 °C due to the expulsion of two water molecules of the halloysite interlayer.⁵¹ The literature^{16,52} reports that the thermal behavior of the polymer/HNT nanocomposites is strongly related to their mesoscopic structure. The homogenous dispersion of the HNTs into the matrix induced an increase in the polymer degradation temperature because of both the barrier effect and entrapment process towards the volatile products.^{16,52,53} Accordingly, the activation energy of the polymer degradation was reduced by the filling of the HNTs indicating that the kinetics was slowed down.^{16,52} In contrast, HNTs sandwiched between two polymer layers did not have any thermal stabilization effects on the nanocomposite systems.¹⁶ On this basis, the specific effect of HNT addition on the kinetics of chitosan degradation can be strictly correlated to the designed multilayer morphology of the nanocomposites. In this regard, thermogravimetry measurements at variable heating rates (β) were conducted with the aim to investigate the non-isothermal kinetics of the polymer degradation of chitosan/HNTs with a different composition. The activation energy (E_{a}) of chitosan

degradation was determined by the Friedman method, which was successfully used to study the kinetics of thermal degradation for materials based on chitin and chitosan.^{15,54} The Friedman method is expressed by the equation

$$\ln\left(\frac{\beta d\alpha}{dT}\right) = \ln[Af(\alpha)] - \frac{E_a}{RT} \quad (2)$$

where $f(\alpha)$ is a function of the extent of conversion (α) that depends on the degradation mechanism, while $d\alpha/dT$ is the first derivative of α with respect to temperature. In addition, A and R are the pre-exponential factor and the gas constant, respectively. According to eqn (2), the E_a value at each α corresponds to the specific slope of the $\ln(\beta d\alpha/dT)$ vs. $1/T$ function. As a general result, E_a does not depend on α for all investigated systems. Fig. 3 shows the dependence of the average E_a values on the composition of the chitosan/HNT nanocomposites.

We observed that the effect of HNT addition on the kinetic degradation of chitosan depends on the filler concentration of the nanocomposites. Compared to pure chitosan, an increase in E_a was detected for composites with $R_{\text{HNT:CHIT}} < 0.5$. Similar results were obtained for chitosan/HNT nanocomposites prepared by the classical casting method, which produced hybrid materials with a homogenous distribution of the filler into the polymer matrix.¹⁵ On the other hand, the presence of larger amounts of nanotubes ($R_{\text{HNT:CHIT}} > 0.6$) slowed down the kinetics of chitosan degradation (Fig. 3). Interestingly, nanocomposites with $R_{\text{HNT:CHIT}} = 1.27$ exhibited a significant E_a reduction (ca. 20%) with respect to that of pure chitosan. According to the literature,¹⁶ a thermal destabilization effect on polymer degradation is consistent with a sandwich-like structure of the nanocomposites. Namely, TG data showed that the formation of a well compacted intermediate layer of halloysite was achieved only in nanocomposites with a large filler content.

2.2.2 Oxidative degradation of chitosan/HNT nanocomposites. DSC experiments were conducted in static air with the aim to investigate the oxidative degradation of chitosan/HNT nanocomposites. The analysis of the DSC thermograms provided the enthalpy (ΔH_{ox}) and the temperature (T_{ox}) of the material degradation under the oxidative atmosphere. It should be noted that T_{ox} was determined from the onset of the DSC peaks. As shown in Fig. 4, T_{ox} was strongly enhanced by the addition of

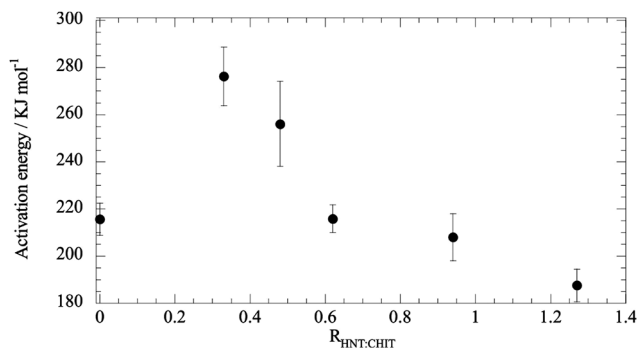


Fig. 3 The average activation energy of chitosan degradation as a function of the composition of the nanocomposites.

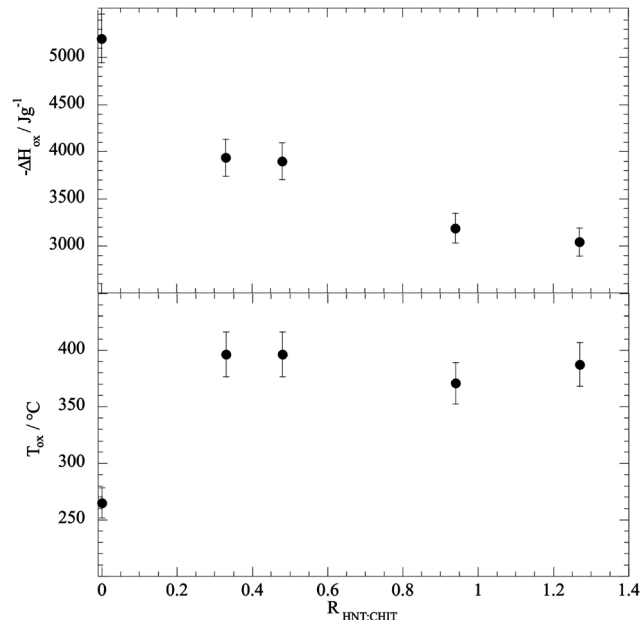


Fig. 4 Enthalpy (up) and temperature (down) of oxidative degradation as functions of the HNT/chitosan weight ratio for the multilayer nanocomposites.

HNTs into chitosan highlighting that the ignition temperature of the oxidation process is much higher for the nanocomposites compared to that for pure polymer. The T_{ox} enhancement indicates that the nanotubes generated a flame retardant effect on chitosan. Similar results were observed for chitosan/sepiolite nanocomposites.⁵⁵ In addition, we detected that ΔH_{ox} decreases upon filling chitosan with the HNTs (Fig. 4). Namely, the amount of heat released during the oxidative degradation is lower for the nanocomposites than that determined for the pristine chitosan confirming the fire retardant action induced by the nanotubes. The significant ΔH_{ox} reduction (ca. 50%) estimated in the composites with a very large filler content ($R_{\text{HNT:CHIT}} = 0.94$ and $R_{\text{HNT:CHIT}} = 1.27$) might be partially due to the formation of a well compacted HNT layer in the middle region.

3. Experimental

3.1 Materials

Chitosan (75–85% deacetylated, $M_w = 50\text{--}190 \text{ kg mol}^{-1}$) and glacial acetic acid are Aldrich products. Halloysite nanotubes ($\text{Al}_2\text{Si}_2\text{O}_5(\text{OH})_4 \cdot 2\text{H}_2\text{O}$; $M_w = 294.19 \text{ g mol}^{-1}$) are from Imerys Ceramics New Zealand Limited. The specific surface of the HNTs is $22.10 \text{ m}^2 \text{ g}^{-1}$.⁴³

3.2 Preparation of multilayer nanocomposites

Chitosan/HNT nanocomposites with multilayer morphology were prepared by means of a sequential casting method. As sketched in Fig. 5, films with a sandwich-like structure (a layer of halloysite between two layers of chitosan) were obtained through the subsequent deposition of aqueous dispersions with variable pH as follows: (1) chitosan (pH = 3.5); (2) HNTs (pH = 6); (3) chitosan (pH = 3.5). This procedure allows us to

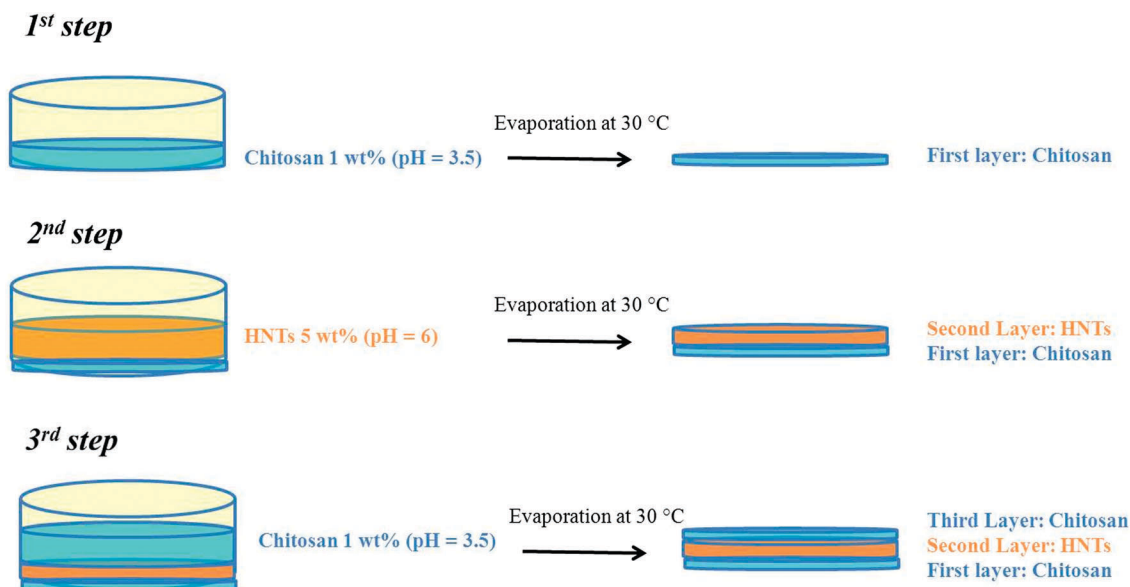


Fig. 5 Schematic representation of the preparation of chitosan/HNT nanocomposites with a three-layered structure.

obtain a well-ordered structure because of the very low solubility of chitosan at neutral pH.⁴⁴

In detail, we prepared a 1 wt% chitosan solution in water under stirring overnight at 30 °C. The pH of the polymer solution was fixed at 3.5 by adding 0.1 mol dm⁻³ of acetic acid dropwise. The obtained solution was poured into a glass Petri dish at 30 °C to evaporate water until the weight was constant. Then, a 5 wt% aqueous dispersion of halloysite was deposited on a chitosan dried film, which is confined to the bottom of the Petri dish. A stable HNT dispersion in water was prepared by sonication and subsequent magnetic stirring overnight at 30 °C. It should be noted that the selected concentration (5 wt%) ensures that the HNT dispersion is highly stable due to hindered precipitation as the nanotube contact distance was achieved.⁵⁶ Once the evaporation was complete, a well compacted HNT layer was obtained. Finally, the casting of a chitosan layer (from the 1 wt% aqueous dispersion) was carried out on a halloysite deposit which allowed obtaining a three-layered structure as shown in Fig. 1. The thickness of the inner HNT layer was systematically varied by changing the volume of its dispersion, while the thicknesses of the outer chitosan layers were kept constant. The weight ratio between the HNTs and the total amount of chitosan ($R_{\text{HNTs:CHIT}}$) ranged between 0.33 and 1.27. Similar to the chitosan/HNT nanocomposites with a homogenous distribution of the filler into the matrix,¹⁵ the prepared films with a multilayer morphology exhibited compact mechanical features.

3.3 Methods

3.3.1 Scanning electron microscopy (SEM). The morphology of chitosan/HNT nanocomposites were studied by using a microscope ESEM FEI QUANTA 200F. Before each experiment, the sample surface was coated with gold in argon by means of an Edwards sputter coater s150a to minimize charging under the electron beam. The measurements were carried out in high-vacuum mode ($<6 \times 10^{-4}$ Pa) for simultaneous secondary electrons.

The energy of the beam was 20 kV, and the working distance was 10 mm. Minimal electron dose conditions were employed to avoid damaging the sample.

3.3.2 Contact angle. Water contact angle measurements were performed using an optical contact angle apparatus (OCA 20, Data Physics Instruments) equipped with a CCD camera with high-resolution power. The SCA 20 software (Data Physics Instruments) was used for data acquisition. The water contact angle just after deposition (θ_i) was measured by the method by placing a droplet of 5.0 ± 0.5 μL onto the sample surface. Both the support and the injecting syringe were maintained at 25.0 ± 0.1 °C. Each sample was analyzed three times, and the average values are reported.

3.3.3 Thermogravimetry. Thermogravimetry (TG) measurements were conducted by using a Q5000 IR apparatus (TA Instruments) under a nitrogen flow of 25 and 10 cm³ min⁻¹ for the sample and the balance, respectively. The weight of each sample was *ca.* 5 mg. Experiments were performed by heating the samples from room temperature to 900 °C in a platinum crucible. The measurements were conducted at variable heating rates (β) to determine the activation energy (E_a) of chitosan degradation. Specifically, β values of 5, 10, 15 and 20 °C min⁻¹ were selected.

3.3.4 Differential scanning calorimetry. Differential scanning calorimetry (DSC) measurements were carried out by means of a DSC 2920 CE apparatus (TA Instruments). The apparatus was calibrated with indium. The pans were in aluminum and the weight of each sample was *ca.* 2 mg. The temperature and the power calibration were determined at variable heating rates in agreement with the recent IUPAC technical report.⁵⁷ The measurements were performed in static air within a temperature range between 0 and 600 °C. The heating rate was set at 10 °C min⁻¹.

4. Conclusions

Multilayer nanocomposites composed of chitosan and halloysite nanotubes (HNTs) were successfully prepared by means of an

innovative casting method based on the sequential deposition of aqueous dispersions with variable pH. SEM images evidenced that the prepared bionanocomposites possess an intermediate halloysite layer that is sandwiched between two chitosan layers. The volume fraction of the middle layer can be easily controlled by changing the experimental conditions employed in the preparation of the composite biofilms. According to the sandwich-like structure, the surfaces of the chitosan/HNT films exhibited a strong hydrophobic character ruling out the presence of nanotubes at the interfaces. The kinetics of thermal degradation of chitosan can be controlled by the HNT content in the nanocomposite. A significant reduction in the activation energy of the chitosan degradation was detected for composite systems with a large filler concentration because of the formation of a well-compacted layer of HNTs in the middle region. In addition, calorimetric measurements showed that all nanocomposites exhibit potential flame retarding capacity compared to pure chitosan as highlighted by the increase in the ignition temperature and the enthalpy reduction for thermal degradation under oxidative conditions. With this study, an easy strategy to prepare multilayer sustainable films with promising surface and thermal properties was proposed. The attained knowledge represents a fundamental point to fabricate composites with a sandwich-like structure that hold potential for several technological purposes.

Conflicts of interest

There are no conflicts to declare.

Acknowledgements

The work was financially supported by the University of Palermo.

References

- 1 A. A. Sapolidis, F. K. Katsaros, G. E. Romanos, N. K. Kakizis and N. K. Kanellopoulos, *Composites, Part B*, 2007, **38**, 398–404.
- 2 M. Makaremi, P. Pasbakhsh, G. Cavallaro, G. Lazzara, Y. K. Aw, S. M. Lee and S. Milioto, *ACS Appl. Mater. Interfaces*, 2017, **9**, 17476–17488.
- 3 Y. Lvov, A. Aerov and R. Fakhruddin, *Adv. Colloid Interface Sci.*, 2014, **207**, 189–198.
- 4 Y. Lvov and E. Abdullayev, *Prog. Polym. Sci.*, 2013, **38**, 1690–1719.
- 5 Y. Stetsyshyn, J. Zemla, O. Zolobko, K. Fornal, A. Budkowski, A. Kostruba, V. Donchak, K. Harhay, K. Awsuik, J. Rysz, A. Bernasik and S. Voronov, *J. Colloid Interface Sci.*, 2012, **387**, 95–105.
- 6 R. F. Fakhruddin and Y. M. Lvov, *Nanomedicine*, 2016, **11**, 2243–2246.
- 7 M. Liu, C. Wu, Y. Jiao, S. Xiong and C. Zhou, *J. Mater. Chem. B*, 2013, **1**, 2078–2089.
- 8 H. Wei, K. Rodriguez, S. Renneckar and P. J. Vikesland, *Environ. Sci.: Nano*, 2014, **1**, 302–316.
- 9 V. K. Thakur and M. R. Kessler, *Polymer*, 2015, **69**, 369–383.
- 10 M. Du, B. Guo, Y. Lei, M. Liu and D. Jia, *Polymer*, 2008, **49**, 4871–4876.
- 11 E. Ruiz-Hitzky, P. Aranda, M. Darder and G. Rytwo, *J. Mater. Chem.*, 2010, **20**, 9306–9321.
- 12 G. Ozkoc and S. Kemaloglu, *J. Appl. Polym. Sci.*, 2009, **114**, 2481–2487.
- 13 G. Gorrasi, R. Pantani, M. Murariu and P. Dubois, *Macromol. Mater. Eng.*, 2014, **299**, 104–115.
- 14 I. Blanco and F. A. Bottino, *Polym. Compos.*, 2013, **34**, 225–232.
- 15 V. Bertolino, G. Cavallaro, G. Lazzara, M. Merli, S. Milioto, F. Parisi and L. Sciascia, *Ind. Eng. Chem. Res.*, 2016, **55**, 7373–7380.
- 16 G. Cavallaro, D. I. Donato, G. Lazzara and S. Milioto, *J. Phys. Chem. C*, 2011, **115**, 20491–20498.
- 17 B. Finnigan, D. Martin, P. Halley, R. Truss and K. Campbell, *J. Appl. Polym. Sci.*, 2005, **97**, 300–309.
- 18 B. Liang, H. Zhao, Q. Zhang, Y. Fan, Y. Yue, P. Yin and L. Guo, *ACS Appl. Mater. Interfaces*, 2016, **8**, 28816–28823.
- 19 G. Huang, J. Yang, J. Gao and X. Wang, *Ind. Eng. Chem. Res.*, 2012, **51**, 12355–12366.
- 20 J. Zasadzinski, R. Viswanathan, L. Madsen, J. Garnæs and D. Schwartz, *Science*, 1994, **263**, 1726–1733.
- 21 L. Netzer, R. Iscovici and J. Sagiv, *Thin Solid Films*, 1983, **99**, 235–241.
- 22 G. Decher, *Science*, 1997, **277**, 1232–1237.
- 23 N. A. Kotov, *Nanostruct. Mater.*, 1999, **12**, 789–796.
- 24 Y. Shimazaki, M. Mitsuishi, S. Ito and M. Yamamoto, *Langmuir*, 1997, **13**, 1385–1387.
- 25 X. Zhang, H. Chen and H. Zhang, *Chem. Commun.*, 2007, 1395–1405.
- 26 M. Liu, Y. Zhang, C. Wu, S. Xiong and C. Zhou, *Int. J. Biol. Macromol.*, 2012, **51**, 566–575.
- 27 G. I. Fakhruddin, F. S. Akhatova, Y. M. Lvov and R. F. Fakhruddin, *Environ. Sci.: Nano*, 2015, **2**, 54–59.
- 28 M. Kryuchkova, A. Danilushkina, Y. Lvov and R. Fakhruddin, *Environ. Sci.: Nano*, 2016, **3**, 442–452.
- 29 D. Tan, P. Yuan, F. Annabi-Bergaya, D. Liu, L. Wang, H. Liu and H. He, *Appl. Clay Sci.*, 2014, **96**, 50–55.
- 30 C. Aguzzi, C. Viseras, P. Cerezo, I. Salcedo, R. Sánchez-Espejo and C. Valenzuela, *Colloids Surf., B*, 2013, **105**, 75–80.
- 31 G. Cavallaro, I. Grillo, M. Gradzielski and G. Lazzara, *J. Phys. Chem. C*, 2016, **120**, 13492–13502.
- 32 Y. Zhao, E. Abdullayev, A. Vasiliev and Y. Lvov, *J. Colloid Interface Sci.*, 2013, **406**, 121–129.
- 33 G. Huang, W. Li, Q. Liu, J. Liu, H. Zhang, R. Li, Z. Li, X. Jing and J. Wang, *New J. Chem.*, 2018, **42**, 168–176.
- 34 P. Luo, Y. Zhao, B. Zhang, J. Liu, Y. Yang and J. Liu, *Water Res.*, 2010, **44**, 1489–1497.
- 35 S. Sadjadi, T. Hosseinejad, M. Malmir and M. M. Heravi, *New J. Chem.*, 2017, **41**, 13935–13951.
- 36 Q. Wang, Y. Wang, Y. Zhao, B. Zhang, Y. Niu, X. Xiang and R. Chen, *CrystEngComm*, 2015, **17**, 3110–3116.
- 37 Y. Liu, J. Zhang, H. Guan, Y. Zhao, J.-H. Yang and B. Zhang, *Appl. Surf. Sci.*, 2018, **427**, 106–113.

- 38 Y. Liu, H. Guan, J. Zhang, Y. Zhao, J.-H. Yang and B. Zhang, *Int. J. Hydrogen Energy*, 2018, **43**, 2754–2762.
- 39 G. Gorrasi, *Carbohydr. Polym.*, 2015, **127**, 47–53.
- 40 G. Gorrasi, V. Bugatti and V. Vittoria, *Carbohydr. Polym.*, 2012, **89**, 132–137.
- 41 R. D. Silva, P. Pasbakhsh, K. L. Goh, S.-P. Chai and J. Chen, *J. Compos. Mater.*, 2014, **48**, 3705–3717.
- 42 E. Joussein, S. Petit, G. J. Churchman, B. Theng, D. Righi and B. Delvaux, *Clay Miner.*, 2005, **40**, 383–426.
- 43 P. Pasbakhsh, G. J. Churchman and J. L. Keeling, *Appl. Clay Sci.*, 2013, **74**, 47–57.
- 44 V. Bertolino, G. Cavallaro, G. Lazzara, S. Milioto and F. Parisi, *Langmuir*, 2017, **33**, 3317–3323.
- 45 R. T. De Silva, P. Pasbakhsh, K. L. Goh and L. Mishnaevsky, *Polymer*, 2014, **55**, 6418–6425.
- 46 T. Wu, Y. Li and D. S. Lee, *Macromol. Res.*, 2017, **25**, 480–488.
- 47 E. A. Naumenko, I. D. Guryanov, R. Yendluri, Y. M. Lvov and R. F. Fakhrullin, *Nanoscale*, 2016, **8**, 7257–7271.
- 48 A. Ali and S. Ahmed, *Int. J. Biol. Macromol.*, 2018, **109**, 273–286.
- 49 S. Farris, L. Introzzi, P. Biagioni, T. Holz, A. Schiraldi and L. Piergiovanni, *Langmuir*, 2011, **27**, 7563–7574.
- 50 I. Blanco, L. Abate, F. A. Bottino and P. Bottino, *Polym. Degrad. Stab.*, 2014, **102**, 132–137.
- 51 G. Cavallaro, G. Lazzara and S. Milioto, *Langmuir*, 2011, **27**, 1158–1167.
- 52 G. Cavallaro, R. Lisi, G. Lazzara and S. Milioto, *J. Therm. Anal. Calorim.*, 2013, **112**, 383–389.
- 53 M. Du, B. Guo and D. Jia, *Eur. Polym. J.*, 2006, **42**, 1362–1369.
- 54 T. Wanjun, W. Cunxin and C. Donghua, *Polym. Degrad. Stab.*, 2005, **87**, 389–394.
- 55 M. Darder, M. López-Blanco, P. Aranda, A. J. Aznar, J. Bravo and E. Ruiz-Hitzky, *Chem. Mater.*, 2006, **18**, 1602–1610.
- 56 G. Cavallaro, G. Lazzara, S. Milioto, G. Palmisano and F. Parisi, *J. Colloid Interface Sci.*, 2014, **417**, 66–71.
- 57 H. Lee, P. D. Fasulo, W. R. Rodgers and D. R. Paul, *Polymer*, 2006, **47**, 3528–3539.